2012

Analysis And Design Optimization Of Resonant Dc-dc Converters

Xiang Fang
University of Central Florida

STARS Citation

Fang, Xiang, "Analysis And Design Optimization Of Resonant Dc-dc Converters" (2012). *Electronic Theses and Dissertations*. 2125.
https://stars.library.ucf.edu/etd/2125

ANALYSIS AND DESIGN OPTIMIZATION OF RESONANT DC-DC
CONVERTERS

by

XIANG FANG
B.S. Tsinghua University, 2007

A dissertation submitted in partial fulfillment of the requirements
for the degree of Doctor of Philosophy
in the Department of Electrical Engineering and Computer Science
in the College of Engineering and Computer Science
at the University of Central Florida
Orlando, Florida

Spring Term
2012

Major Professor: John Shen and Issa Batarseh

ABSTRACT

The development in power conversion technology is in constant demand of high power efficiency and high power density. The DC-DC power conversion is an indispensable stage for numerous power supplies and energy related applications. Particularly, in PV micro-inverters and front-end converter of power supplies, great challenges are imposed on the power performances of the DC-DC converter stage, which not only require high efficiency and density but also the capability to regulate a wide variation range of input voltage and load conditions. The resonant DC-DC converters are good candidates to meet these challenges with the advantages of achieving soft switching and low EMI. Among various resonant converter topologies, the LLC converter is very attractive for its wide gain range and providing ZVS for switches from full load to zero load condition.

The operation of the LLC converter is complicated due to its multiple resonant stage mechanism. A literature review of different analysis methods are presented, and it shows that the study on the LLC is still incomplete. Therefore, an operation mode analysis method is proposed, which divides the operation into six major modes based on the occurrence of resonant stages. The resonant currents, voltages and the DC gain characteristics for each mode is investigated. To obtain a thorough view of the converter behavior, the boundaries of every mode are studied, and mode distribution regarding the gain, load and frequency is presented and discussed. As this operation mode model is a precise model, an experimental prototype is designed and built to demonstrate its accuracy in operation waveforms and gain prediction.

Since most of the LLC modes have no closed-form solutions, simplification is necessary in order to utilize this mode model in practical design. Some prior approximation methods for converter's gain characteristics are discussed. Instead of getting an entire gain-vs.-frequency curve, we focus on peak gains, which is an important design parameters indicating the LLC's operating limit of input voltage and switching frequency. A numerical peak gain approximation method is developed, which provide a direct way to calculate the peak gain and its corresponding load and frequency condition. The approximated results are compared with experiments and simulations, and are proved to be accurate. In addition, as PO mode is the most favorable operation mode of the LLC, its operation region is investigated and an approximation approach is developed to determine its boundary.

The design optimization of the LLC has always been a difficult problem as there are many parameters affecting the design and it lacks clear design guidance in selecting the optimal resonant tank parameters. Based on the operation mode model, three optimization methods are proposed according to the design scenarios. These methods focus on minimize the conduction loss of resonant tank while maintaining the required voltage gain level, and the approximations of peak gains and PO mode boundary can be applied here to facilitate the design. A design example is presented using one of the proposed optimization methods. As a comparison, the L-C component values are reselected and tested for the same design specifications. The experiments show that the optimal design has better efficiency performance.

Finally, a generalized approach for resonant converter analysis is developed. It can be implemented by computer programs or numerical analysis tools to derive the operation waveforms and DC characteristics of resonant converters.

ACKNOWLEDGMENTS

I would like to express my sincere gratitude to my advisors Dr. Issa Batarseh and Dr. John Shen, for their tremendous supports and continuous inspirations to my research works throughout my Ph.D. studies. What I have learned from them is not only the spirit of doing research but also the ability to think independently. I would also like to thank Dr. Nasser Kutkut for his precious and patient guidance during his supervision of Florida Energy Systems Consortium (FESC) in UCF. I am greatly grateful for my other dissertation committee members, Dr. Thomas Xinzhang Wu and Dr. Wasfy Mikhael, for their valuable guidance and kind suggestions.

I would like to express my deep appreciation to Dr. Haibing Hu, who introduced me to the area of the resonant converter topology and kindly gave me insightful suggestions for my academic research.

It is a great honor for me to be part of the Florida Power Electronics Center (FPEC) at the University of Central Florida. My study and research life in FPEC was full of joy and hard work, which is an unforgettable and precious memory to me. I would like to thank all my fellow colleagues for the inspiration and the support. I especially appreciate the generous help of Dr. Ala Hussein and Dr. Mingyao Ma provided on formatting and typesetting the electronic file of the dissertation.

In the end, I would like to thank my beloved wife, Shujie, for the love and encouragement she gave to support me through every difficulty, for the enjoyment and happiness she brought to my life.

TABLE OF CONTENTS

LIST OF FIGURES

LIST OF TABLES

CHAPTER ONE: INTRODUCTION

1.1 Background and Challenges

The techniques of power conversion are about processing and delivering electric power; power converters are needed ubiquitously in this age of electricity. The power conversion is an important link between the harvested or supplied power source to the end-user electronic products or the energy transmission or storage applications. From the field of renewable energy generation to the power supply of a portable digital device, all the rapid advancements in the technology impose intense challenges on the power electronics. In the past decades, achieving high power efficiency and high power density is constantly demanded by the development of electricity generation, transmission and power supply technologies, and has become the focus of the power conversion research.

Nowadays, the world's energy structure is undergoing a fundamental readjustment: as the traditional fossil fuel based energy sources such as oil, gas and coal being the major cause of numerous environmental pollution problems, people are actively seeking renewable energy sources such as solar, wind and hydro power and accordingly developing the energy technology as an alternative [1]. As shown in Figure 1.1 [1], the renewable energy is only 19.4% of the total power generation, and there is a huge potential for the future of the renewable energy. Among these renewable energy sources, the solar power with its advantages of clean, reliable, quiet and low maintenance cost is having an exponential growth as seen in Figure 1.2 [1, 2].
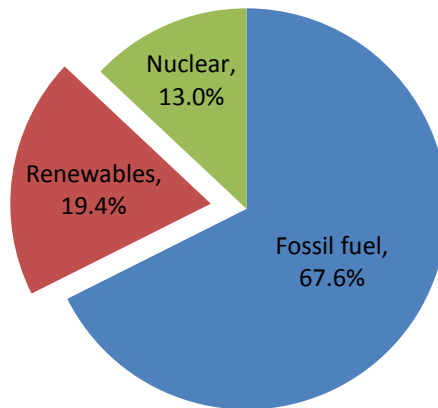
Figure 1.1 Energy share of global electricity generation in 2010

Worldwide Solar PV Capacity, 1995-2010
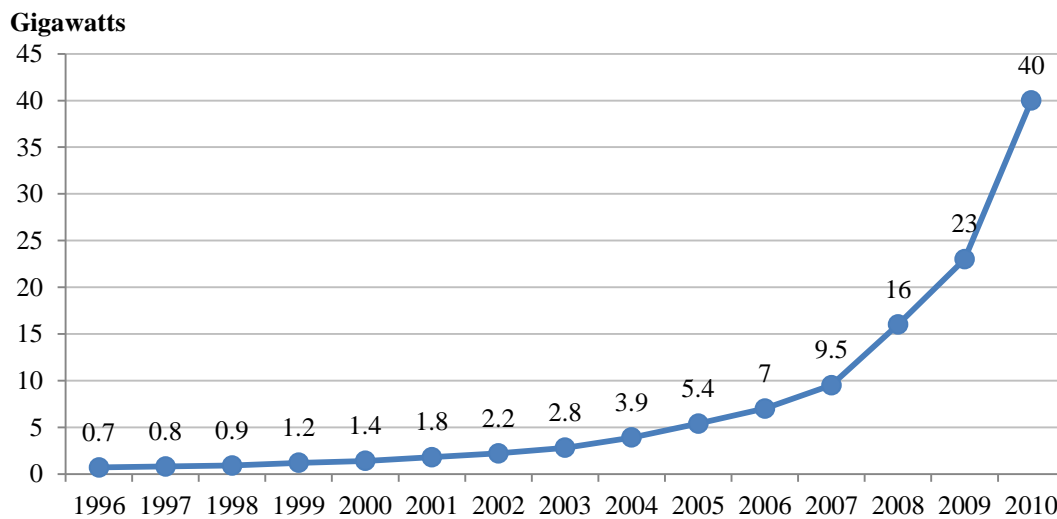
Figure 1.2 The growth of global solar PV capacity

There are several kinds of system structure for photovoltaic power applications [3-7], which are summarized and illustrated in Figure 1.3. The stand-alone off-grid system is usually for residential or small-scale applications which can provide electricity to where utility power is inaccessible like RV's and boats or remote areas. The grid-interface central system consists of a large array of PV panels and one or several centralized AC inverters directly connected to the

2

power grid. It is usually for large-scale PV power farm applications. The third type system is the grid-interface micro system, which has small-scale power rating (150W – 2kW) but connected to the grid but has the flexibility for large-scale applications having mass amount of micro systems work together. In contrast to the central system, a micro system only connect to single or several PV panels, which can maximize the energy production by implementing max power point tracking (MPPT) for each single module and has no mismatch losses for keeping each module independent[8, 9]. Also, it represents better reliability and safety for the module independence that can proof against whole system failure caused by single unit. However, its disadvantage is the high cost as each PV panel requires a micro-inverter unit. The common part in the three systems is the DC/DC power stage. Although in some micro system single DC/AC stage structure is used, to achieve high power efficiency it usually requires DC/DC then DC/AC two stage structure. The technical challenge for the DC/DC converter is that the input source has wide variation range. Like other renewable energy system, the PV panels are persistently affected by the changing environment factors such as cloud shadow, temperature fluctuations, sun's angle and etc. The converter should be able to regulate the PV panel output to a desired stable voltage level for the next DC/AC stage. Increasing the power density is another major challenge especially for stand-alone systems and micro systems as small profile units will ease the installation and transportation of the PV modules.

Stand-alone Off-grid System

PV Panel   DC/DC   DC Bus
                  Converter

Grid-interface Central System

PV Array   Centrlized Inverter   AC Grid

                  DC/DC   DC/AC
                  Converter   Inverter

Grid-interface Micro System

                  Microinverter   AC Grid

PV Panel   DC/DC   DC/AC
                  Converter   Inverter

PV Panel   DC/DC   DC/AC
                  Converter   Inverter
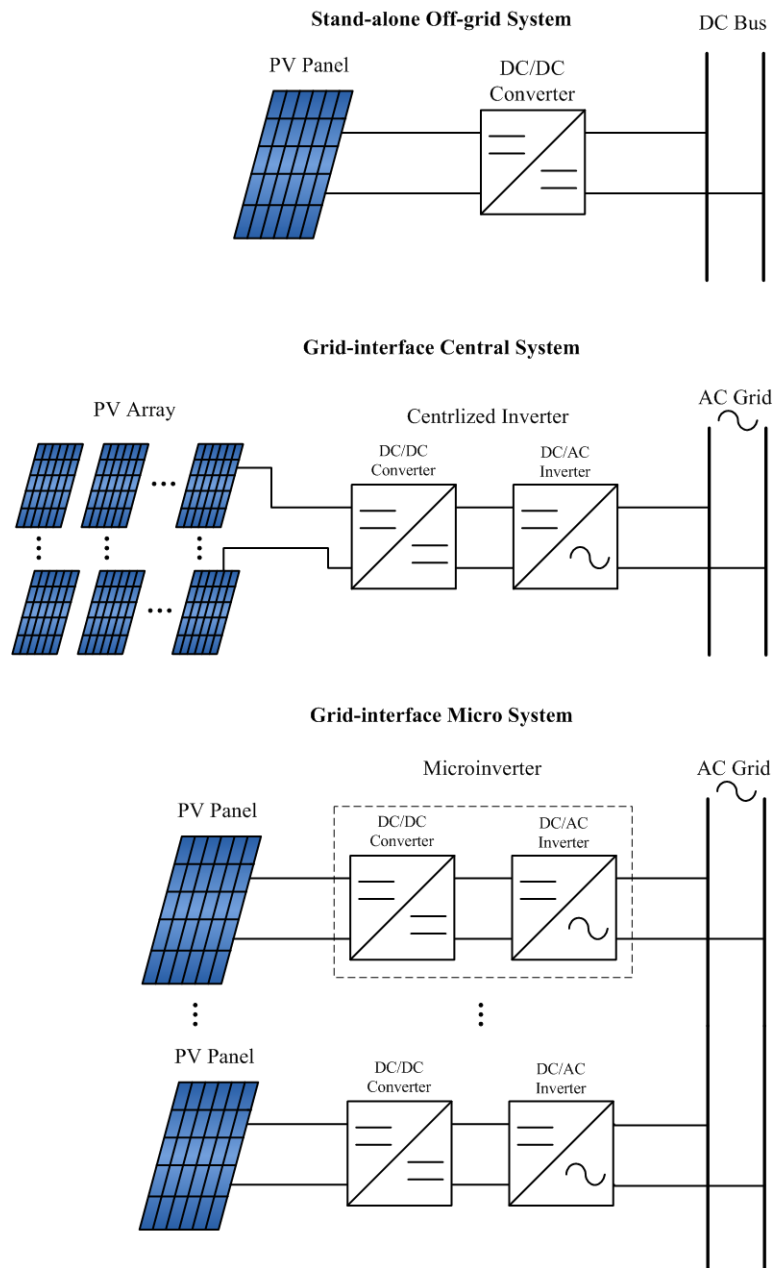
Figure 1.3 The photovoltaic power system structures

Besides the field of energy, the power conversion plays a vital role in the computing

system and consumer electronic products as well. As the trend of integrated circuit development is

towards smaller size and faster computing speed, it leads to smaller, yet more powerful electronic

devices. After over 50 years since the Moore's Law was proposed, it still uncannily holds true

4

today that the transistors' number in an integrated circuit chip doubles every two years. According to this prediction, the computational power will continue its exponential-like increase. Although it seems that following this trend the power consumption for the same level computing capability will decrease as the transistor density and speed increases and the required supply voltage reduces, the challenges of the power supply are more stringent on the accuracy of the regulated voltage, the quickness of the dynamic response and the effectiveness of the power delivery. Likewise, the portable consumer electronics like smart phones and ultraportable notebooks are experiencing a rapid growth and have the potential to become dominant in the future consumer electronics market. All these fast-pace advances in the industry impose great challenges on power conversion technology, which require the converter to achieve high power efficiency in order to prolong the battery life for mobile devices and high power density to make convenient small profile and light weight products.
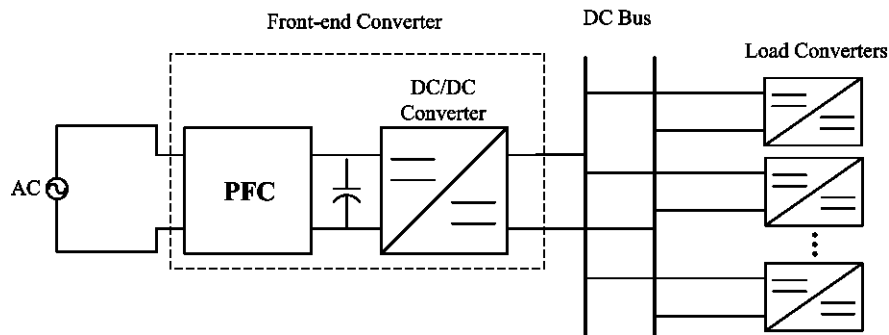
Figure 1.4 The front-end converter structure

The distributed power systems (DPSs) having multiple converter stages located closed to their point of use eliminate the shortcomings of the centralized or modular systems [10-13], and therefore are commonly employed in the modern digital electronic systems such as communication infrastructures, server and data center, and various electronic products. The architecture of DPS is illustrated in Figure 1.4 [12, 14].

5

The two-stage architecture of DPS contains two DC/DC converter parts: one is in the front-end converter which should has high efficiency performance over wide load condition and meet the hold-up time requirement for lost AC line condition, and the other is the point-of-load regulator which should have fast transient response to the load change and reduce the power losses by placing near to the load. Also, since high power density can help build compact and cost-effective digital systems, the demand of high power density is persistent for DPS and the required efficiency is targeted higher and higher, as shown in Figure 1.5 [15-17] and Table 1.1 [18].
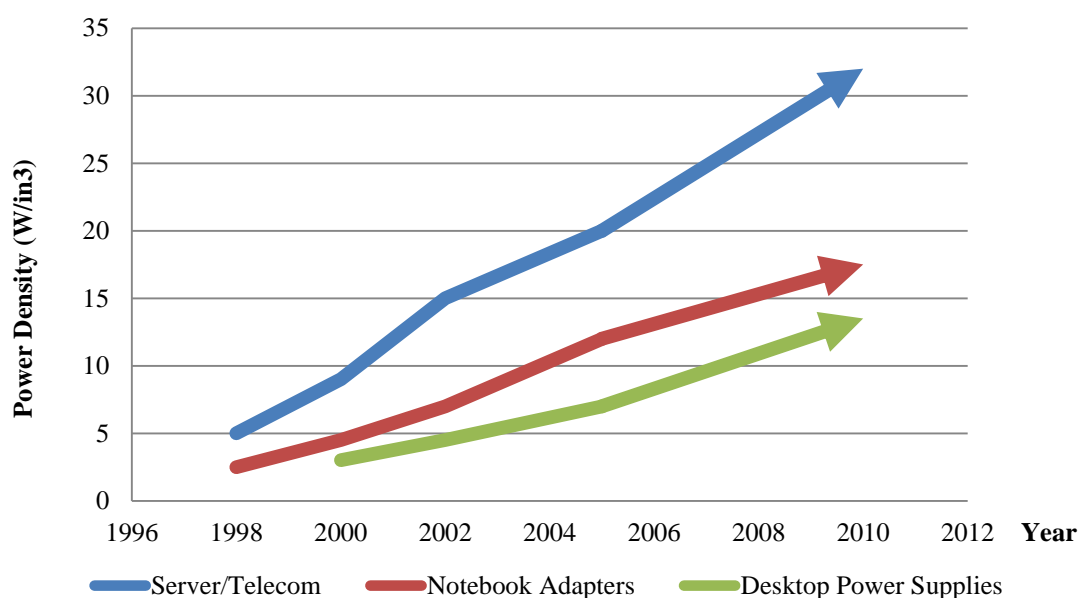
Figure 1.5 The power density trends in power supplies

From the above introduction, it can be seen that to meet the challenges the converter topology should be capable of achieving both high efficiency and power density, yet adaptable for a wide fluctuated operating condition. The resonant converter is a suitable candidate for such requirements and an introduction to the resonant topologies is given in the next section.

Table 1.1 Front-end Converter Development Trend Projections

		2003	2008	2013
Front-end Converters	Cost ($/W)	0.1 – 0.2	0.095 – 0.14	0.08 – 0.125
	Density (W/in^3)	3 – 10	8 – 18	13 - 38
	Efficiency	80 – 85%	88 – 94%	92 – 96%

1.2 Introduction to Resonant Converters

Resonant DC/DC converters are the class of converters which have L-C resonant tank serving as a major part in power conversion process. The fundamental concept of the resonant converter is that the circulating energy in an L-C resonant circuit is manageable by changing the operating frequency, and therefore the converter can condition the input power to the desired output voltage.

In general, a resonant converter consists of a switch network, a resonant tank and a rectifier as seen in Figure 1.6[19, 20]. The switch network which could be half-bridge or full-bridge configuration is used to generate a square voltage excitation to the next resonant tank part. The resonant tank is used to circulate and deliver the energy, who usually exhibits sinusoidal current and voltage waveform during some subintervals of a switching cycle. Unlike the PWM converters, the resonant frequency of the L-C network is typically comparable to the switching frequency, and therefore the current or voltage variation during one cycle has much larger

7

amplitude in contrast to the low-frequency ripple of the PWM converter. The resonant tank is widely employed in DC/AC inverter to filter out the undesired high order harmonic components of the square-wave input to generate pure sinusoidal AC output, of which the system structure is similar to the resonant converter but without the rectifier stage. In an inverter, the resonant tank behaves like a frequency selector, whereas for a converter the purity of the sinusoidal waveform is not a concern as the rectifier and the output low-pass filter will convert the AC to DC. The various resonant behaviors of an L-C tank determine the different characteristics of the resonant converters.
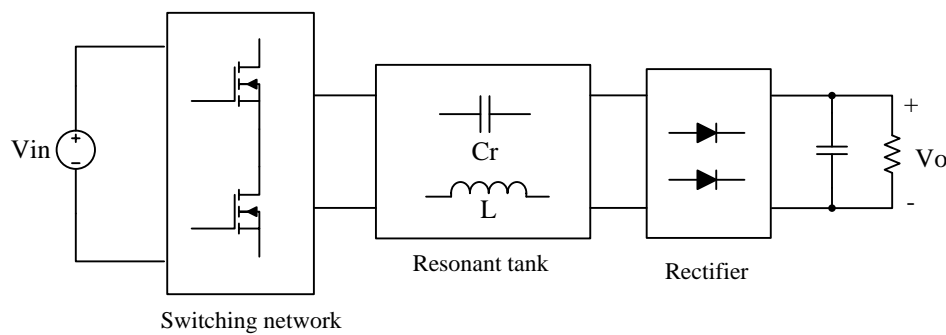
Figure 1.6 The general scheme of a DC-DC resonant converter

The major advantage of the resonant converter is their ability of achieving zero voltage switching (ZVS) or zero current switching (ZCS), which indicates that the voltage or current for the converter switches crosses zero respectively during the switching transitions. Such mechanisms can help the converter get rid of some switching losses, which occur at the instants that the switches turn on or off. Comparing to PWM converters like buck, boost or buck-boost, the resonant converter can operate in a higher switching frequency without the obstacle of increasing the switching losses. Also, the periodic energy commutation via the resonant L-C elements become more frequent with the raise of operating frequency, and the required inductance

or capacitance can be lower and hence the size of these passive components can be reduced so that the power density is improved. Another benefit from the soft-switching nature of the resonant topology is that the "noise" generated by the converter components can be minimized with the smooth switching transitions, and low electromagnetic interference (EMI) can be achieved. [21]

Although the resonant converter is superior in many aspects regarding power efficiency and power density, it is not perfect. Because of its resonance, which requires that the switching frequency is comparable to the resonant frequency, the resonant current and voltage waveforms exhibit large ripples within switching cycle, whereas for PWM converter such variations are relatively small [22-25]. Therefore, the peak values of current or voltage ripples determine the current/voltage stresses over the converter components, and thus need to be considered in selecting the components. The large variation of the resonance also increases the current circulating in the resonant tank, which increases the conduction losses and may offset the advantage of low switching losses. This shortcoming will particularly affect the efficiency in light load condition, which makes it difficult to optimize the converter for a wide load range.

There is a wide variety in the L-C resonant tank topologies. The most commonly known resonant converter topologies are the series resonant converter (SRC), the parallel resonant converter (PRC) and the series-parallel resonant converter (SPRC) [19, 26]. Among other resonant tank configurations with three or more L-C elements, the LLC converter is one of the most representative topologies, which attracts a lot of attentions in recent years and is widely used in numerous applications [27-35].

1.2.1 Two-component Resonant Converters

<u>*Series Resonant Converter*</u>

The SRC circuit is illustrated in Figure 1.7. The resonant tank of SRC consists of a resonant capacitor C_r and a resonant inductor L_r connected in series. The output load resistance is in series with the resonant tank and the impedance of the resonant tank Z_r is a function of the switching frequency, and hence the voltage across the output impedance can be modulated by the switching frequency. At resonant frequency $f_r = 1/(2\pi\sqrt{L_rC_r})$, the resonant impedance $Z_r = 0$ reaches its minimum and the normalized output voltage gain ($M = nV_o/V_{in}$, the transformer turns ratio n is included as if n is equal to 1) becomes unity. It is the max gain of SRC, since Z_r magnitude becomes larger for the switching frequency above or below resonance and the voltage divided to output accordingly will decrease. The DC characteristic plot is shown in Figure 1.8.
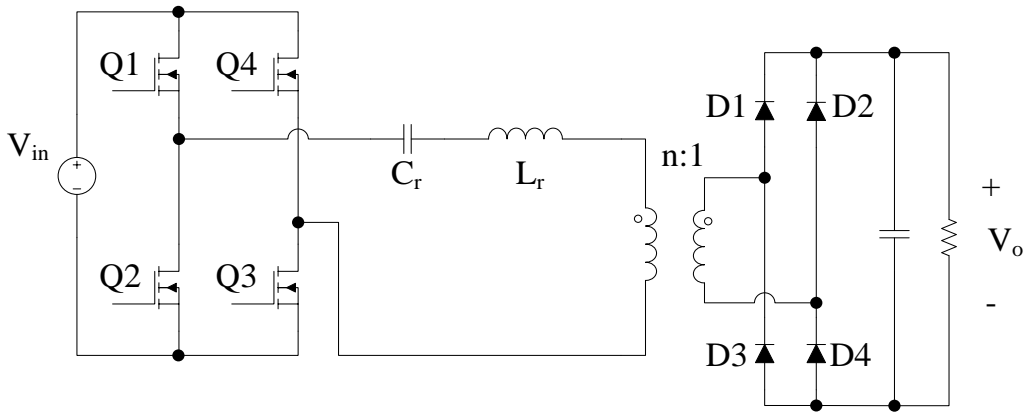
Figure 1.7 The full-bridge series resonant converter (SRC)

For the frequency region above the resonance, the total input impedance will appear inductive, which makes the input current lag the input voltage, and thus ZVS condition is

attainable. ZVS is preferable for converters that use MOSFETs and diodes, since it minimizes the switching losses and the EMI effect. On the other hand, below the resonant frequency is the capacitive impedance region, where ZCS can be achieved. ZCS condition is more favorable for reducing the switching losses for IGBT devices, but cannot reduce the switching loss in MOSFET converters. Also, the resonant behavior in the ZCS region of SRC is more complicated than in ZVS due to the sub-harmonic effect. The resonant tank responds to the signal with the resonant frequency component more strongly than other frequency, and it is possible that some high order harmonic of a low switching frequency input coincides with the resonance. In this case, the gain and frequency relationship is no longer monotonic for low switching frequency and therefore these operation regions should be generally avoided.
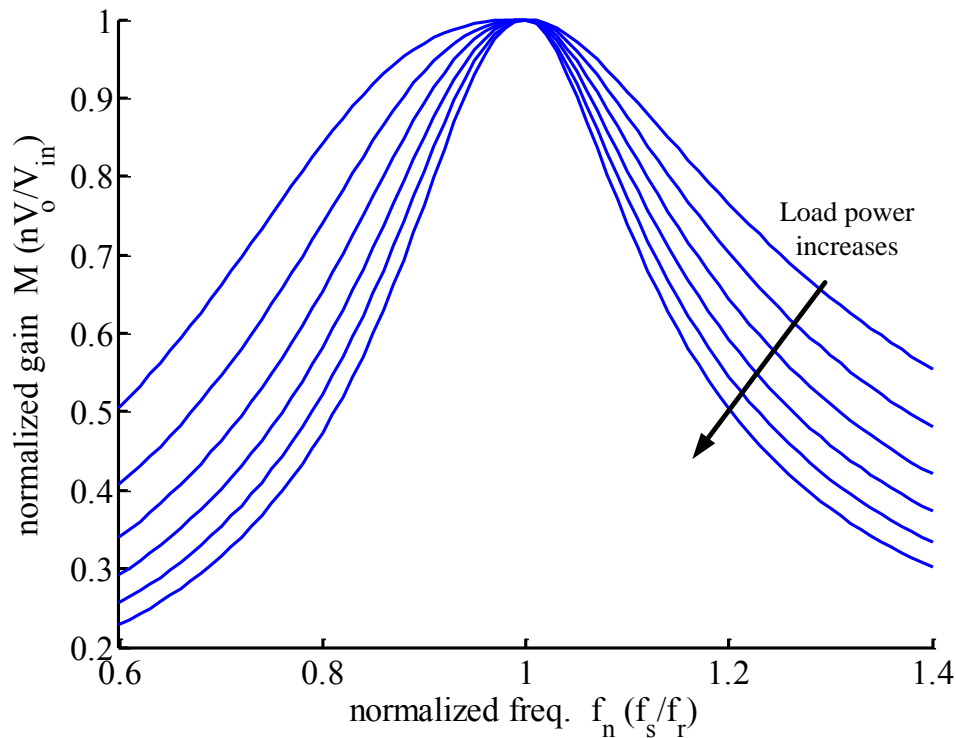
Figure 1.8 The DC characteristics of SRC

It can be observed from the DC characteristic plot (Figure 1.8) that the gain curves are less steep for lighter load condition. In other words, in order to regulate an increased input voltage, the required frequency variation range will be wider for light load comparing to heavy load. In theory, the gain curve becomes flat for zero load condition, which makes SRC incapable of zero load regulation. Another problem for the high frequency operation (above the resonance) is that the turn-off switching loss is increased. Therefore, SRC is not suitable for wide input and load applications.

Parallel Resonant Converter

The parallel resonant converter (PRC) topology is shown in Figure 1.9. Its resonant tank also has two resonant components as SRC, but the capacitor C_r is in parallel with the output rectifier. Another difference is that the output stage is an L-C filter rather than a capacitor filter, which is an inductively coupled output and equivalent to a current source.
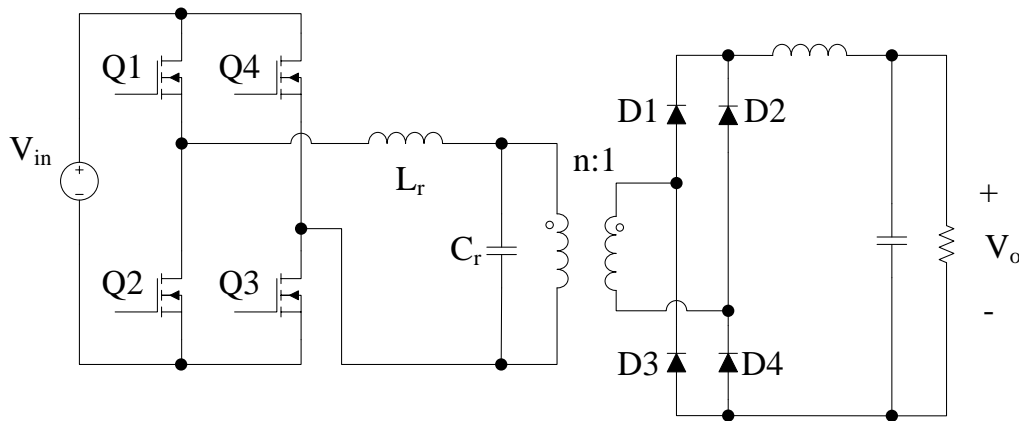
Figure 1.9 The full-bridge parallel resonant converter (PRC)

The peak gain of PRC is affected by the load resistance, whereas for SRC the peak gain at resonance is unity and load-independent. The peak gains occur at a frequency below the resonant frequency, and the peak frequency will be lower for a heavier load condition. The peak value can be larger or smaller than 1, which allows the converter to work in a wider gain range if properly designed. The DC gain plot is shown in Figure 1.10.
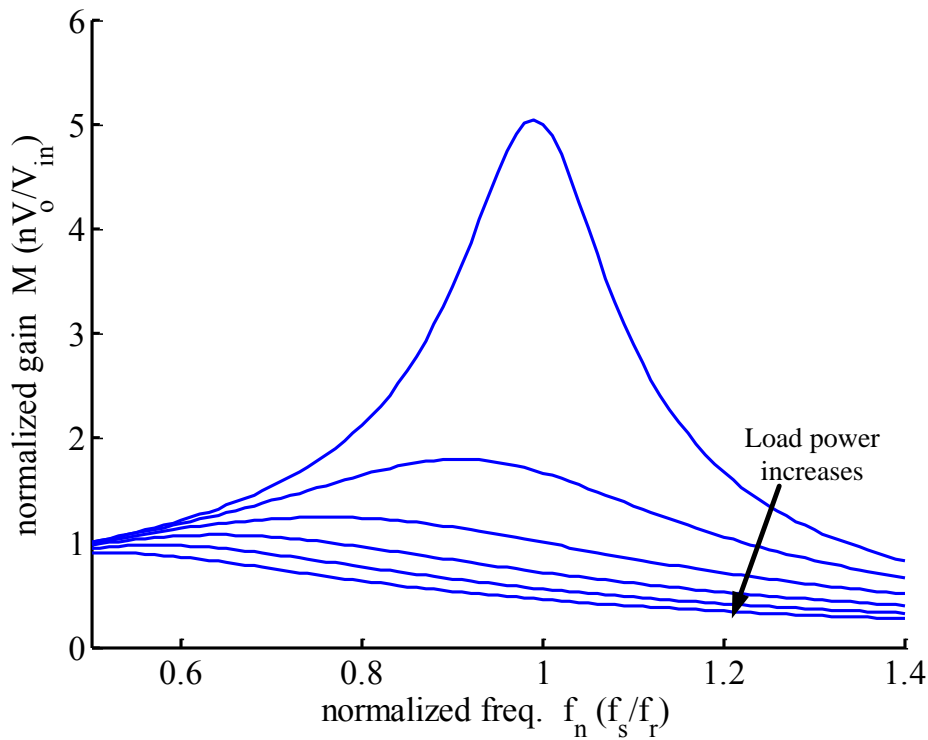
Figure 1.10 The DC characteristics of PRC

The same analysis can be applied to PRC that in order to achieve ZVS the converter should be limited in the above peak gain frequency region. However, the peak frequency is variable depending on the load condition and the tank parameters: the peak point shifts to lower frequency and smaller gain value as the load increases. Another notable feature of the DC gain is that the curve slope is steeper for lighter load condition in contrary to SRC. Provided the same

input and load range, the required frequency variation to regulate the voltage is narrower for PRC than for SRC. The drawback of PRC is the same circulating current problem causing high conduction loss and poor efficiency for light load condition, since the input impedance is inductive for ZVS condition, which is dominated by the inductive part and less affected by the load resistance resulted in a relatively large resonant current even for large load resistance.

1.2.2 Three-component Resonant Converters

LCC Resonant Converter

The SPRC, also known as the LCC resonant converter, is a combination of SRC and PRC as seen in Figure 1.11[36-38]. The resonant tank has three resonant elements: L_r and C_r in series, C_p in parallel with the rectifier input. Consequently, the converter has two resonant frequencies: $f_0 = 1/(2\pi\sqrt{L_r C_r})$ is the short circuit resonant frequency, and $f_\infty = 1/(2\pi\sqrt{L_r C_r||C_p})$ is the open circuit resonant frequency, where $C_r||C_p = C_r C_p/(C_r + C_p)$.
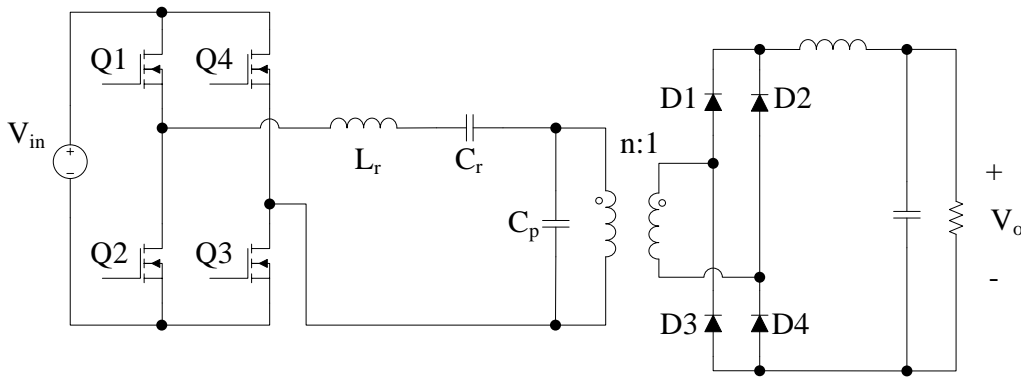
Figure 1.11 The full-bridge LCC resonant converter

14

The DC gain of the SPRC is illustrated in Figure 1.12 (where $f_r = f_\infty$). It can be seen that at f_0 it is the load-independent operating point similar to the SRC where all the gain curves cross the unity point. However, affected by the presence of C_p the gain may reach its peak at a higher frequency above f_0. As aforementioned, in order to operate in the preferable ZVS region, the converter with MOSFET switches should be working on the right slope of a gain curve. Therefore, the LCC cannot operate at the open circuit resonant frequency, which is the highest efficacious point for the series part of the resonant tank impedance is at its minimum magnitude with the inductance and capacitance canceled each other.
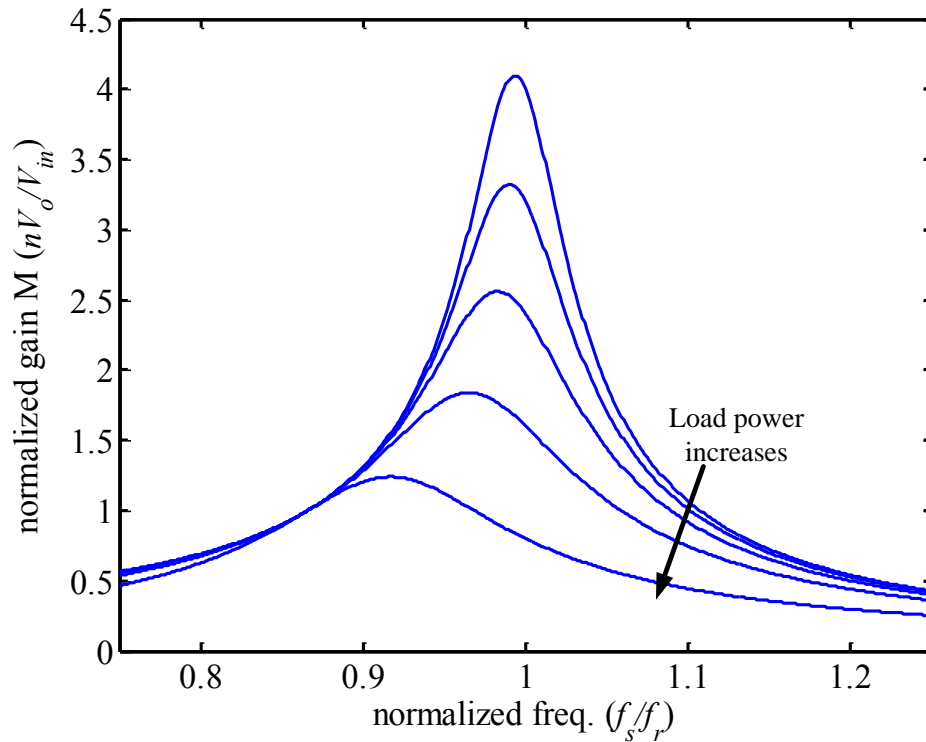
Figure 1.12 The DC characteristics of LCC

The LCC possesses the advantages of PRC that it is capable of handling zero load condition and the gain-frequency curves have steep slope for light load condition. In the

15

meantime, the resonant current is not as large as PRC and thus the circulating energy is limited, which is one of the merits of SRC.

LLC Resonant Converter

The LLC resonant converter is also a three-resonant-component converter as shown in Figure 1.13. Unlike the LCC, the LLC resonant tank has an inductor L_m in parallel to the transformer primary side (or rectifier input) instead of a capacitor. The parallel inductor is denoted as L_m for the reason that it is usually implemented by the magnetizing inductor of the transformer. Although the magnetizing inductor exists for every transformer, which makes SRC look the same as LLC, L_m in SRC is much larger than the resonant inductor L_r and will not participate in the resonance, while in the LLC L_m has comparable inductance with L_r and can no longer be ignored in the resonance. Since the magnetizing inductor is embodied in the transformer and the resonant inductor can be implemented by the leakage inductance of the transformer as well, the SRC circuit structure can be converted to the LLC topology at no extra costs [39-41].
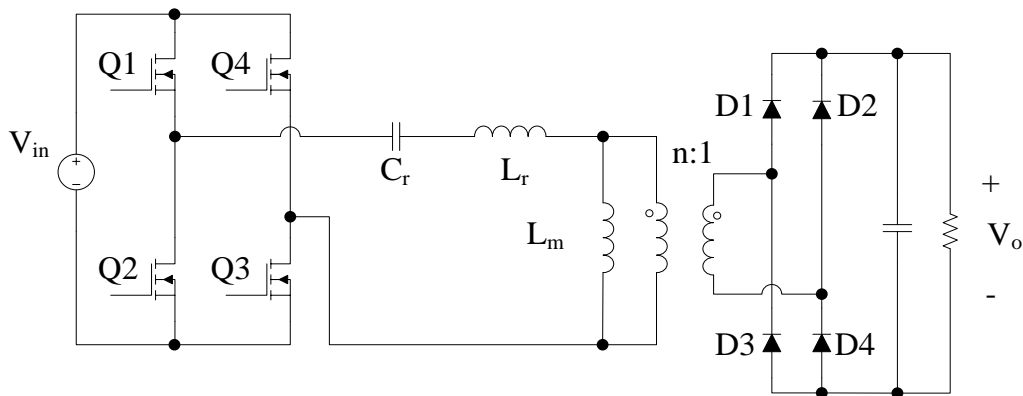
Figure 1.13 The full-bridge LLC resonant DC-DC converter

The LLC converter has likewise two resonant frequencies: $f_0 = 1/(2\pi\sqrt{L_r C_r})$ is the short circuit resonant frequency, and $f_\infty = 1/(2\pi\sqrt{(L_r + L_m)C_r})$ is the open circuit resonant frequency. But f_0 is larger than f_∞, which indicates that the load-independent unity gain point occurs at a higher frequency than the peak gain point based on the previous LCC analysis as shown in Figure 1.14 (where $f_r = f_0$). This feature of the LLC grants the highest efficiency operation point reachable within ZVS region to the converter, which is given up by the LCC in consideration of ensuring ZVS. Besides, the LLC combines the advantages of SRC and PRC: the range of gain is wide as the gain can be above or below 1; the span of operation frequency is contracted as different gain curves for different load condition converge to the unity gain point at f_0.
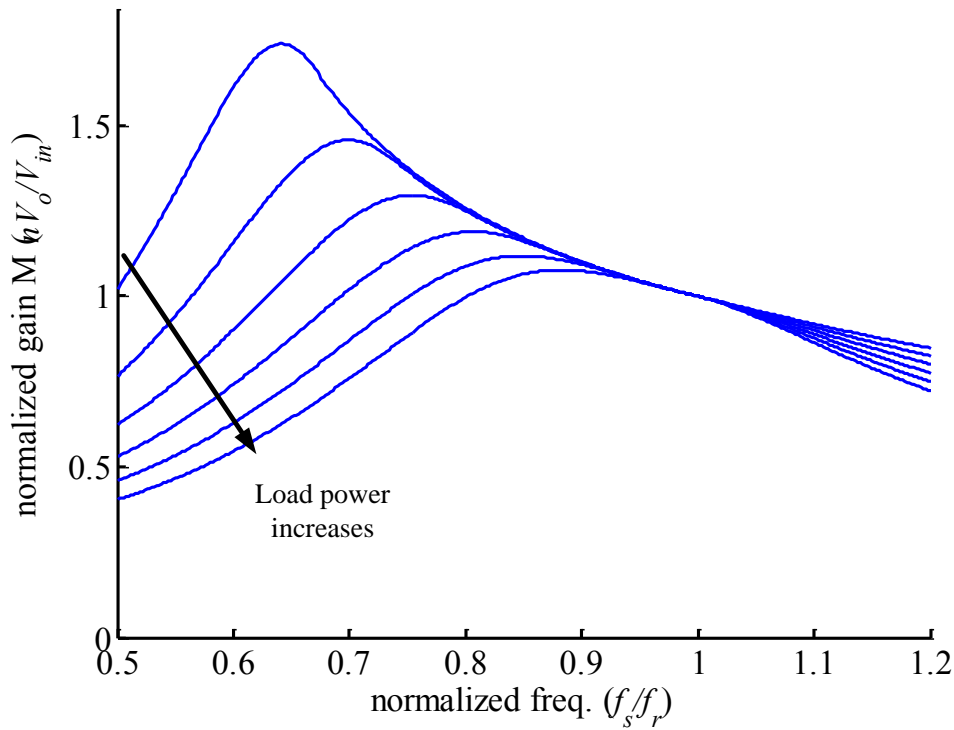
Figure 1.14 The DC characteristics of LLC

1.3 Objectives and Outline

The primary objective of this dissertation is to give a thorough and systematic analysis of the operation of the resonant converter, particularly the LLC resonant converter, whose topology has the potential to achieve high power density and high power efficiency for wide input range applications. The dissertation is divided into five chapters, which are organized as follows:

The first chapter gives the background introduction of the DC-DC conversion techniques in the micro-inverter architecture for solar energy generation and in the front-end converter of the distributed power system. For both application areas, the technology development calls for high efficiency performance and low profile size of the converter stage. To meet these challenges, the resonant converter topologies are the suitable candidates for their natural soft switching characteristic. By achieving soft switching, the switching losses can be greatly reduced to benefit the power efficiency, and the operating frequency can be pushed higher in order to improve the power density. Another advantage of using the resonant converter topology rather than conventional phase-shift PWM converter is that for wide input or load variation conditions it is a strenuous task for the PWM converters to maintain the same level competence for all operation points, whereas the challenge for the resonant converter is not as impossible as for PWM converters. Among the resonant topologies, the LLC draws a lot of attentions for its favorable property of achieving zero voltage switching while covering wide input and load range.

In Chapter Two, the operation and DC characteristics of the LLC converter are investigated. Due to the complex operation modes of the LLC, a lot of efforts and various analysis methods have been made to explore the unique characteristics of the converter.

The prior analysis methods are summarized into three categories: the frequency domain method, the state-plane method and the time-domain method. The frequency domain method is about developing the AC equivalent circuit and deriving the DC characteristics by using sinusoidal waveform assumption, of which the representative and widely used method is called Fundamental Harmonic Analysis (FHA). The FHA offers a simple and straightforward way to examine the voltage conversion gain, but the result is not satisfactory for the poor accuracy in the operating region deviated from the resonant frequency. Besides, the FHA has no insight about the varied operation modes of the LLC. The state-plane method uses the state space diagram to study the relation of the resonant voltages and currents, and the gain and load information can be derived from the diagram by trigonometry. The state-plane approach can deliver the precise operation waveforms of the converter but requiring the prior knowledge of the operation modes, and is cumbersome to use in practice comparing with the FHA. The time domain method focuses on solving the operating waveforms of the resonant converter and hence the gain. Numerous studies on the LLC are based on time domain analysis. As some concentrates on one or several interested and favorable operation modes, the study on the modes for wide range of input, load and frequency condition is incomplete.

A generalized and methodical analysis of the LLC operation modes is carried out in this chapter, in which six major modes are defined and investigated. The resonant behavior and the DC characteristics of each mode are discussed as well. It is found that the continuous conduction modes have explicit solution for the gain, whereas the discontinuous conduction modes need the help of numerical tools to find the solution. The mode boundaries and distribution are presented in order to provide a comprehensive overview of the effect of operating condition onto the operation mode. To verify the analysis, an experimental prototype was built and the multiple resonant mode

waveforms were observed as stated by the analysis. The gain-frequency curves for different load level obtained from the experiments are in well agreement with the result predicted by the mode model, and have relatively larger deviation with the result derived from the FHA.

The voltage gain prediction result generated by the analysis method presented in Chapter Two, despite its high accuracy, is time consuming to compute. Chapter Three explores the approximation approaches to simplify the analysis method and facilitate its use in aiding the LLC rapid design or evaluation process. A literature review of some prior approximation methods is presented. Then, the approximation based on the operation mode model is proposed. Rather than making estimation for the entire gain curve, it focuses on getting the peak gain point information. The peak gain is considered an essential parameter in design as it marks the max conversion gain that the LLC is capable of in conditioning for a certain load power level. In addition, the peak gain point is the boundary point between ZVS and ZCS region (ZVS region is where the switching frequency is above the peak point, and ZCS is the region below the peak). Furthermore, the polarity of the gain curve slope should remain unchanged to ensure the control loop stability, and it imposes the converter to operate only one side, the high frequency side, of the peak gain point. All in all, the frequency of the peak gain is lower limit of the permissible switching frequency of the LLC. By taking advantage of the curve fitting technique and the Newton-Raphson method, a peak gain approximation approach is developed, which provide a straight way to calculate the peak gain point without any nonlinear equation solving involved. The approximate results is compared with the circuit simulation result and proved to have adequate accuracy. Not only the peak value for a given resonant tank configuration and switching frequency is given by the approximation; the load condition at the peak gain can also be derived from it. Together, the estimated results providing the gain-frequency-load relation can be

employed conveniently to expedite the converter design process. Besides the peak gain, another important and useful knowledge from the operation mode distribution is the scope of PO mode. As this mode possesses the merit of zero rectifier reverse recovery current along with other favorable characteristics of the LLC, the converter operation will be benefitted from the restriction of only operating in PO mode. Unfortunately, though the resonant frequency serves as the boundary between PO and NP/NOP mode, the other side border with PON/PN mode is not easy to obtain as tackling transcendental equation involved. Hence, the PO and PON mode boundary estimation method is proposed to ease this process. A linear curve fitting method is developed to attain the PO/PON boundary, and an error analysis is provided to study the variation of the boundary for different LLC parameters.

Chapter Four is dedicated to the design optimization of the LLC resonant converter. Some existing design methods and optimization processes of the converter are discussed. The basic objective of the converter design is to provide satisfactory performance suiting the application specifications, which should not only cover the normal operation requirements but also be capable of handling extreme cases. Within the scope of guaranteed specified operation, the optimization target is to increase the power efficiency, power density or reliability, or reduce costs. We divide the LLC design into three cases: the first is for narrow input voltage variation, the second is for wide input voltage variation, and the third is for no reverse recovery performance. For the first scenario, the converter has a stable operation condition and it should be set to the resonant point of the LLC which is the maximum efficiency point, and the optimization consideration majorly focuses on this point. For the second scenario, the worst case of the converter operation should be considered, which is at the minimum input voltage and full load condition, and the LLC needs to provide sufficient large gain to regulate this worst condition. The peak gain placement design

21

method is developed for this scenario, which set the worst condition at the peak gain point of the LLC in order to minimize the resonant tank currents. For the third scenario, it is obvious that the LLC should only operate in PO or OPO mode according to the operation mode analysis. Therefore, in a similar way of the peak gain placement, we use the PO/PON boundary to deal with the worst operating point. To demonstrate the effectiveness of the proposed optimal design method, a LLC converter prototype is built and tested. Besides using the optimal parameters from this method, other L-C tank configuration schemes based on other methods are also tested and compared. The comparison verifies the performance superiority provided by the proposed approach. A general discussion on the LLC optimization is presented, which abstract the issue into mathematical problem that is independent of specific application cases.

Chapter Five presents a generalized analysis method of resonant converters. A resonant converter is characterized by its resonant tank. The equivalent circuit of a resonant tank may vary through different resonant conditions. Inspired by the LLC analysis, the resonant tank behavior can be classified into three resonant stages, stage P, N and O. The resonant stage equivalent circuits can be constructed using the normalized parameters to simplify the analysis. For a pure L-C tank circuit, the resonant variables are designated as the capacitor voltages and inductor currents, which is enough to represent all the operating waveforms of a converter. These variable functions are a combination of sinusoid and linear terms. An iterative process is developed to find the expressions of each resonant variable. These variables are restrained by the symmetry and continuity conditions and the stage constraints, which can be used as boundary conditions to build simultaneous equations of resonant variables. Hence, the unknowns can be solved using numerical calculation software and the resonant tank's current/voltage waveforms and the DC characteristics are obtained. Several analysis examples are given to demonstrate the procedure.

The LLC resonant DC-DC converter is explored in the aspects of operation analysis, model approximation and design optimization, and the analysis approach is generalize to other resonant topologies. However there are other areas to be covered for resonant converters, the future works and research interests are given in the end.

CHAPTER TWO: OPERATION ANALYSIS OF LLC RESONANT CONVERTER

2.1 Introduction

The LLC resonant converter exhibits attractive potentials in switching-mode power supply applications demanding high power density and high efficiency as we discussed in the first chapter. The LLC converter have been studied for a long time since the topology was first proposed and studied in 1994 by A.K.S. Bhat[42], and various methods and techniques have been used in the converter operation analysis and modeling. However, due to the complex interaction between the LLC resonant components, there is no simple and explicit way to analyze its operation and characteristics [43, 44]. The frequency domain analytical method simplifies the topology by making sinusoidal waveform approximations and using AC equivalent circuits at the sacrifice of model accuracy, and furthermore they cannot depict the variation of operation modes by solving transfer functions. Another approach is by employing state-plane analysis, from which the dynamic response of the resonant state variables can be precisely represented on the state-plane trajectory. However, it is sometimes difficult to interpret and found cumbersome in practical use. Other methods focus on the converter's resonant behavior in time domain, which can therefore be referred to as time-domain analysis. In steady state, the circuit periodic operation can be divided into multiple resonant stages, and the circuit equations for each stage can be built and solved. However, these mode equations are nonlinear and may not have explicit solutions, and therefore some studies apply assorted approximations to the operation waveform in order to solve the equations for a certain mode. While these methods may be more accurate than the frequency

domain method, their dependence on a certain mode can limit the usage covering a wide range of operation condition without knowing the mode transition and distribution. Although some discussion on the various modes has been given in [44], there is no prior study on mode boundary and distribution.

In this chapter, an overview of the prior LLC analysis methods are presented; the operation mode are analyzed in detail, and the mode equations are given and solved for each mode to give a precise description of the converter resonant behavior and DC characteristic; the mode distribution under different operating frequency and load conditions is discussed.

2.2 Review of Prior LLC Analysis Methods

The prior LLC analysis methods can be generally divided into three categories: the frequency domain method, the state-plane method and the time domain method.

2.2.1 Frequency Domain Method

In a resonant converter topology, the input of a resonant tank is a square-wave voltage excitation signal generated by the switch network pre-stage. If we ignore the higher harmonics of the square wave voltage and treat it as purely sinusoidal, the resonant tank can be analyzed using its AC equivalent circuit, which greatly reduces the difficulty in analysis. The transfer function of the resonant tank and the output rectifier stage can therefore be derived, and its frequency domain response can be studied to obtain the DC characteristics of the converter. This frequency domain method is called the fundamental harmonic analysis (FHA), which is proposed by R. L. Steigerwald [45] in 1988.
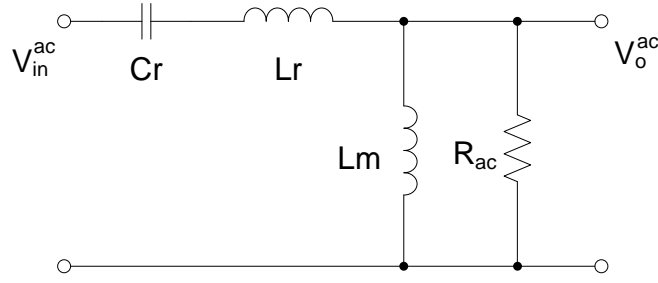
Figure 2.1 AC equivalent circuit for the LLC resonant converter

For the LLC resonant converter, the AC equivalent circuit is shown in Figure 2.1. The square wave voltage input magnitude for full bridge switch network is equal to the input voltage V_{in}, while for half bridge it is equal to half V_{in}. To simplify the discussion, the analysis here is for full bridge configuration and the result can be converted to half bridge case by simply substituting V_{in} to $\frac{1}{2}V_{in}$. To include the load resistance in the AC circuit, it needs to be converted to equivalent AC impedance to the primary side of the transformer, which is shown in Figure 2.2.
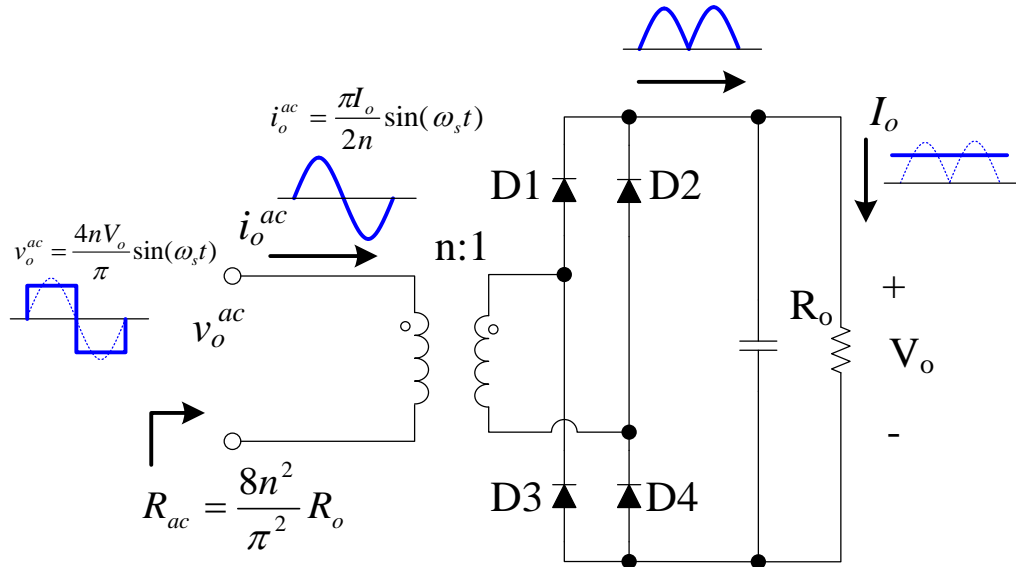
Figure 2.2 Derivation of equivalent AC load impedance R_{ac}

26

Assuming the output voltage is stable, the input voltage drawn by the rectifier is also in square waveform, of which the fundamental component is $\frac{4}{\pi}nV_o$; assuming the input current of the rectifier is a sine signal, the average of the rectified current is the output current, and therefore the amplitude of the rectifier input current is $\frac{2}{\pi n}I_o$. So, the AC equivalent impedance of the transformer is

$$R_{ac} = \frac{8n^2}{\pi^2} R_o \tag{2.1}$$

From the equivalent AC circuit, the DC voltage gain can be derived using AC analysis method as the following:

$$M = \frac{nV_o}{V_{in}} = \frac{\frac{4}{\pi}nV_o \sin(\omega_s t)}{\frac{4}{\pi}V_{in} \sin(\omega_s t)} = \left| \frac{f_n^2(m-1)}{(mf_n^2-1) + jQ(m-1)(f_n^2-1)f_n} \right| \tag{2.2}$$

where

$$f_n = \frac{f_s}{f_r}, \qquad f_r = \frac{1}{2\pi\sqrt{L_r C_r}}, \qquad m = \frac{L_r + L_m}{L_r}, \qquad Q = \frac{\sqrt{\frac{L_r}{C_r}}}{R_{ac}}$$

It can be seen from the expression (2.2) that the gain is affected by the switching frequency f_s, the quality factor Q and the inductors ratio m and the resonant frequency of L_r and C_r. For a given converter design, the LLC circuit parameter is determined and unchanged, and therefore the gain is the function of operating frequency and load condition. The gain-vs.-frequency curves for different load conditions are plotted in Figure 2.3.
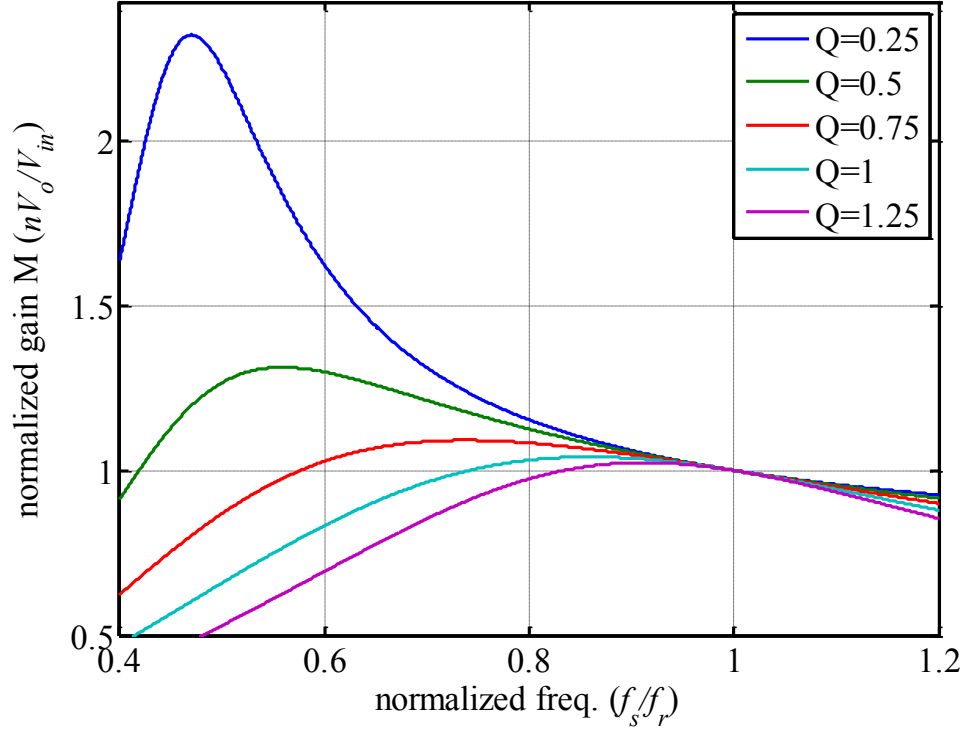
Figure 2.3 The LLC gain curves derived from FHA method (*m=5*)

As illustrated in Figure 2.3, the normalized voltage gain of the LLC converter tends to rise higher than 1 when the switching frequency moves below the L_r-C_r resonant frequency f_r. The gain curve will reach its peak somewhere below f_r, and trend of the peak gain frequency is that it moves towards f_r with the increase of load. In general, the heavier the load grows, the lower the gain becomes accordingly. All these observations holds true for the actual performance of the LLC.

Also, one interesting feature of the gain curves is that they all converge at the unity point when the switching frequency is equal to the resonant frequency; in other words, this unity gain point is load independent and the converter operated at this point does not need to change its switching frequency for any level of output power as long as the input voltage is the same.

However, this statement about the resonant operating point does not stand true for all load condition, the light load condition to be more specified, and more details can be found in Chapter 2.3.1.

The FHA can also be applied to the study of the impact of parasitic components in the LLC resonant converter. In [46-48], such study is carried by including the secondary-side leakage inductance (L_{lks}) and the wiring capacitance of the transformer and the junction capacitance (C_{jc}) of rectifier diodes as shown in Figure 2.4 [46], from which it is found that L_{lks} causes the resonant frequency to shift lower than $1/2\pi/\sqrt{L_r C_r}$ and the corresponding normalized gain to move higher than 1, and C_{jc} leads to a gain rise in high switching frequency region.
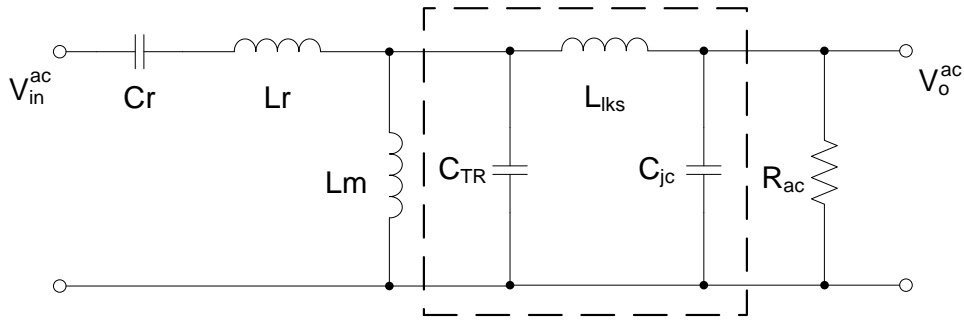
Figure 2.4 AC equivalent circuit of LLC converter including parasitic components

The reason the FHA is imprecise is that the high-order harmonics are omitted during the analysis process. Besides the odd order harmonic components of the square waveform in V_{in} and rectifier input voltage, the currents through the resonant tank and the rectifier is also not sinusoidal. The tank has different resonant states and may work in discontinuous mode, which all bring distortion to the fundamental harmonic assumption.

The FHA can be improved by including high order harmonic components of the voltage and current signals [49]. The steady-state solutions for the resonant converter can be derived as

29

well as the converter gain, by using Fourier-series analysis and superposition principle. The more the number of harmonics is included, the smoother the waveforms become. However, the accuracy improvement of this Fourier-series approach is aimed at the continuous conduction mode, while the harmonic distortion caused by discontinuous rectifier current at some operation mode has not been addressed. In [50], the extended FHA is proposed. While the analysis is for the LCC resonant converter, the concept can be applied to the LLC as well. In this method, the rectifier current in discontinuous mode is studied, and its fundamental component is derived. Then, the equivalent rectifier input impedance for this mode can be obtained accordingly. This modification can help improve the DC gain prediction precision in discontinuous mode. The paper [51] uses describing functions to analysis the circuit. There are two major assumptions in [51]: one is assuming the resonant current to be sinusoidal; the other is to only consider fundamental harmonic component of the tank input voltage (which is a square wave) and the magnetizing inductor voltage v_m (which is also the primary side transformer input voltage) and current i_m. Note that v_m and i_m are described by using piecewise function, and then the Fourier series expansions are performed to express v_m and i_m so that their fundamental component can be obtained. Hence, the equivalent impedance of the transformer input can then be calculated, and the output gain can be derived from the voltage dividend law. Since the piecewise function is used to represent v_m and i_m, the derived fundamental components are more precise in depicting the voltage and current waveforms than FHA, and thus the gain prediction results show higher accuracy. However, the computation complexity increases, especially in solving the phase angle between input voltage and current. The numerical calculation tools are still needed in solving the related nonlinear equations. All these modified methods based on FHA increase the model complexity and lost its virtue of simplicity.

Although the FHA approach has limited accuracy in the DC gain prediction result, it provides an intuitive and straightforward way to understand the characteristic of the LLC. However, FHA or the other similar frequency domain approaches give no much detail about the operation current or voltage behavior of the converter, and thus fails to reveal the multiple resonant modes. Therefore, the frequency domain method is inadequate in converter design practice.

2.2.2 State-Plane Method

The state-plane analysis for the resonant converter is a method that uses state-plane diagram to describe the relation between state variables (usually assigned as the resonant currents and voltages) [52-55]. By dividing the time domain behavior of the resonant converter into different resonant stage, each stage will contribute an arc or line part of the resonant variable trajectory on the state plane. For a steady-state performance, the trajectory is a closed loop on the state plane. After obtaining the state-plane diagram, the resonant variables' behavior can be solved graphically using geometry. The converter gain can also be derived from the state plane. This method has been employed to study the characteristics of various resonant converter topologies [55-59]. In [60, 61], the generalized approach of applying state-plane analysis to resonant converters are proposed.
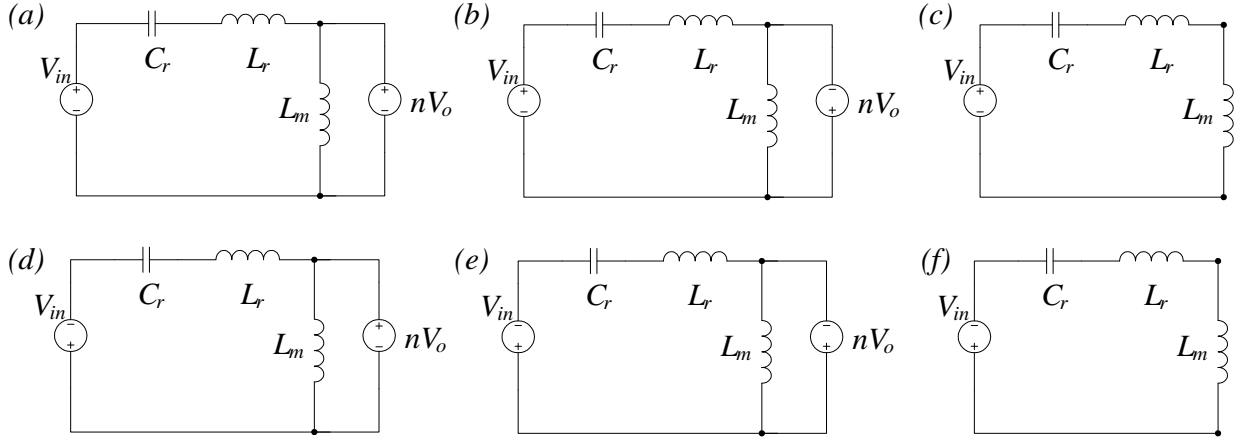
Figure 2.5 The equivalent circuits of the six resonant stages of the LLC converter

Regarding the LLC resonant converter, the resonant current i_r, the capacitor voltage v_C and the magnetizing current i_m are the resonant variables, and therefore the state plane is a three-dimension space. The resonant tank can be divided into six different stages as shown in Figure 2.5, and for each stage the singular point can be obtained, which is the circle center of the piecewise resonant-state trajectory. However, the radius of the partial circle and the conduction angle denoted as the duration time of a resonant stage is not easy to determine, which require the knowledge of the initial condition of the resonant variables. An addition relation between the tank currents and the output current can be utilized to solve the problem as the average output current should be equal to the following expression

$$I_o = \frac{1}{T_s} \int_0^{T_s} |i_r - i_s| dt \qquad (2.3)$$

where both i_r and i_m are piecewise functions of the resonant stages occurred in one switching cycle, and T_s is the switching period.

To start the state-plane analysis, the following resonant variables are selected as the state variables: C_r voltage v_C, L_r current i_r, and the transformer input current $i_o = i_r - i_m$. The

32

voltages are normalized by nV_o, and the currents are normalized by nV_o/Z_r ($Z_r = \sqrt{L_r/C_r}$). Then, the designated state variables can be plotted on the normalized state plane. Also, note that the load condition is represented in normalized form as $p_{on} = P_o Z_r/(nV_o)^2$.
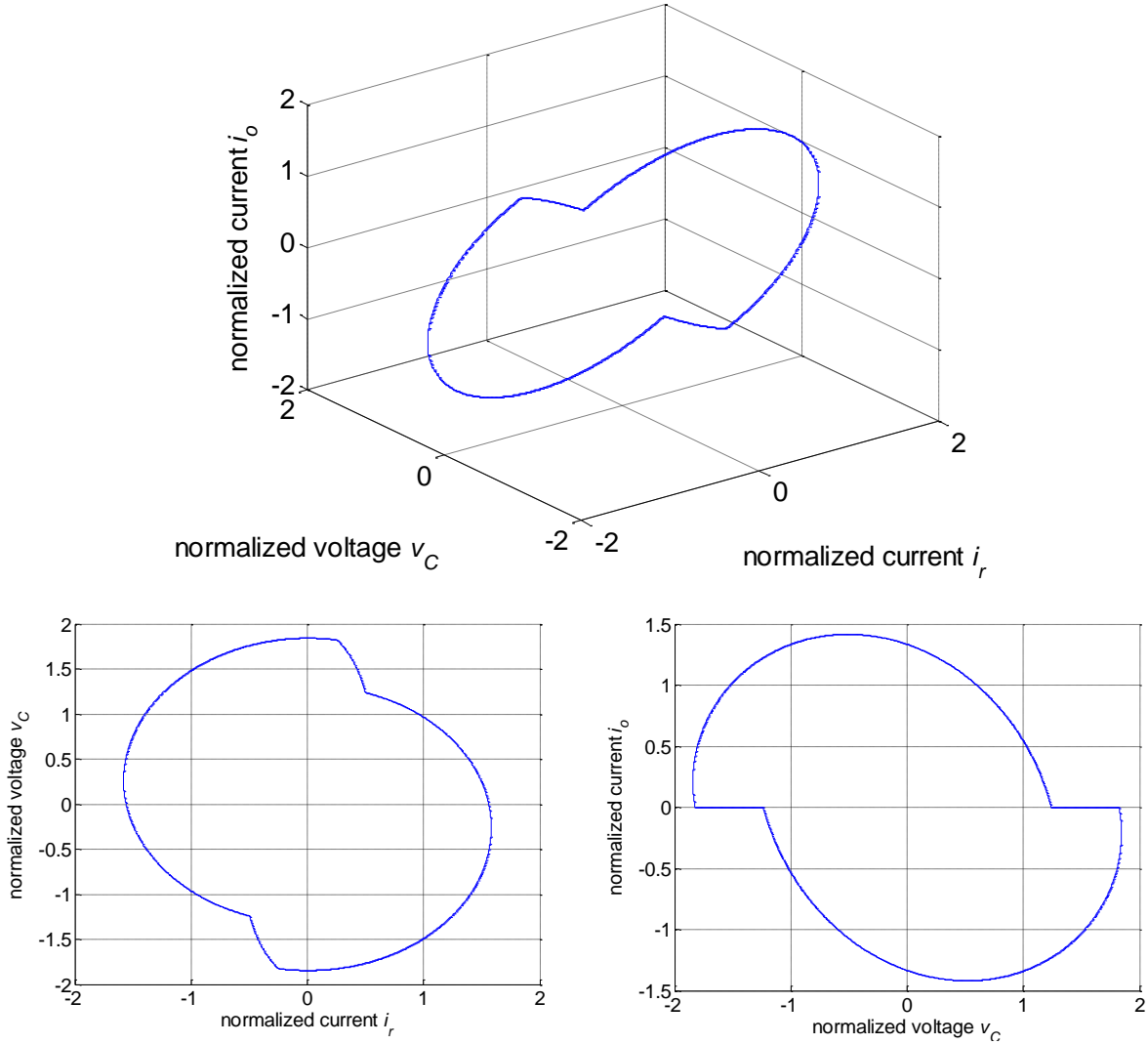
Figure 2.6 The state-plane diagram of the LLC converter in DCM (*m=5, fn=0.7, pon=0.6*)
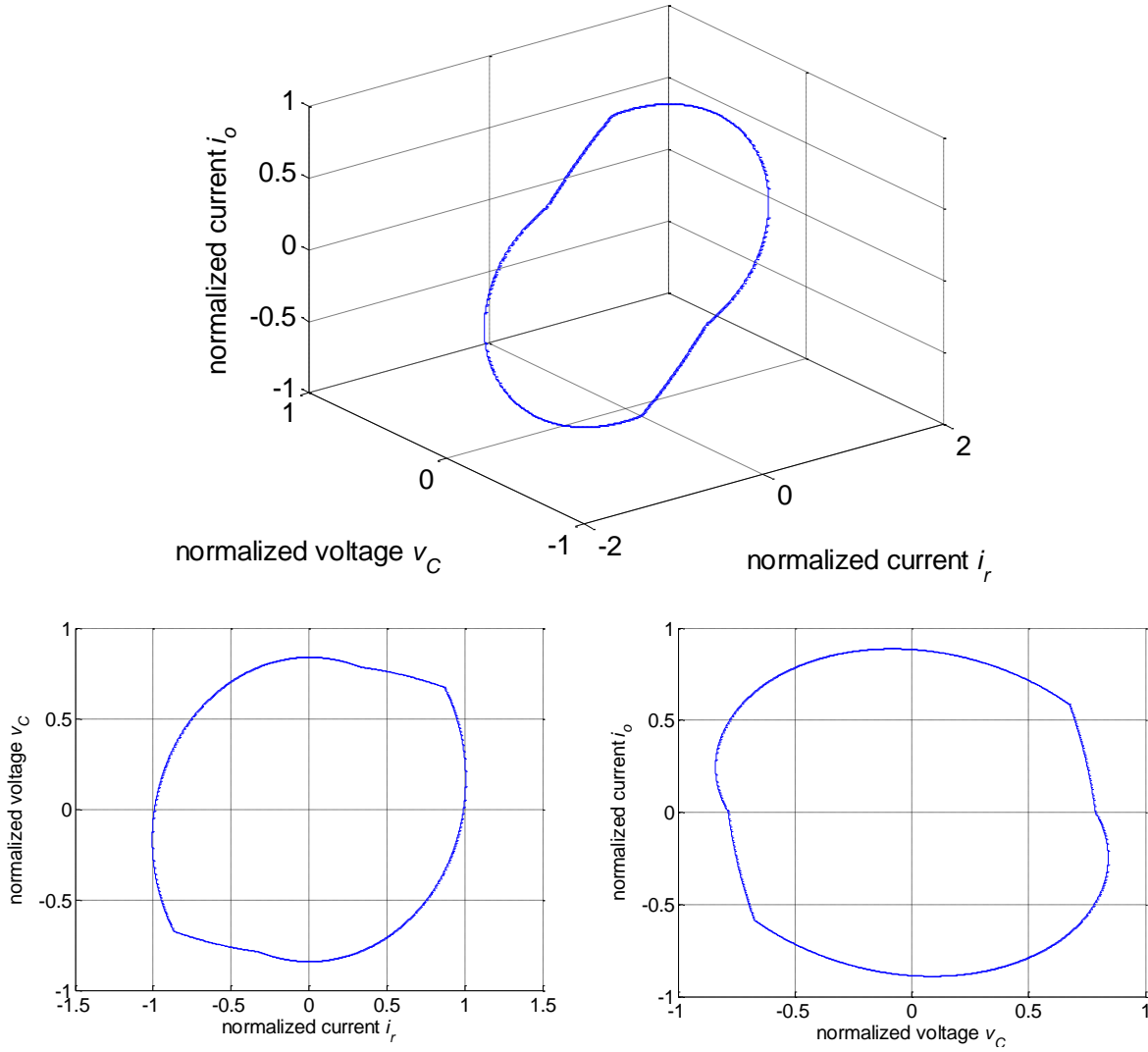
Figure 2.7 The state-plane diagram of the LLC converter in CCM (*m=5, fn=1.2, pon=0.6*)

Figure 2.6 is a typical state-plane diagram of the LLC converter in DCM, in which it can be seen that i_o remains zero on part of the state trajectory, whereas Figure 2.7 shows the state-plane diagram in CCM. The time variance is implicit on the diagram, but the conduction angle is related to the time span of a resonant stage. Not all the six resonant stages necessarily appear on the trajectory, and such difference in the sequence of the stages forms the various operation

modes of the converter. As a result, to carry out a thorough state-plane analysis the operation modes should be known beforehand, for which the detail analysis can be found in Chapter 2.3.

In the state-plane analysis, the information of the gain is contained in the singular point coordinate of the state-plane trajectory, and is connected with the output current through equation (2.3) and the switching frequency as the closed-loop trajectory represents one switching cycle. Hence, the gain can be expressed in terms of the output load and the switching frequency, which is not as obvious and intuitive as the FHA method. But unlike FHA's approximate result, the state-plane method provides precise solution of the steady-state characteristics, and the exact resonant voltage and current waveform can be obtained. Furthermore, the peak values of the resonant variable can be read directly on the state plane, which provides a convenient way to study the voltage or current stress on the converter components. The drawback of the state-plane analysis is about its high complexity lay in clarifying the multiple resonant stages and extracting the DC characteristic information. The calculation of the radii of the state trajectory require the help of numerical tools to get the stage initial condition, and this iterative process is time consuming and impractical for a quick evaluation of the circuit. With these obstacles, the state-plane approach turns out not as popular as the frequency domain method in the LLC resonant converter design.

2.2.3 Time Domain Method

In the state-plane method, the LLC has different state trajectory for different operation modes, and the modes are formed by the different subinterval resonant stages. The time domain method is a collective name for those approaches that is about analyzing the periodic resonant current and voltage waveforms and sorting these operation modes.

35

In [44], the analysis is performed, and in total six resonant intervals and eleven resonant modes are presented. The classification of the six subintervals is literally the same as the six resonant stages presented in the state-plane method as shown in Figure 2.5. The appearance pattern of these intervals is studied and given in [44]. The LLC operation mode is divided in a manner based on the converter gain, which organizes the operation into buck and boost types possessing different sets of modes according to the switching frequency and the continuous or discontinuous conduction condition. However, it perplexes the mode analysis to some extent, as some mode exists in both buck and boost or can span below or above resonance, and some mode only occurs in a boundary condition. Also the boundaries between each mode are unclear, and the converter gain relation with the switching frequency or the load power is absent. In the next section, a systematic study on the operation modes is presented, and six major operation modes, instead of eleven, are provided.

Although the LLC converter has multiple operation modes, not all modes are desirable in practical applications. Therefore, some time-domain analysis is only aimed at several preferable modes [62-64]. In [62, 63], only the DCM that has a monotonic increased gain with a decreased switching frequency in the below resonant frequency region, named and defined as PO mode in Chapter 2.3.2, is analyzed. The mode equations for the resonant currents and voltages are developed, and the necessary boundary conditions to solve it are presented. Due to the complexity of the equations, the paper uses numeral calculation tool to solve the mode parameters and no symbolic answer is given. Since exact waveforms can be obtained, it is employed to estimate the power losses and therefore can help the LLC design.

2.3 Operation Modes of the LLC Converter

The difficulty in the LLC converter analysis is described in previous sections, which makes the operation analysis impossible to find universal accurate equations or expressions applied to all operation condition. Instead, the operation is divided into different operation modes and the individual characteristics of each mode can be solved and studied. In this section, a generalized analysis of the LLC converter's multiple resonant operation modes is investigated.

The operation in one switching cycle can be divided into different resonant stages, and for different operation mode the composition of these stages are different, which can therefore be used to distinct and mark the modes. For each operation mode, the circuit equations are developed, from which the exact current and voltage waveforms are solved.

To generalize the analysis, the circuit variables including current, voltage, frequency, power, are normalized by the following base coefficients:

- Base frequency: $f_{base} = 1/(2\pi\sqrt{L_r C_r})$

- Base voltage: $V_{base} = nV_o$

- Base current: $I_{base} = nV_o/Z_r$

- Base power: $P_{base} = (nV_o)^2/Z_r$

where $Z_r = \sqrt{L_r/C_r}$. The normalized variables are the variables divided by the corresponding base coefficient and will be denoted with a subscript n.

Although the resonant frequency by common definition is the frequency at which the resonant tank gives the peak output response, in the following discussion the resonant frequency f_r

is referred as the resonant frequency of L_r and C_r, which is the base frequency f_{base}, unless stated otherwise.

2.3.1 Resonant Stages

The resonant tank of the LLC has a dual resonant mechanism that the resonance can be formed by L_r and C_r along or with L_m joining them. There are six possible resonant stages, which can be characterized by the switching state and the L_m voltage condition. Since the duty cycle of the LLC is fixed to 50%, which uses variable frequency control to regulate the voltage, the resonant tank waveforms in one half switching cycle are symmetrical in reverse direction to the other half. To simplify the discussion, the analysis will focus on one half switching cycle, where the input voltage of the resonant tank is positive that in full bridge configuration it is when Q1, Q3 turn on and Q2, Q4 turn off, and in half bridge configuration it is when upper switch is on. In this case, there are three resonant stages only depending on the L_m voltage condition:

1. Positive clamped stage $v_m = nV_O$ (denoted as stage P)

2. Negative clamped stage $v_m = -nV_O$ (denoted as stage N)

3. Cut-off stage $v_m = nV_O$ (denoted as stage O)

The equivalent circuits for the three stages are shown in Figure 2.8.
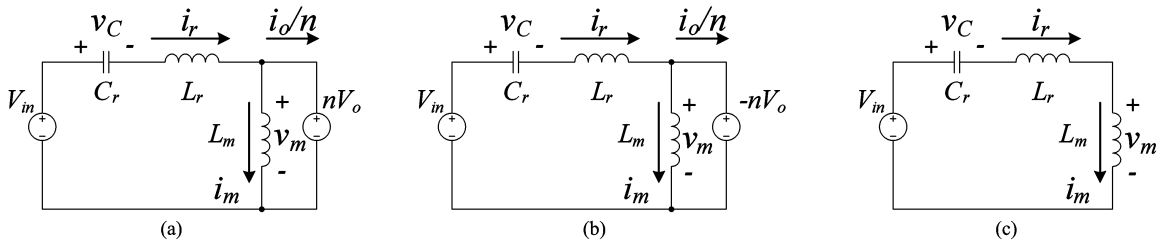
Figure 2.8 The LLC resonant tank equivalent circuits in the half switching cycle: (a) stage P, (b) stage N, (c) stage O

For stage P, the magnetizing inductor L_m is clamped to nV_O, and hence i_m increases linearly. L_r and C_r are in resonance and i_r waveform is sinusoidal. The secondary-side rectifiers conduct through D1 and D4 and the output current i_o should be always positive in this stage. We choose the inductor currents i_r and i_m and the capacitor voltage v_C as the resonant state variables, and they can be described by the following:

$$
\begin{aligned}
i_{rPn}(\theta) &= I_{rPn}\sin(\theta + \theta_{P0}) \\
i_{mPn}(\theta) &= I_{mPn} + \theta/(m-1) \\
v_{CPn}(\theta) &= -I_{rPn}\cos(\theta + \theta_{P0}) - 1 + 1/M
\end{aligned}
\tag{2.3}
$$

where

$$
\theta = 2\pi f_r t, m = (L_m + L_r)/L_r, M = nV_o/V_{in}
$$

and I_{rPn} is the normalized magnitude of the sinusoidal L_r current in stage P, θ_{P0} is the initial phase angle of i_{rPn}, and I_{mPn} is the initial L_m current when stage P starts. As the output current is restrained in one direction, it requires that $i_{rPn} > i_{mPn}$ in stage P.

Stage N operates similarly to stage P as L_m is not in the resonance of Lr and Cr, but v_m is clamped to $-nV_O$ instead of positive nV_O. The magnetizing current i_m is decreasing linearly, and from the secondary side D1, D4 are off and D2, D3 are conducting. The resonant current and voltage can be expressed as

$$
\begin{aligned}
i_{rNn}(\theta) &= I_{rNn}\sin(\theta + \theta_{N0}) \\
i_{mNn}(\theta) &= I_{mNn} - \theta/(m-1) \\
v_{CNn}(\theta) &= -I_{rNn}\cos(\theta + \theta_{N0}) + 1 + 1/M
\end{aligned}
\tag{2.4}
$$

where I_{rNn} and I_{mNn} are the normalized current parameters, θ_{N0} is the initial phase angle of i_{rNn}. The current constraint of this stage is $i_{rNn} < i_{mNn}$.

In stage O, L_m joins the resonance with L_r and C_r, whereas the secondary side is cut off from the prime side; the rectifier diodes are turned off, and thus no current flows to the output. The resonant currents i_r and i_m are equal and in pure sinusoidal waveform, but the resonant frequency decreases to $f_r / \sqrt{m}$. The expressions of the resonant variables are given by

$$
\begin{aligned}
i_{rOn}(\theta) &= i_{mOn}(\theta) = I_{rOn} \sin(\theta / \sqrt{m} + \theta_{O0}) \\
v_{COn}(\theta) &= -\sqrt{m} I_{rOn} \cos(\theta / \sqrt{m} + \theta_{O0}) + 1/M \\
v_{mOn}(\theta) &= \frac{m-1}{\sqrt{m}} I_{rOn} \cos(\theta / \sqrt{m} + \theta_{O0})
\end{aligned}
\tag{2.5}
$$

where I_{rOn} is the normalized current parameter and θ_{O0} is the initial phase angle. The constrain condition of stage O is that $|v_m|$ should be less than nV_O to avoid letting the rectifier conduct.

2.3.2 Operation Modes

The LLC converter's operation modes are formed by the different combinations of the three resonant stages defined in the previous section. We use this combination to indicate the modes; for example, if an LLC operation in the half cycle starts fist in stage P and then ends in stage O, then it would be named as PO mode. Generally the converter could operate in six major modes which are PO, PON, PN, NP, NOP and OPO.

The modes that contain stage O are Discontinuous Conduction Mode (DCM), as during stage O the output current is discontinued and there is only current circulating in the resonant tank, whereas those without stage O are Continuous Conduction Mode (CCM). The load condition for DCM is usually heavier than CCM at the same switching frequency level, while the DC gain is higher in DCM than in CCM.

As the name suggested, this mode begin with stage P and ends in stage O. In stage P, the current i_r and i_m start from the same negative initial value and then they diverge in different wave shapes: i_m increases linearly as L_m is clamped to $+nV_o$, while i_r varies sinusoidally as L_r and C_r are in resonance. When i_r and i_m converge at the end of stage P, the rectifier is turned off and the resonant tank is cut off from the output and moves to stage O. In stage O, v_m decreases in sinusoidal wave shape but should be kept above $-nV_o$, or otherwise the resonant tank will enter stage N within the half cycle. The voltage and current waveforms of this mode is illustrated in Figure 2.9.
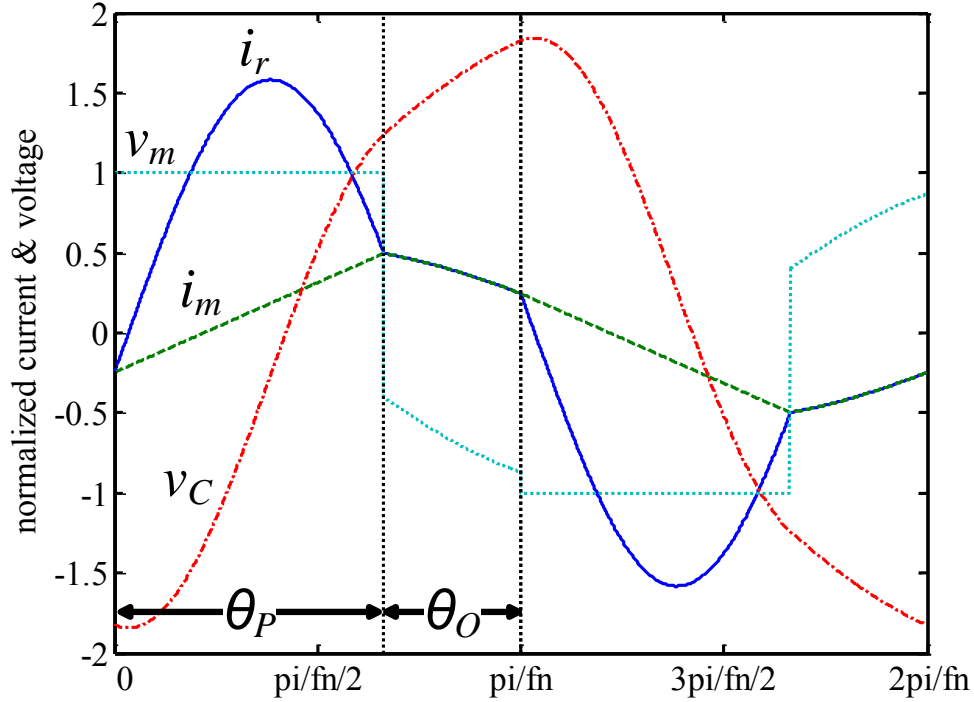
Figure 2.9 The LLC operating waveforms in PO mode ($m=5, f_n=0.7, p_{on}=0.6$)

The inductor current is negative at the start of this mode indicating that the switch current lags the switch voltage, and the resonant tank appears as an inductive load to the bridge. Therefore, the ZVS condition is always achieved in this mode. The DC voltage gain M increases monotonically with the decrease of f_n, and gain curves for various loads converge to 1 at $f_n=1$, as seen in Figure 2.10. In other words, the peak gains do not occur in this mode. The gain variation caused by the load change is moderately small, which indicates that the corresponding frequency change can be narrow to regulate a load variation in this mode. The slope of the gain-frequency curves in PO mode is always negative, which ensures the control stability in the closed-loop design. Also, since the mode is ending with stage O, the output current remains zero when the switches switch, and hence it eliminates the reverse recovery loss of rectifier diodes. In consequence, PO mode is the preferable operation mode of the LLC converter.
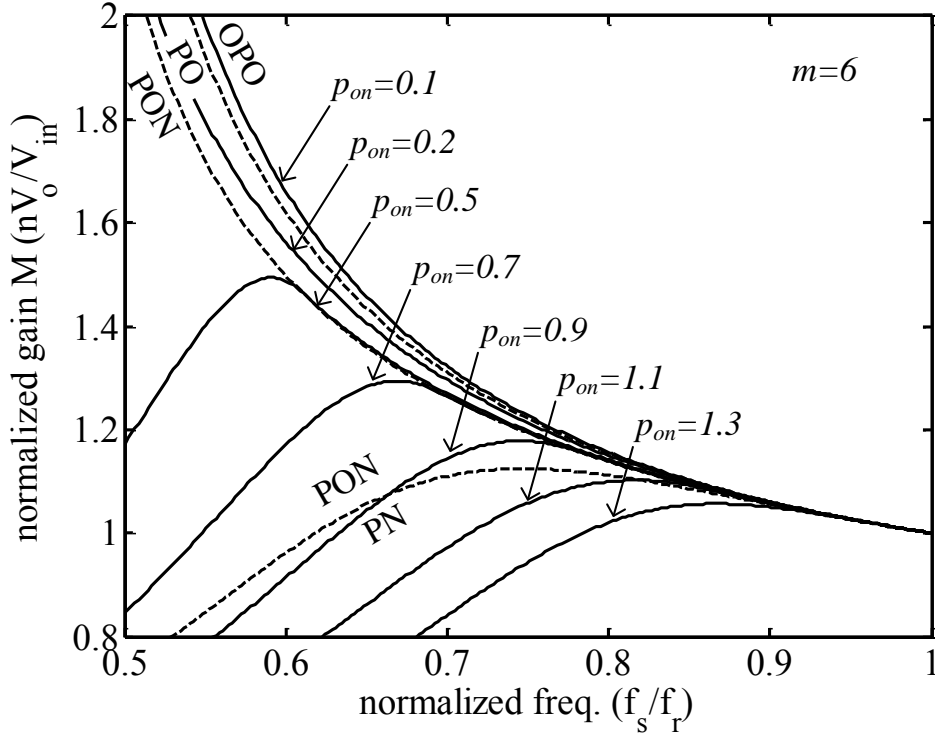
Figure 2.10 The normalized gain curves of the LLC converter in PO, PON,PN and OPO mode, as the mode boundaries are marked in dash lines

PON Mode

PON mode has an addition stage N in the end comparing to PO mode, and it is likely to occur under relatively heavier load or lower switching frequency condition. Although the first two stages of PON mode are the same as PO mode, i_r and i_m in PON start with different initial values at the start since the mode ends in stage N rather than stage O, and the inductor currents is not required to converge at the cycle end. The L_m voltage is clamped to nV_o in stage P, and decreases in stage O and, as stage O ends, it falls down to $-nV_o$ that it turns on the rectifier and L_m is reversely clamped to $-nV_o$, which starts stage N. The resonant tank current i_r in stage N varies sinusoidally below i_m. Before i_r and i_m converge again, the half switching cycle ends. The waveforms are shown in Figure 2.11. Since the output current is not zero at the switching instants,

43

the secondary side diodes have reverse recovery losses. Since the start inductor current value may not always be negative as in PO mode, the ZVS condition could be lost in this mode. Also, the gain-frequency relation for a constant load condition is no longer monotonic and a gain curve may reach its peak and fall below 1 in this mode. The converter should avoid operating below the frequency of peak gain as it is the ZCS region and could cause control instability.
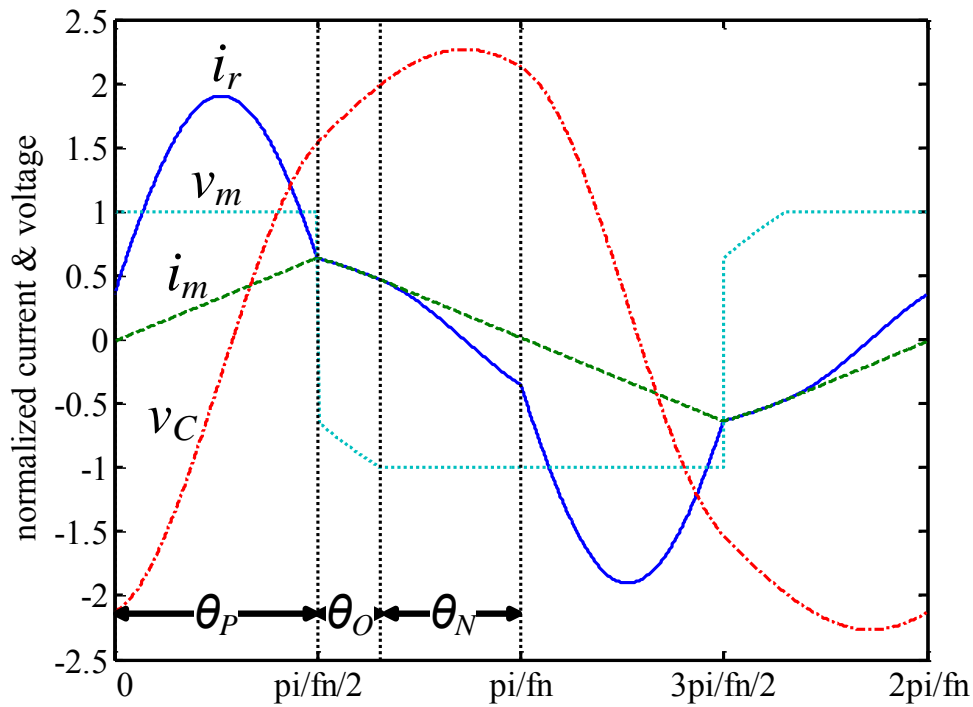
Figure 2.11 The LLC operating waveforms in PON mode ($m=5,f_n=0.6,p_{on}=0.6$)

PN Mode

PN mode is a continuous conduction mode without the cut-off stage O. and is for heavy load condition. The duration of stage O in PON mode will be shortened if the load increases. Eventually, when the length of stage O shrinks to 0, the LLC enters PN mode. Throughout the switching period, L_m does not have the resonant stage and thus i_m varies as a triangle waveform

(see Figure 2.12). Like PON mode, the inflection point of the gain curve, where the first derivative of the curve is zero, can be found in this mode and this mode is mainly in ZCS region. For the same switching frequency, the DC gain of PN mode is lower than in PON or PN mode.
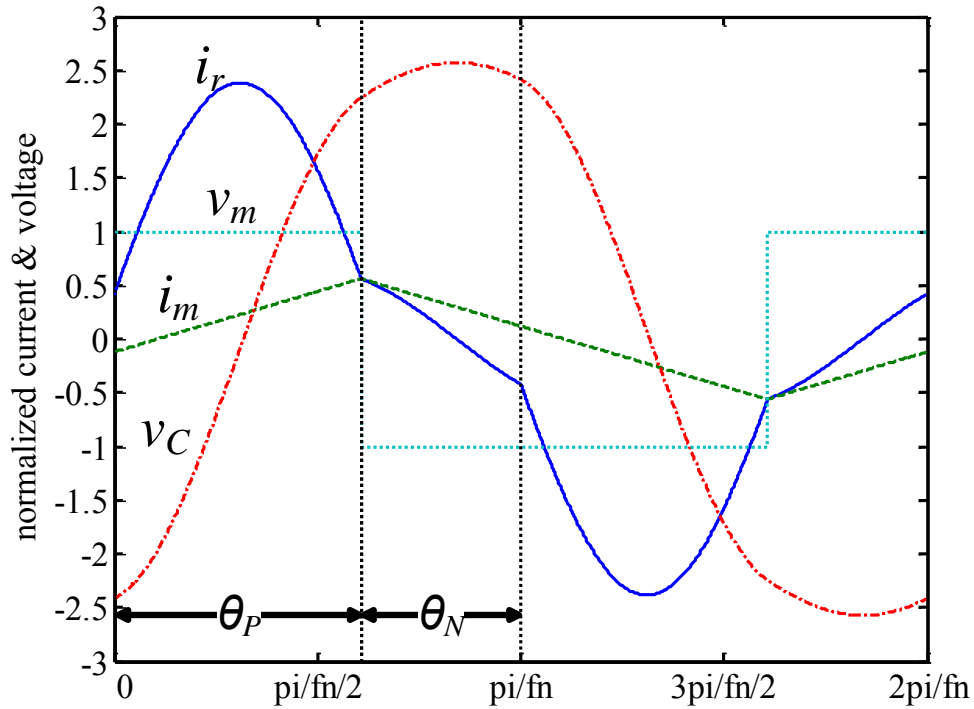
Figure 2.12 The LLC operating waveforms in PN mode ($m=5, f_n=0.7, p_{on}=1$)

NP Mode

NP mode is also a CCM and can be found under heavy load, and its operating waveforms are plotted in Figure 2.13. For this mode, the LLC has not enough time to finish stage P and enter other stage before the half cycle ends. From the stage constraint, the current i_r is higher than i_m when stage P ends, and the symmetry requires that i_r is lower than i_m at the start of the half cycle which indicates that the mode begins with stage N. NP mode shares the same two stages with PN

mode but in different order, and thus the mode equations and solutions of this two mode are very similar too. In fact, the two modes are the only two CCM that has closed-form solutions.
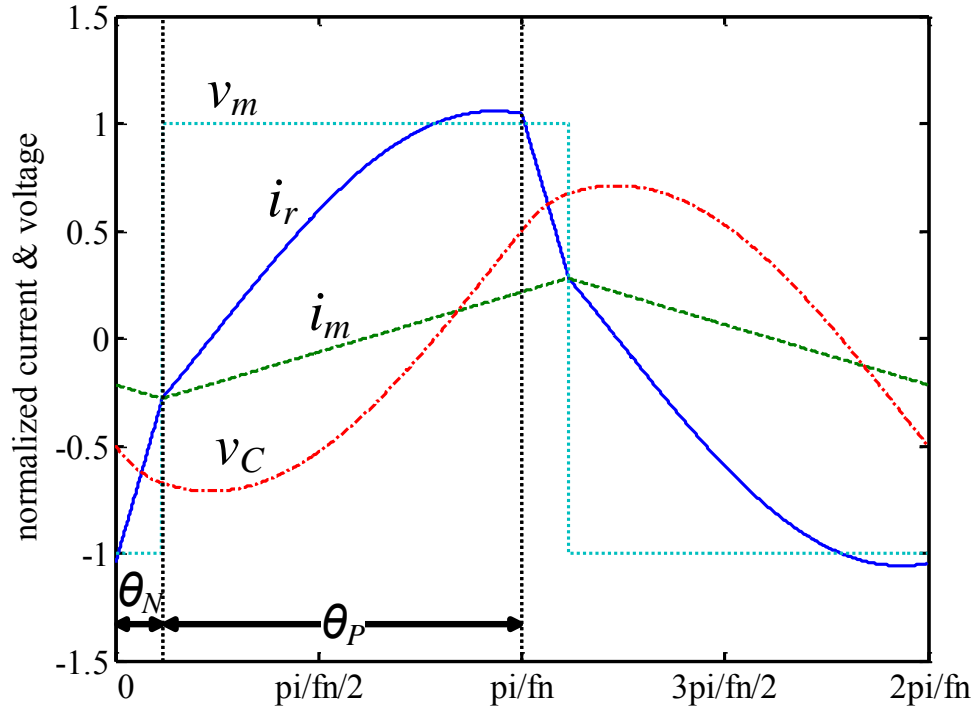
Figure 2.13 The LLC operating waveforms in NP mode ($m=5,f_n=1.4,p_{on}=0.6$)

NP mode occurs when the switching frequency is above resonant frequency f_r. The voltage gain M of this mode is lower than 1 and decreases as f_n increases. Although the tank's input impedance is inductive, the gain-frequency relation is also monotonic and the whole mode is within ZVS region as in PO mode, NP mode has additional rectifier diode reverse recovery losses as the output current is not zero at the switching instants. In order to reduce the power losses we could limit the switching frequency below f_r to avoid this mode.
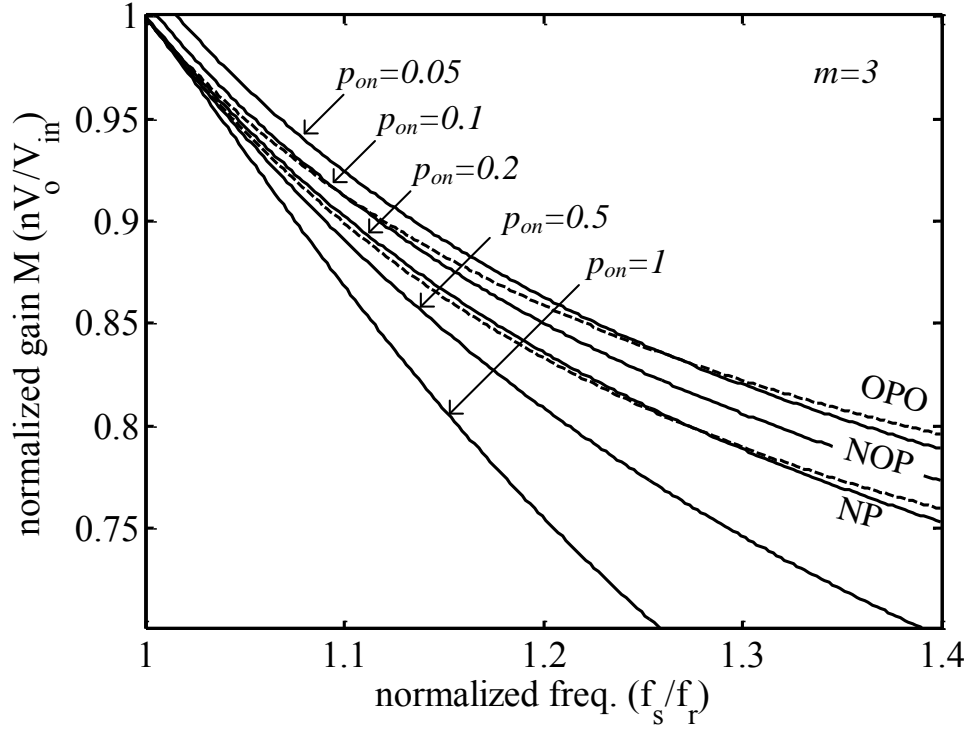
Figure 2.14 The normalized gain curves of the LLC converter in NP, NOP and OPO mode, as the mode boundaries are marked in dash lines

NOP Mode

NOP mode is also in the above-resonant-frequency region with NP mode, but it is in relatively lighter load condition and has an additional cut-off stage O between stage N and P. At the end of stage N the L_m voltage is not high enough ($v_m < nV_o$) to immediately turn on the secondary side rectifier so that v_m will not clamp to output voltage and the tank enters stage O. After accumulating sufficient voltage stress to the rectifier in stage O, the rectifier will start to conduct again and L_m will be clamped by output, and then the resonant tank enters stage P. The NOP mode waveforms are illustrated in Figure 2.15. Similar to NP mode, the gain in NOP mode decreases with the increase of switching frequency and they suffer the same reverse recovery current problem as the output current is still flowing when the switches switch.

47
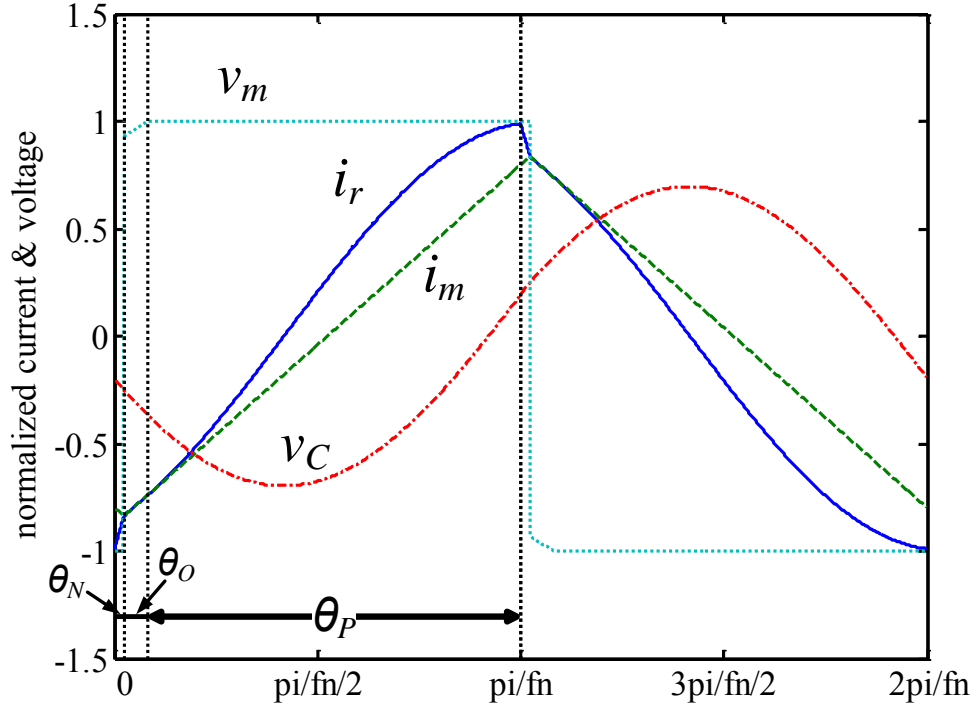
Figure 2.15 The LLC operating waveforms in NOP mode ($m=2.5, f_n=1.25, p_{on}=0.2$)

OPO Mode

OPO mode has two stage O's, and it exits in light load condition. At the start of the half switching cycle, v_m is not high enough to turn on the rectifier and start stage P, and thus the LLC operates in stage O. Until the magnetizing inductor has built up high enough voltage to let the rectifier conduct, stage O changes to stage P. After stage P, v_m is not low enough to start stage N, and thus this mode ends up in stage O as well. Figure 2.16 shows its current and voltage waveforms. OPO mode has relatively higher gain than other modes and exists for a frequency range from below to above the resonant frequency f_r.
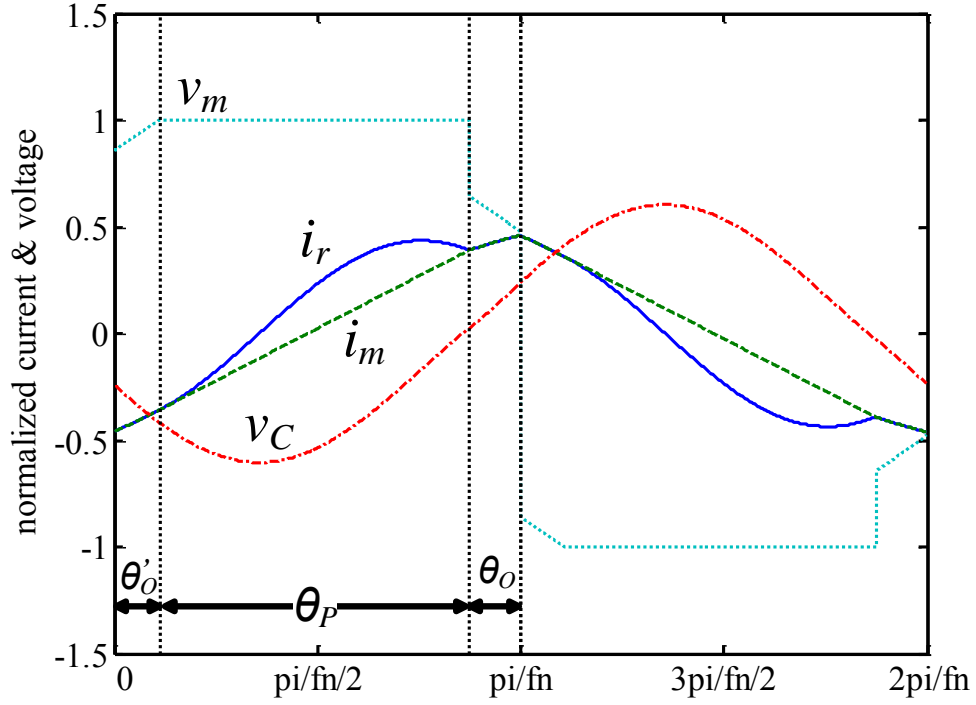
Figure 2.16 The LLC operating waveforms in OPO mode ($m=5, f_n=0.8, p_{on}=0.1$)

Other Modes

Besides the six major operation mode described above, there are admittedly other possible stage combinations, but the reason they are not included as the major modes is because that either some of them only occur in some certain conditions and can be treated as a special boundary case of a major mode, or some exist only in ZCS region losing the desirable merit of the LLC and are therefore considered trivial. More discussion on the boundary mode will be covered in the later part of the mode distribution section.

For low switching frequency (usually lower than $f_r/\sqrt{m}$), the tank current may ring for more than 2 complete half cycles within each half switching period, which is quite similar to the

sub-harmonic effect of the series resonant converter [19, 65]. Operation in these high-order harmonic modes is typically circumvented, and therefore the detail analysis is considered trivia.

2.3.3 Experiment Operation Waveforms

To demonstrate the waveforms of the operation modes, an experimental full-bridge LLC converter prototype with 210V output rating has been built. The resonant frequency is set to 140 kHz with a 3.9 µH L_r and 330 nF C_r. The magnetizing inductor L_m is set to 11 µH and thus m is 3.82. The transformer turns ratio n is 10/70.

The experiment waveforms in different operation modes are given in Figure 2.17.
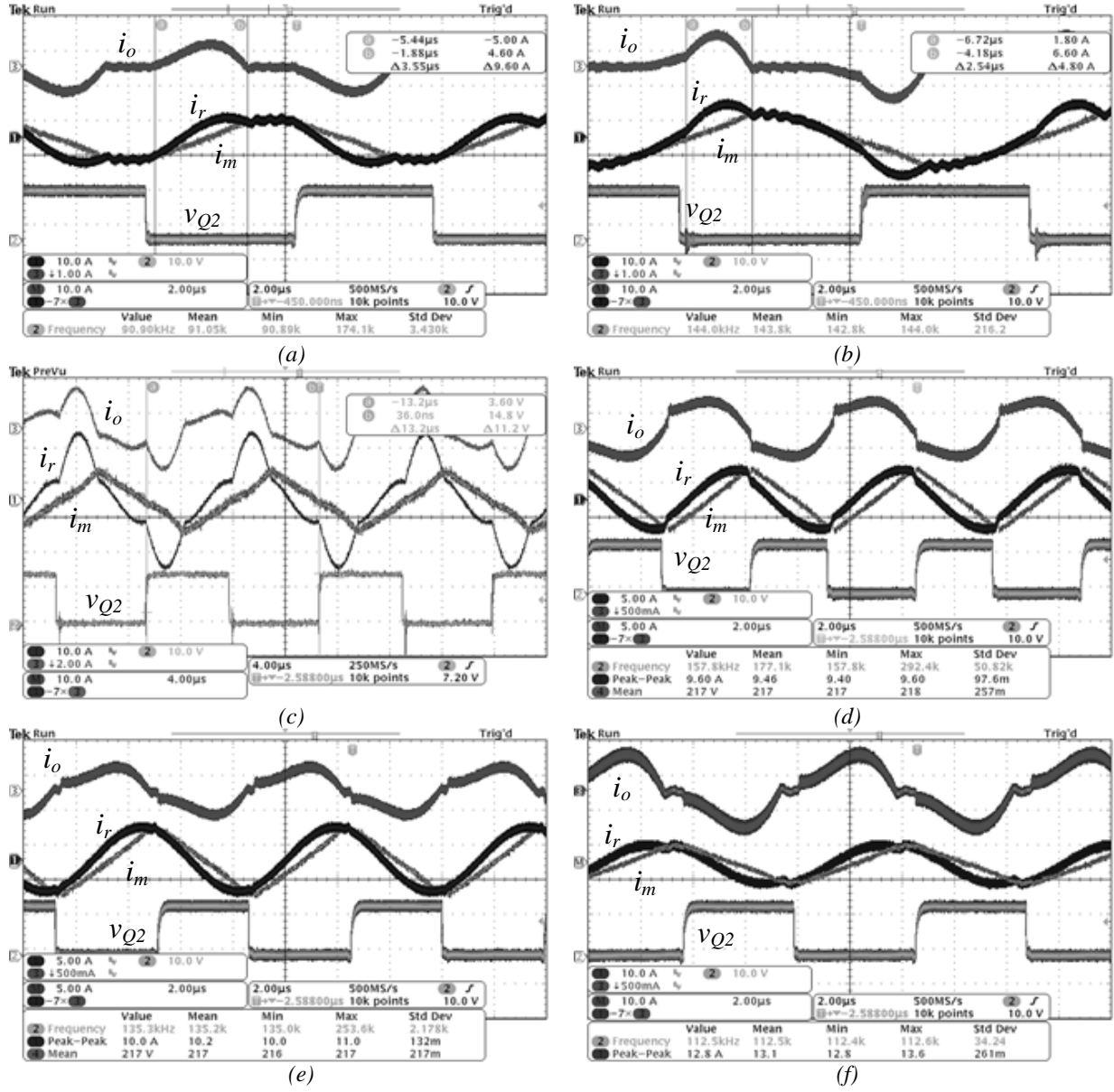
Figure 2.17 Experimental operating waveforms for the six modes of the LLC converter: (a) PO mode, (b) PON mode, (c) PN mode, (d) NP, (e) NOP mode, (f) OPO mode

The resonant and output currents are measured using current probe, and the magnetizing current, as there is no way to directly measure it, is obtained using the math function of the oscilloscope given that $i_m = i_r - i_o/n$. When Q2 driving signal goes low, Q2, Q4 are off and Q1, Q3 are on, which is the half cycle that the previous analysis and discussion are focused on. For the

whole switching cycle, it can be seen that the current waveforms in one half cycle are turned upside-down comparing to the other half. The current i_o shown in Figure 2.17 is equal to zero in stage O, and it is positive in stage P and negative in stage N, which provides a way to identify the resonant stages. For NOP and NP mode waveforms the duration of stage N and O is relatively short, judging from current i_o waveform we can still recognize the difference of NOP and NP mode. The experiment results are in good agreement with the mode analysis.

The detailed comparisons between the waveforms from the experiments and generated by the operation mode equations at the corresponding operation points are given in Figure 2.18 (PO mode), Figure 2.19 (PON mode) and Figure 2.20 (PN mode). Note that the current functions produced by the mode equations are de-normalized using the experiment circuit parameters in order to have the same scale with the measured waveforms. The operation conditions of the three modes are listed in Table 2.1.

Table 2.1 Operation Conditions of the Experimental Waveforms

PO mode (Figure 2.18)	PON mode (Figure 2.19)	PN mode (Figure 2.20)
$P_o = 60W$ $V_{in} = 17.7V$ $V_o = 212V$ $f_s = 90.9kHz$	$P_o = 60W$ $V_{in} = 10.4V$ $V_o = 215V$ $f_s = 74.5kHz$	$P_o = 260W$ $V_{in} = 36.8V$ $V_o = 210V$ $f_s = 78kHz$
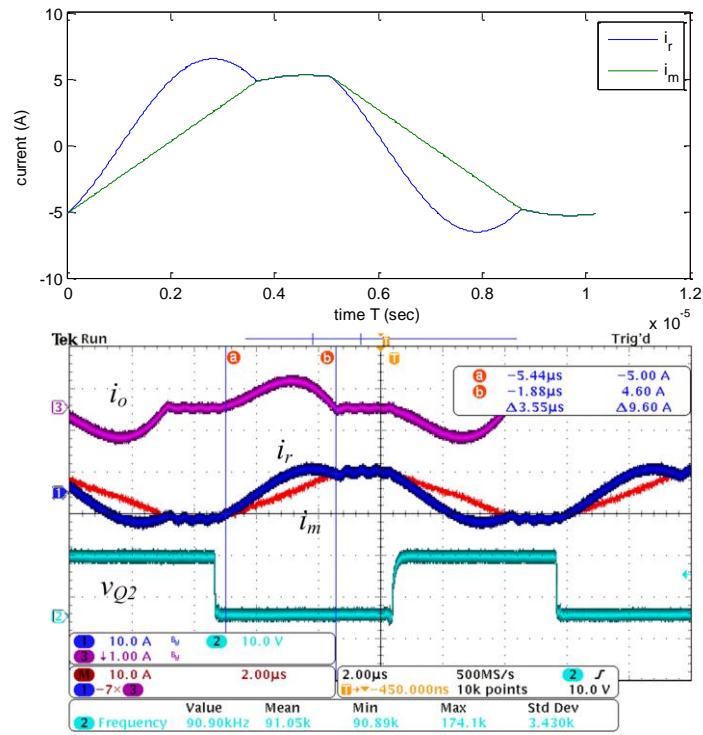
Figure 2.18 PO mode current waveforms comparison between mode model and experiment
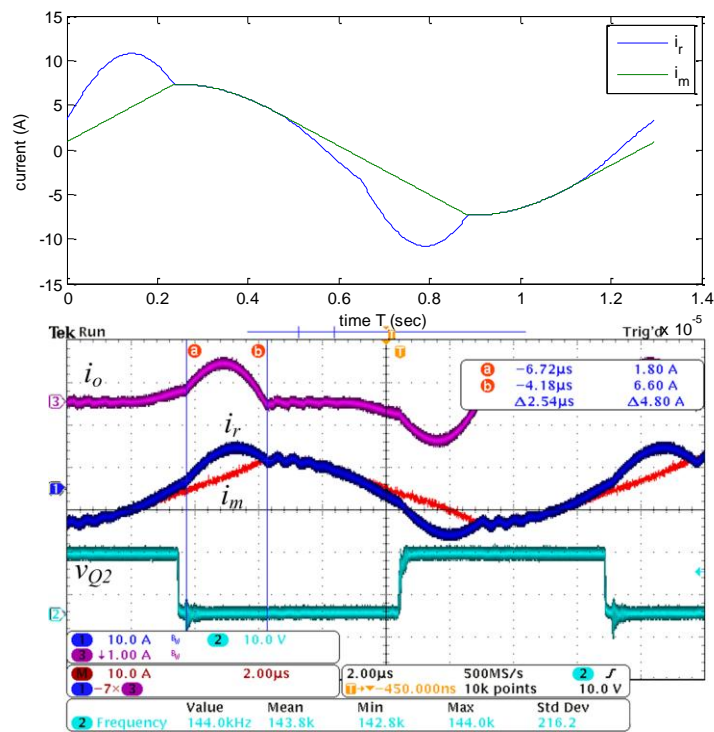
Figure 2.19 PON mode current waveforms comparison between mode model and experiment

53
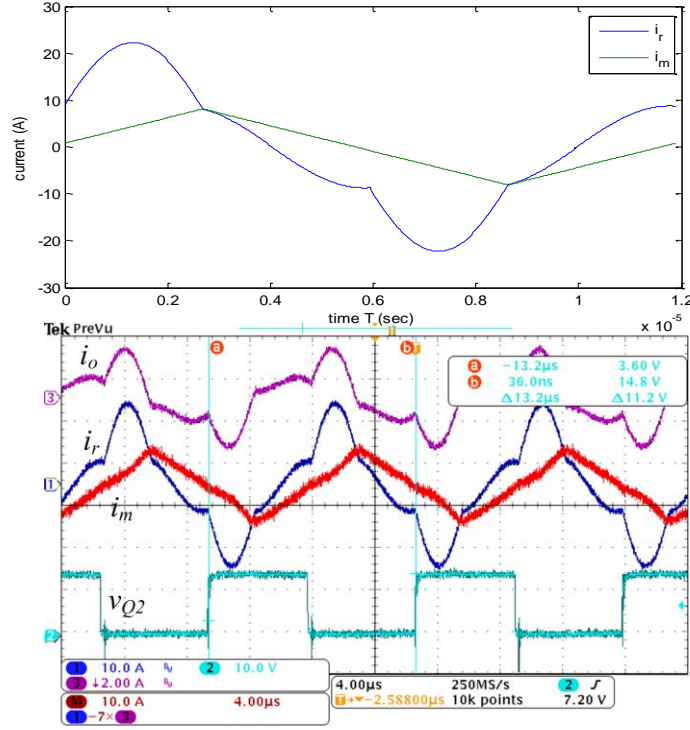
Figure 2.20 PN mode current waveforms comparison between mode model and experiment

It can be seen from the comparison that the current magnitudes and the time intervals of each resonant stage from the mode analysis match the experimental results. It validates the operation mode analysis method and shows the high accuracy of the approach.

2.3.4 Solving the Operation Mode Equations

The resonant state variable expressions are given in the stage analysis, but to solve them the initial and boundary conditions must be found. For each operation mode these conditions can be found at the edge between stages and the boundary of the switching cycle. The boundary constraints can be obtained from the following aspects:

1. From the continuity of the inductor current and capacitor voltage, the resonant state variables of two adjacent stages should be equal respectively at the joints of the two stages.

54

2. By symmetry, the initial values of the state variables should be opposite to their initial values in the half cycle period.

3. From the stage constraints, the absolute value of v_m should increase to nV_o at the end of stage O, while the polarity of v_m is dependent on the following stage, positive if followed by stage P or negative if followed by stage N; the end values of i_r and i_m should be equal at the end of stage P or stage N since entering other stage will change the inequality relation between the two current variables. Note that this constraint condition is only valid for the instant of stage transition and does not hold if the switch cycle ends before a stage changes to another stage.

The above boundary conditions are summarized by the following equations:

- Continuity conditions:

$$
\begin{aligned}
i_{rXn}(\theta_X) &= i_{rYn}(0) \\
i_{mXn}(\theta_X) &= i_{mYn}(0) \\
v_{CXn}(\theta_X) &= v_{CYn}(0)
\end{aligned}
\tag{2.6}
$$

where subscripts X and Y is used to denote the two different adjacent stages

- Symmetry conditions:

$$
\begin{aligned}
i_{rXn}(0) &= -i_{rYn}(\theta_Y) \\
i_{mXn}(0) &= -i_{mYn}(\theta_Y) \\
v_{CXn}(0) &= -v_{CYn}(\theta_Y)
\end{aligned}
\tag{2.7}
$$

where X and Y denotes the first and last resonant stages in the half switching cycle

- Stage constraint conditions:

    For stage O:

$$
v_{mOn}(\theta_O) =
\begin{cases}
1, & \text{followed by stage P} \\
-1, & \text{followed by stage N}
\end{cases}
\tag{2.8}
$$

For stage P:

$$i_{rPn}(\theta_P) = i_{mPn}(\theta_P) \tag{2.9}$$

For stage N:

$$i_{rNn}(\theta_N) = i_{mNn}(\theta_N) \tag{2.10}$$

Applying these equations properly to an operation mode as the boundary conditions is not enough to solve the unknown current or phase parameters in the state variable expressions unless the normalized switching frequency f_n, the inductor ratio m and the DC gain M are known. However, one important aspect of the analysis is to predict the converter behavior, and the M-f_n relation is a key DC characteristic to be interpreted and explored. Given the context, the DC gain M should be rather treated as an unknown parameter. Therefore, in order to solve one mode, another parameter, the normalized load power p_{on}, needs to be brought in to establish an additional constraint condition. In the LLC design or evaluation, it is reasonable to include load condition as the power rating is usually a given parameter in specification or the output condition is known in the application. Since the output current is discontinued in stage O, only stage P and N involve in the energy delivery procedure. Thus, the normalized output power can be expressed as

$$p_{on} = \frac{f_n}{\pi}\left[\int_0^{\theta_P}(i_{rPn} - i_{mPn})d\theta + \int_0^{\theta_N}(i_{mNn} - i_{rNn})d\theta\right] \tag{2.11}$$

where θ_P, θ_N represent the length of stage P and N respectively. Note that π/f_n ($= \pi f_r/f_s$) is the half cycle period in phase angle term.

Taking p_{on}, f_n and m as known parameters and along with the applied boundary conditions, we can find sufficient equations to solve for the voltage gain M and the resonant state variables.

Since i_m waveform is sinusoidal in stage O and linear in stage P or N, the boundary equation about i_m in (2.6) will lead to a transcendental equation with the mixture of trigonometric and linear terms if a mode contains stage O. Hence, all discontinuous conduction modes, PO, PON, NOP and OPO, have no closed-form solutions and rely on numerical calculation tools to solve the mode equations, whereas the continuous conduction modes, PN and NP, can be solved analytically.

To solve PN mode, substitute the resonant variable functions (2.3) and (2.4) into the boundary conditions (2.6), (2.7), (2.9) and (2.11), and the simultaneous equations are constructed as follows:

$$
\begin{aligned}
I_{rPn}\sin(\theta_P+\theta_{P0})-I_{rNn}\sin(\theta_{N0})&=0\\
I_{rPn}\cos(\theta_P+\theta_{P0})-I_{rNn}\cos(\theta_{N0})+2&=0\\
I_{rPn}\sin(\theta_{P0})+I_{rNn}\sin(\theta_N+\theta_{N0})&=0\\
I_{rPn}\sin(\theta_P+\theta_{P0})+I_{rNn}\sin(\theta_{N0})-\pi/[f_n(m-1)]&=0\\
I_{rPn}\cos(\theta_{P0})+I_{rNn}\cos(\theta_N+\theta_{N0})-2/M&=0\\
I_{rNn}\cos(\theta_{N0})-1-1/M+p_{on}\pi/(2f_n)&=0
\end{aligned}
\tag{2.12}
$$

Note that $\theta_P+\theta_N=\pi/f_n$. After proper manipulation of (2.12), we arrive at the following equations:

$$
\begin{aligned}
\sin\theta_P&=\frac{M}{2}\frac{\pi}{(m-1)f_n}\cos(\frac{\pi}{2f_n})\left[\cos(\frac{\pi}{2f_n})+\sin(\frac{\pi}{2f_n})\cot\theta_{N0}\right]\\
\cos\theta_P&=\frac{M}{2}\frac{\pi}{(m-1)f_n}\cos(\frac{\pi}{2f_n})\left[\cos(\frac{\pi}{2f_n})\cot\theta_{N0}-\sin(\frac{\pi}{2f_n})\right]-M
\end{aligned}
\tag{2.13}
$$

where

$$
\cot\theta_{N0}=\left(2+\frac{2}{M}-p_{on}\frac{\pi}{f_n}\right)\Big/\frac{\pi}{(m-1)f_n}
$$

By substituting (2.13) into the Pythagorean trigonometric identity, $\sin(\theta_P)^2 + \cos(\theta_P)^2 = 1$, it yields a quadratic polynomial equation about M, given f_n and p_{on} as known parameters. Hence, closed-form solutions for PN mode can be derived.

For NP mode, the solving of the mode equations has similar process with PN mode. The following equations can be used to derive the explicit expression of DC gain:

$$
\begin{aligned}
\sin\theta_N &= \frac{M}{2}\frac{\pi}{(m-1)f_n}\cos(\frac{\pi}{2f_n})\left[\cos(\frac{\pi}{2f_n})+\sin(\frac{\pi}{2f_n})\cot\theta_{P0}\right] \\
\cos\theta_N &= \frac{M}{2}\frac{\pi}{(m-1)f_n}\cos(\frac{\pi}{2f_n})\left[\cos(\frac{\pi}{2f_n})\cot\theta_{P0}-\sin(\frac{\pi}{2f_n})\right]+M
\end{aligned}
\tag{2.14}
$$

where

$$
\cot\theta_{P0} = \left(-2+\frac{2}{M}+p_{on}\frac{\pi}{f_n}\right)\Big/ \frac{\pi}{(m-1)f_n}
$$

2.3.5 Voltage Gain Obtained from Mode Equations

The gain characteristics can be obtained by solving the operation mode equations. To verify the model's accuracy, the experimental prototype in the previous section 2.3.3 is used here to measure the gain at different operation condition and compare with the results predicted by the mode analysis. The circuit specifications are listed in Table 2.2, and the corresponding base coefficients for parameter normalization are listed in Table 2.3.

Table 2.2 The Specifications of the Experimental LLC Converter Circuit

Parameters	Values
Output voltage V_o	210V
Resonant capacitor C_r	330nF
Resonant inductor L_r	3.9uH
Magnetizing inductor L_m	11uH
Transformer turns ratio n	10/70

Table 2.3 The Base Coefficients of the Experimental LLC Converter Circuit

Parameters	Values
Base frequency f_{base}	140kHz
Base voltage V_{base}	30V
Base current I_{base}	8.73A
Base power P_{base}	262W
Inductors ratio m	3.82

The voltage gain is measured at three load power level: 50W, 100W and 150W, of which the normalized load power is $p_{on} = 0.191, 0.382, 0.573$. The comparative gain curves are plotted in Figure 2.21, from which it can be seen that the mode analysis provides precise gain predictions over a wide range of operation frequency and load conditions.
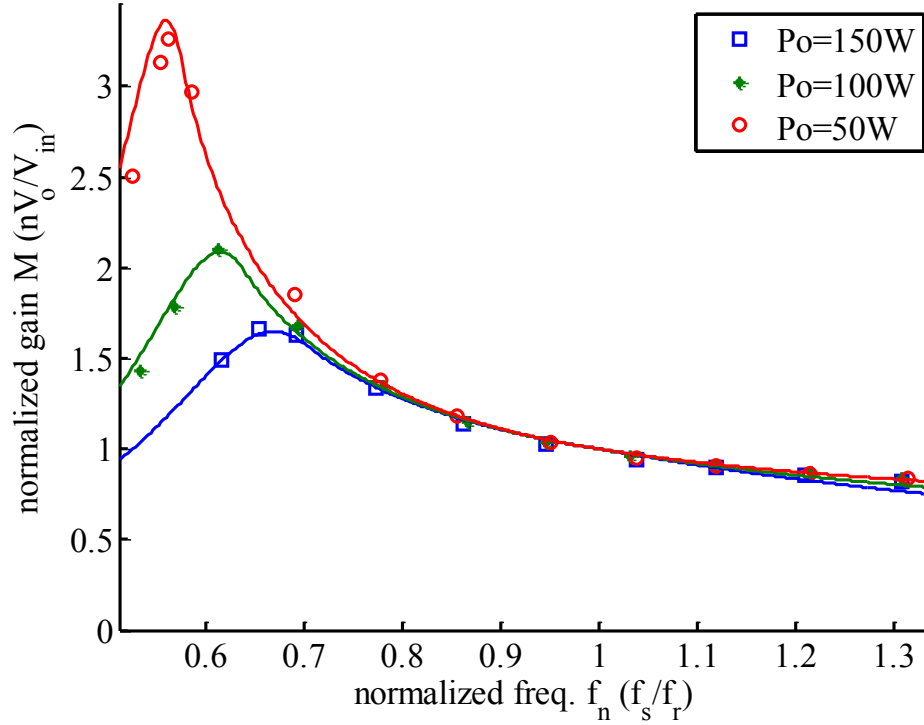
Figure 2.21 Gain curves comparison between mode analysis result (solid lines) and experimental results (markers)

In addition, the comparative gain plots between the mode analysis and the FHA are shown in Figure 2.22. Note that in FHA the quality factor Q is used to indicate the output load resistance, while the normalized load power p_{on} is used in our operation mode analysis model. The corresponding relationship between Q and p_{on} can be derived from their definitions, which is given as follows: $Q = p_{on}\pi^2/8$. It can be seen that there are large deviations between the two methods, especially in low frequency region and heavy load condition. For intermediate load, the voltage gain from FHA is lower than the gain from operation mode model in the below resonance region ($f_n < 1$). It seems that FHA's gain has a smaller peak compared to the mode model, but actually for continuously decreasing load power, the peak gain of FHA rises faster than the mode model and will eventually catch up and exceed the peak of mode model in extreme light load

condition (as seen in Figure 2.23). In the operation region above resonant frequency, the FHA generally gives higher gain prediction than the operation mode. Since almost all gain curves from both methods converge at the resonant frequency and the gain changing rate above resonance is relatively flat, the difference between the two methods is very small comparing with the low frequency region. The zoom-in gain plot enlarging the area around the resonant frequency is shown in Figure 2.24.
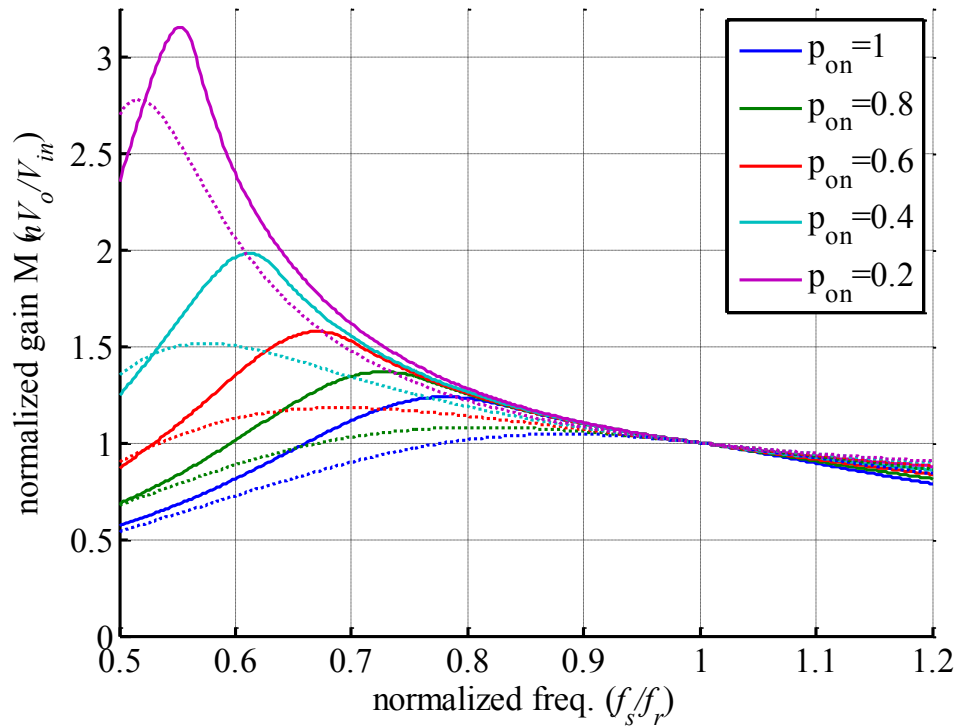
Figure 2.22 Gain curves comparison between mode analysis method (solid lines) and FHA method (dash lines) for $m=4$
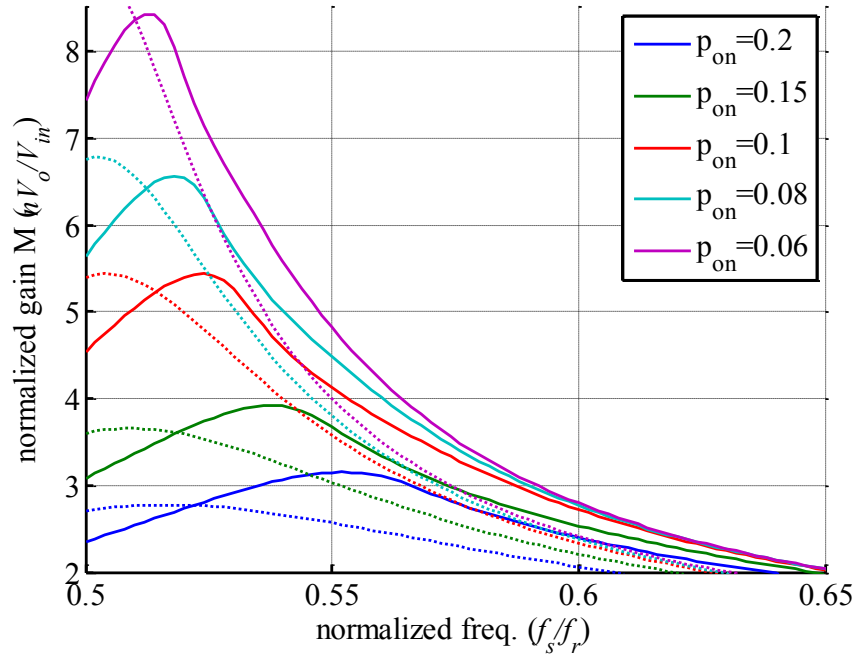
Figure 2.23 Gain curves comparison between mode analysis method (solid lines) and FHA method (dash lines) at light load condition for *m=4*
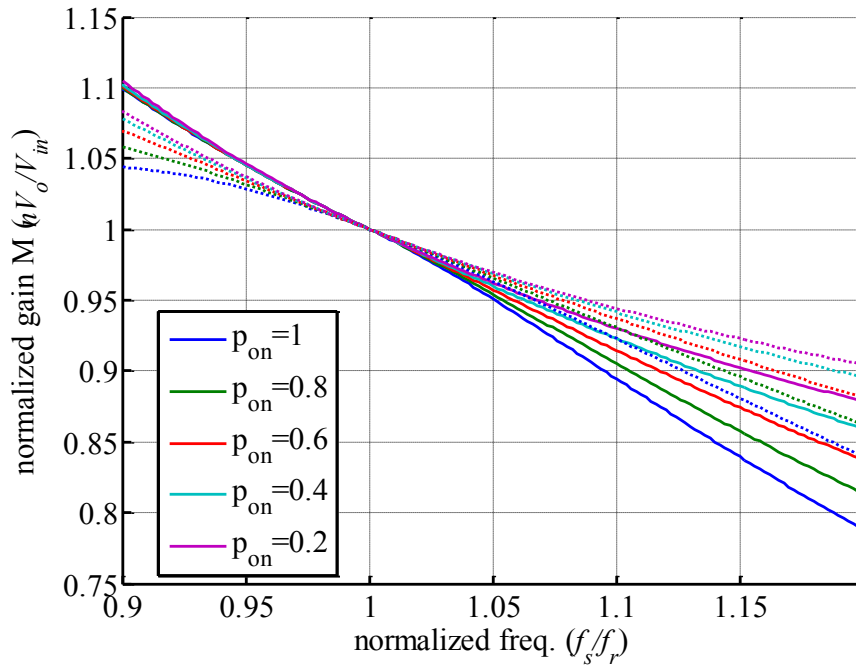
Figure 2.24 Gain curves comparison between mode analysis method (solid lines) and FHA method (dash lines) around the resonant frequency for *m=4*

2.4 Mode Distribution of the LLC Converter

Although solving the mode equations provides precise gain prediction and resonant current/voltage waveforms, one solution is limited for a mode. The operation modes have different load, gain and frequency distribution. Without this knowledge, the converter operation analysis is discrete and incoherent and it hampers the usability of the method. Therefore, in order to obtain a complete picture of the LLC mechanism and a continuous voltage gain curve, knowing the boundaries and distribution of modes is essential to apply the appropriate mode equations according to the load and frequency condition. In this section, we present a thorough investigation of the LLC mode distribution.

2.4.1 Mode Boundary

The transition between operation modes is marked by the mode boundary. For some modes, the mode edges are one of the six operation modes but happen in some special operating condition. In some case, the mode boundaries could be a particular boundary mode differed than the six modes. In addition to the 6 major modes, there are three boundary modes that only occurs at the boundaries between the 6 modes, which are OP mode occurred at the boundary between NOP and OPO mode, P mode occurred at resonant frequency f_r and O mode occurred at zero load condition.

The boundary has additional constraint on the mode equations, which renders the simultaneous equations solvable without the relation equation of load p_{on} given in (2.11). In other words, the load p_{on} can be calculated using its expression after solving the mode equations and its

relations with switching frequency and voltage gain for the boundary mode can be obtained. The following discussion will include the added boundary mode constraints.

The boundary mode of PO and PON is PO mode as P and O are the sharing stages of the two. In the boundary PO mode, stage O also shares some property of stage N at its end, which is that the final v_m value in stage O is $-nV_o$. Exceeding the $-nV_o$ lower limit will lead the converter to stage N, where v_m is always clamped to $-nV_o$. If v_m reaches $-nV_o$ before the half cycle finishes, the LLC would start to operate in PON mode. Thus, the boundary condition is given by

$$v_{mOn}(\theta_O) = -1 \tag{2.15}$$

With this condition, as discussed before, the load power p_{on} and gain M of this mode are uniquely determined by m and f_n.

The boundary mode between PON and PN is PN mode. For PN mode, it requires that the initial v_m of stage N is low enough ($v_m \leq -nV_o$) to turn on the rectifier so that the converter can directly enter stage N after stage P without the transition of stage O. Therefore, in boundary PN mode the initial v_m of stage N should be equal to $-nV_o$. To evaluate v_m at the start of stage N, the first order derivative of the resonant current i_r is used as i_m and i_r converge at the border of stage P, N, and the boundary constraint can be expressed as

$$(m-1)\frac{di_{rNn}(0)}{d\theta} = (m-1)I_{rNn}\cos(\theta_{N0}) = -1 \tag{2.16}$$

Since PN mode has closed-form solution, the gain and load of the boundary PN mode is given as

$$M = \frac{m-1}{\sqrt{m^2 - \left[(2m-1)\sin(\frac{\pi}{2f_n}) + \frac{\pi}{2f_n}\cos(\frac{\pi}{2f_n})\right]\left[\sin(\frac{\pi}{2f_n}) - \frac{\pi}{2f_n}\cos(\frac{\pi}{2f_n})\right]}} \quad (2.17)$$

$$p_{on} = \frac{2f_n}{\pi}\left[1 + \frac{1}{M} + \frac{1}{m-1}\right]$$

NP and NOP mode's boundary occurs above resonant frequency, which is NP mode. In contrast to the PN and PON boundary, for NP mode the instant v_m value at the start of stage P should be larger than nV_o to let L_m be clamped by the output. Therefore, the boundary condition at the edge of NP mode to NOP mode is

$$(m-1)\frac{di_{rPn}(0)}{d\theta} = (m-1)I_{rPn}\cos(\theta_{P0}) = 1 \quad (2.18)$$

Similarly, the gain and load expressions on the mode boundary can be derived as below:

$$M = \frac{m-1}{\sqrt{m^2 - \left[(2m-1)\sin(\frac{\pi}{2f_n}) - \frac{\pi}{2f_n}\cos(\frac{\pi}{2f_n})\right]\left[\sin(\frac{\pi}{2f_n}) + \frac{\pi}{2f_n}\cos(\frac{\pi}{2f_n})\right]}} \quad (2.19)$$

$$p_{on} = \frac{2f_n}{\pi}\left[1 - \frac{1}{M} + \frac{1}{m-1}\right]$$

Since OPO mode's operation frequency spans from below to above the resonant point and it has two adjacent modes, which are PO and NOP mode. For $f_n<1$, OPO mode borders with PO mode, and the boundary mode is PO mode. The same constraint of boundary NP mode (2.18) applies here at the start of stage P which is also the beginning of the switching cycle. For $f_n>1$, OPO mode borders with NOP mode, and their boundary is OP mode based on their sharing stages, which does not belong to the six major modes. Boundary conditions (2.6) and (2.7) apply to both OP and PO modes, and OP mode equations have the same number of unknown parameters as PO mode. However, OP mode has one more constraint than PO mode, which is provided in equation (2.8). Hence, OP mode can be solved without knowing p_{on}.

Another unique boundary mode is called P mode, which can be found at the resonant frequency point. At resonant frequency ($f_n=1$), stage P will dominate the whole half cycle while stage O or N vanishes, which forms the boundary P mode. In P mode, as $\theta_P = \pi$, the resonant inductor current i_r and capacitor voltage v_C are pure sinusoidal and the magnetizing current i_m is a triangle waveform. From the symmetry conditions (2.7), it is easy to solve the mode equations, and the following equations can be derived

$$I_{mPn} = -\frac{\pi}{2(m-1)}$$

$$M = 1$$

(2.20)

It can be seen that the normalized DC gain is always equal to 1 in P mode, which means the unity gain is load-independent. This property makes P mode a favorable mode in the converter design, as setting the converter to work at the resonant frequency for the normal input voltage can narrow the operating frequency range. Furthermore, this mode without stage O has no energy circulating stage, which will benefit the power efficient, and the output current converge to zero at the switching instants that there is no reverse recovery losses for the rectifiers. All this features make P mode achieve the highest efficiency than other modes. Therefore, many studies focus on optimizing the converter performance on this mode.

The load-independent property holds true in the entire P mode, but it does not always stands at the resonant frequency for all the load conditions. For light load, the converter may enter OPO mode region. The constraint (2.18) on the starting point of stage P for the boundary NP mode can be applied as the constraint for P and OPO mode boundary. Substitute (2.18) in (2.11) and let $f_n = 1$, and the boundary load power expression can be derived as

$$p_{on} = \frac{2}{\pi} I_{rPn} \cos(\theta_{P0}) = \frac{2}{\pi(m-1)} \tag{2.21}$$

If the load is lighter than this boundary value, the LLC will be operated in OPO mode, in which the gain is no longer unity and load-independent.

It is worth noticing that the border point of P and OPO mode also serves as the dividing point of PO, NP, NOP and OPO mode at the resonant frequency. For NOP and OPO's boundary, OP mode will reach the same load condition at $f_n=1$: as f_n approaches 1, θ_P approaches π and θ_O approaches 0, the limit of load power p_{on} of OP mode is the same as (2.21) defined. The PO/OPO and NP/NOP boundary have the same constraint condition of (2.18), which also leads to the same load value (2.21) at $f_n=1$. Hence, the boundaries between OPO, PO, NOP and NP all converge to the same load point defined by (2.21).

Another interesting operation point on P mode is also a congregating point of mode boundaries. PN, PON and PO are the modes that can only be found in $f_n<1$ region, while NP and NOP is located in $f_n>1$ region, and P mode serves as the border line separating them. It is observed that as f_n approaches 1, the boundary PO mode of PO/PON and the boundary PN mode of PON and PN converge to one load point at resonant frequency, at which the normalized load power p_{on} can be derived from (2.11), (2.16) and (2.18) as

$$p_{on} = \frac{2}{\pi} \frac{2m-1}{m-1} \tag{2.22}$$

This point plays an important role in the mode approximation process, which will be covered more in the next chapter.

O mode is the operation mode for zero load operation. If the load drops to zero, the converter will operate without energy delivering stage that only stage O will exit for the entire

switching cycle. In this mode, no power flows to the output and all energy is circulating in the primary-side resonant tank, and the resonant waveforms are purely sinusoidal excited by the square input voltage. Ideally, input voltage can be arbitrarily small since the output voltage held up by the output capacitor is cut off from input. However, there is limitation on the maximum value of V_{in}. To prevent turning on secondary-side rectifiers, L_m voltage should not exceed nV_o or $-nV_o$ ($|v_m| \leq nV_o$), and this condition can be described as

$$v_{mOn}(\theta) = \frac{m-1}{\sqrt{m}} I_{rOn} \cos(\theta/\sqrt{m} + \theta_{O0}) \leq \frac{m-1}{\sqrt{m}} I_{rOn} \leq 1 \tag{2.23}$$

From the symmetry condition (2.7), we can derive an equality, which is

$$\sqrt{m} I_{rOn} \cos(\frac{\pi}{2 f_n \sqrt{m}}) = \frac{1}{M} \tag{2.24}$$

After combining (2.23) and (2.24), the gain limit can be expressed as

$$M \geq \frac{m-1}{m \cos[\pi/(2\sqrt{m} f_n)]} \tag{2.25}$$

Note that when f_n approaches $1/\sqrt{m}$, the limit of gain M is infinity, as it is the resonant frequency of L_m, L_r and C_r. It indicates that in this circumstance the converter will not be able to regulate the output voltage for any input voltage level at zero load condition. In practice, the LLC is not likely to work in low frequency region since the operation region of the LLC converter is set in the ZVS zone whose frequency range is above $\sqrt{m}$. If the input voltage exceeds the limit, the converter will be unable to maintain the required output level in zero load condition. Instead, the output voltage will become

$$V_o = \frac{m-1}{m \cos[\pi/(2\sqrt{m} f_n)]} \frac{V_{in}}{n} \tag{2.26}$$

2.4.2 Mode Distribution

Since the boundaries between every operation mode are studied in the previous section, the operation mode distribution can then be obtained. The equation solving process is similar to the gain solving except that the load condition for the mode boundary is treated as an unknown parameter and is solvable given the operating frequency. Therefore, the mode distribution should include the gain and the load distribution. Figure 2.25 shows the distribution of the operation modes in a range of switching frequency, load power and gain, which is generated by solving boundary mode equations using MATLAB.

PO mode in the gain-vs.-frequency plot has only a narrow strip area, but in the load-vs.-frequency plot it has a triangle shaped area. As the switching frequency moving from low to high towards the resonance, the gain span of PO mode becomes smaller while the load span is increased. Because of this characteristic, PO mode provides a relatively stable working point close to the resonant frequency for the wide load variation and small input voltage fluctuation situation. If the input voltage is wide-ranging, PO mode is capable to regulate it as long as the output load power is low, since it requires a wide frequency range. At an increased load, the LLC will enter PON mode from PO mode earlier as the operating frequency reduced. For PON mode, it can be seen from its distribution that at low frequency, the gain span and the load span are wide, which indicates that the converter has to vary the frequency substantially to follow the change of input voltage or load power. PN mode occurs in low gain and heavy load region; since the majority of PN mode is in ZCS region, it generally should be avoided.
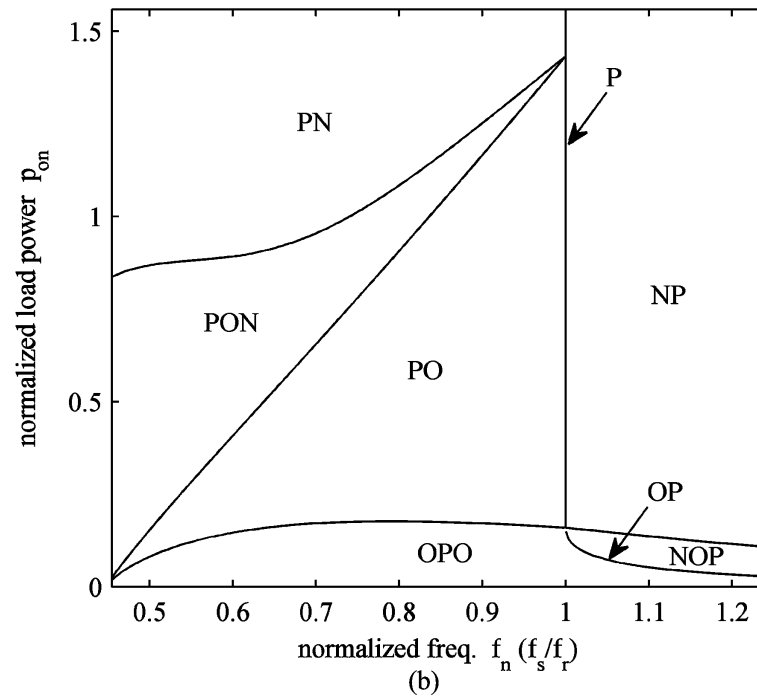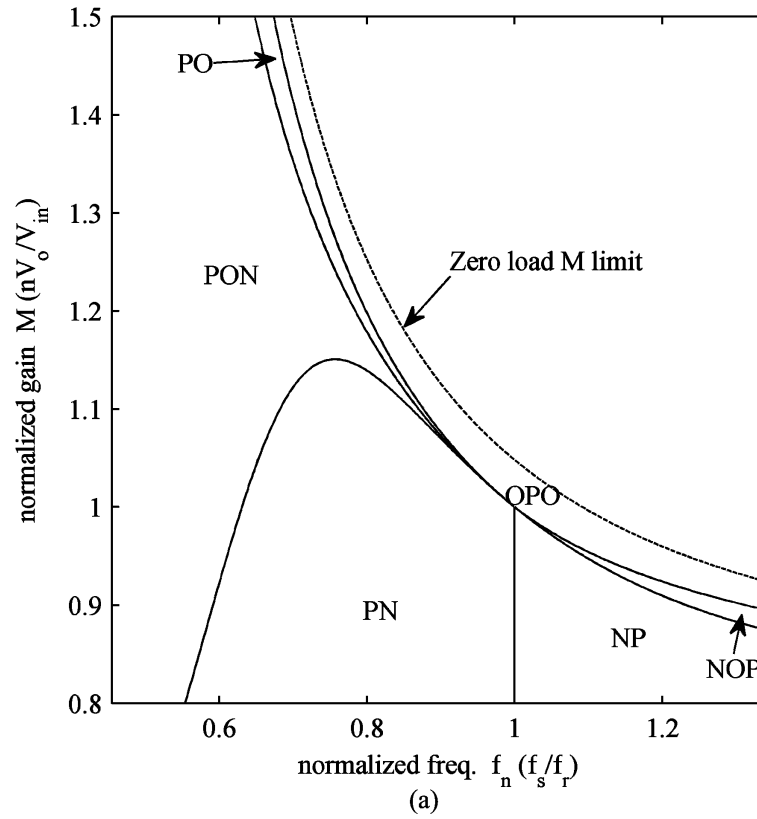
Figure 2.25 LLC mode boundaries and distribution with *m=5*: (a) gain-frequency distribution and the zero load gain limit (the dash line); (b) load- frequency distribution

70

When $f_n > 1$, the major area in the load distribution map (Figure 2.25(b)) is covered by NP mode, and NOP mode occupy the light load region. From the gain distribution (Figure 2.25(a)), the voltage gain in NP and NOP mode is all below unity. OPO mode is the only operation mode that spans both below and above the resonance, also it is the only mode that has a gain greater than 1 in above resonance region. The LLC will enter OPO mode in close-to-zero load condition, which is inescapable for any operation frequency.

CHAPTER THREE: NUMERICAL APPROXIMATIONS OF THE LLC CONVERTER

3.1 Introduction

The LLC operation mode solving involves dealing with transcendental equations if the converter operates in DCM, which is difficult to derive an explicit expression of the DC characteristics. Although CCM has closed-form solutions, they are not the favorable operation mode of the LLC and provide little use in practice. Since the precise gain-frequency relation cannot be given in a simple and direct form, approximations are usually made to simplify the model in order to facilitate the applications. There are numerous approximation approaches based on different analytical model. A discussion on these approaches is presented in this chapter.

The operation mode model proposed in Chapter Two separate the LLC performance in different mode region, which make it even more complicated to obtain a full gain curve if it spans more than one mode. To avoid the complexity in solving the full voltage gain characteristic curve, we focus on the peak gain points instead. In the design procedure of the LLC converter, the peak voltage gain is a key parameter as it indicates the converter's capability in voltage regulation, which determines the minimum input voltage. The switching frequency at the peak gain is the lowest permissible operating frequency, as the slope of gain-frequency curve is reverse to positive below the peak, which will make the control loop unstable. Also, the LLC converter should operate above the frequency of the peak gain to stay in ZVS, since the peak gain is the boundary between ZVS and ZCS region. As aforementioned, many methods have been proposed to improve gain prediction accuracy or simplify the calculation, but there is no direct method to evaluate the

peak gain without using simulation tools or graphical method. The approximation method gives not only the peak gain value as a function of the switching frequency but also the corresponding load power, which can be conveniently employed to facilitate the converter design. The estimated results agree well with simulations and are proved by the experiment.

Besides peak gain approximation, the linear estimation of mode boundary between PO and PON mode is also investigated in this chapter. This boundary could be useful as it defines the border of the most desirable operation mode PO mode and is easier to obtain, and thus it is handy in drawing the operating region of the converter.

3.2 Discussion on Some Prior Approximation Methods

It is shown in previous analysis that the exact solution of the LLC operation is difficult to deduce and therefore inconvenient to use due to the resonant tank non-linearity. Various approximations are made to simplify the analysis. Frankly speaking, every analysis method has some degrees of approximation. The frequency domain methods like FHA are under the assumption that some voltage or current signals are pure sinusoidal. The state-plane or time domain methods are based on the use of ideal circuit components. There is no "exact" exact solution for a converter analysis. However, the discussion in this chapter is mainly about the design-oriented approximations made on time-domain converter waveforms to reduce the analytical and computational complexity.

One approximation approach for PO mode is to assume that the resonant current during stage O remains constant [66]. In stage O, L_m joins the resonance with L_r and C_r, and the characteristic frequency becomes $f_r/\sqrt{m}$. Although the actual resonant current i_r still varies

73

sinusoidally in this stage, the current looks flat if $f_r/\sqrt{m}$ is much smaller than the switching frequency, the output load resistance is low and the stage O duration is short compared with the switching cycle. Based on this approximation, the DC gain function can be derived directly from PO mode equations, which is given by

$$M = \left[1 - \frac{1-f_n}{4(m-1)} \left(\frac{\pi}{f_n} \right)^2 \right]^{-1} \tag{3.1}$$

where $f_n \leq 1$, since it only applies to PO mode. It can be seen that the gain is increased at a decreased f_n and m, which lines with the trends of real PO mode model. But the gain function is irrelevant to the load condition, which is obviously not true. However, as the approximated current waveforms will be more close to the actual ones at increased load condition, this function is used for full load to determine a proper m to meet the minimum input voltage requirement in the design procedure [66]. Other parameters of the converter waveforms can be obtained as well, such as the voltage and current stress across the capacitor and MOSFETs, which can help select the proper power devices.

This approximation introduces large errors in gain prediction because of the fact that the stage O resonant current is actually sinusoidal. To make up the deficiency, a modified approximation is proposed in [67], which, though still based on the observation that i_r looks flat in stage O, it only assumes that the start and end value of the stage O current is the same. By proper manipulating the mode equations, the load condition is linked to the parameters of the current waveforms and so is the gain. In [67], the approximation is used to estimate the "most important electrical quantities useful for the design of the converter" and the gain function is

74

buried in the L_m expression (Equation (42) in [67]). The explicit gain function can therefore be derived from it using the common symbols defined in this dissertation as follows:

$$M = \frac{\dfrac{\pi}{p_{on}} + 2(m-1)}{\dfrac{\pi^2}{2} + \dfrac{2(m-1)}{\eta}} \tag{3.2}$$

where η is the expected efficiency at minimum V_{in} and maximum load. Note that it is not a function of the switching frequency; it is because that, provided the stage O current assumption, the switching frequency is already determined by the load. So, the gain expression is only for one operation point at full load but not the entire curve, and the relation is employed to calculate L_m.

The problem in common of the approximations in [66, 67] is that the constrain condition on stage O current is too strong that some factor influencing the gain may be lost in the derivation.

Another approximation method is focused on the output current i_o through the rectifier [68], which assume that the rectifier current is a half sinusoidal pulse. Since the average i_o is the DC output current, the magnitude of i_o can be simply obtained from the load current. However, obtaining the conduction angle λ of the rectifier is not an easy job. To overcome this difficulty, an approximation method is presented in [68], from which λ can be expressed as a function of the normalized switching frequency f_n, normalized load power p_{on} and the inductors ratio m. After knowing the waveform of i_o, its fundamental component can be found and therefore the frequency domain method can be carried out in the subsequent derivation of the converter gain. From this perspective, it is similar to the describing function analysis method[51]. In summary, the gain acquired is a function of f_n, p_{on} and m, and the complete DC characteristic curve can be provided by this function, even though the approximation is targeted to PO mode. A comparison

with FHA is given, and it is seen that the differences are found in the below f_r region that the peak gain point has higher gain and lower frequency in the proposed method, while in the above f_r region the gain curves are mostly the same from the two methods. Another observation is that the resonant operating point is not truly load-independent but rather nearly independent at the vicinity frequency. From the mode analysis in Chapter, it is known that this statement only holds true for light load condition ($p_{on} < 2/\pi/(m-1)$) and for normal load the converter is load-independent at f_r. This method is less accurate for smaller m, as the sinusoid-like pulse of rectifier current i_o is the difference of the sinusoidal i_r and linear i_m in stage P or N, and the more flat i_m is, the more sinusoidal the i_o pulse shape becomes. Overall, the proposed approximation has improved accuracy over FHA and does not involve iterative computation keeping the calculation straightforward.

3.3 Peak Gain Approximation

From mode analysis, we know the peak of a gain curve can only occur in two modes, PN and PON mode. From PO or NP mode, if the switching frequency decreases and the load increases continuously, the resonant tank will eventually enter PON or PN mode region, where the gain curve will slow down its increase and finally starts to fall. The peak gain points also mark the boundary of inductive and capacitive impedance of the resonant tank; in other words, it is the ZCS and ZVS boundary. The resonant tank current i_r is synchronized with the input excitation voltage having no phase difference, which requires that i_r crosses zero at the moment the switches turn on or off. This zero current crossing condition can be expressed as

$$i_{rPn}(0) = i_{rNn}(\theta_N) = 0 \tag{3.3}$$

By applying this peak gain condition, the peak gain point in the two operation mode, PN and PON is study respectively.

3.3.1 Peak Gain in PN Mode

For PN mode, the voltage gain has closed-form solution, which can be derived from (2.13) in Chapter Two, but with the peak gain condition (3.3) a simple expression for gain can be found. From the symmetry conditions (2.6), it has the constraint $v_{CPn}(0) = -v_{CNn}(\theta_N)$. Substituting the expressions of i_r and v_C in stage P, N into (3.3) and (2.6), the peak gain of PN mode can be derived as

$$M_{pk} = \frac{2}{I_{rPn} - I_{rNn}} \tag{3.4}$$

where I_{rPn} and I_{rNn} are the normalized current magnitude of the resonant inductor L_r during stage P and N respectively. Their expression can be obtained by properly manipulating the mode equations (2.12), which give that

$$
\begin{aligned}
I_{rPn} &= \frac{\pi}{2(m-1)f_n \sin\theta_P}, \\
I_{rNn} &= \frac{\pi}{2(m-1)f_n \sin\theta_N}
\end{aligned}
\tag{3.5}
$$

where

$$
\begin{aligned}
\theta_P &= \frac{1}{2}\left[\frac{\pi}{f_n} + \cos^{-1}\left(\cos\frac{\pi}{f_n} - \frac{\pi}{2(m-1)f_n}\sin\frac{\pi}{f_n}\right)\right] \\
\theta_N &= \frac{1}{2}\left[\frac{\pi}{f_n} - \cos^{-1}\left(\cos\frac{\pi}{f_n} - \frac{\pi}{2(m-1)f_n}\sin\frac{\pi}{f_n}\right)\right]
\end{aligned}
$$

By substituting (3.5) into (3.4), an explicit expression of the peak gain is attained. It can be seen that the peak gain M_{pk} is a function of inductors ratio m and the switching frequency f_n.

When operating in PN mode, the LLC is under relatively heavy load condition and the operating frequency of the peak gain point is closed to resonant frequency f_r. This load power at the peak gain point can also be derived from (2.12), which is shown as follows:

$$p_{on} = \frac{1}{2(m-1)}\left(\tan\frac{\theta_P}{2} - \tan\frac{\theta_N}{2}\right) \tag{3.6}$$

It is also a function of m and f_n. Now, both the gain and load relation with m and f_n are developed and the peak gain trajectory can be plot on the mode distribution map as shown in Figure 3.1. However, PN mode is not a favorable mode for the converter for its low peak gain that it should generally be avoided and is less likely to come across in normal LLC operation.
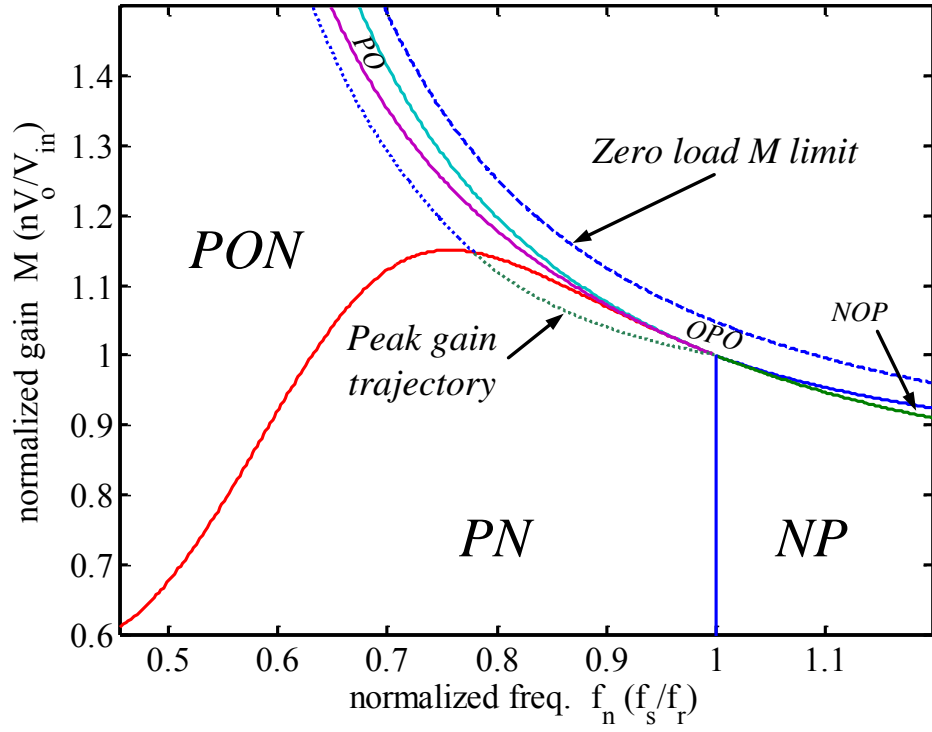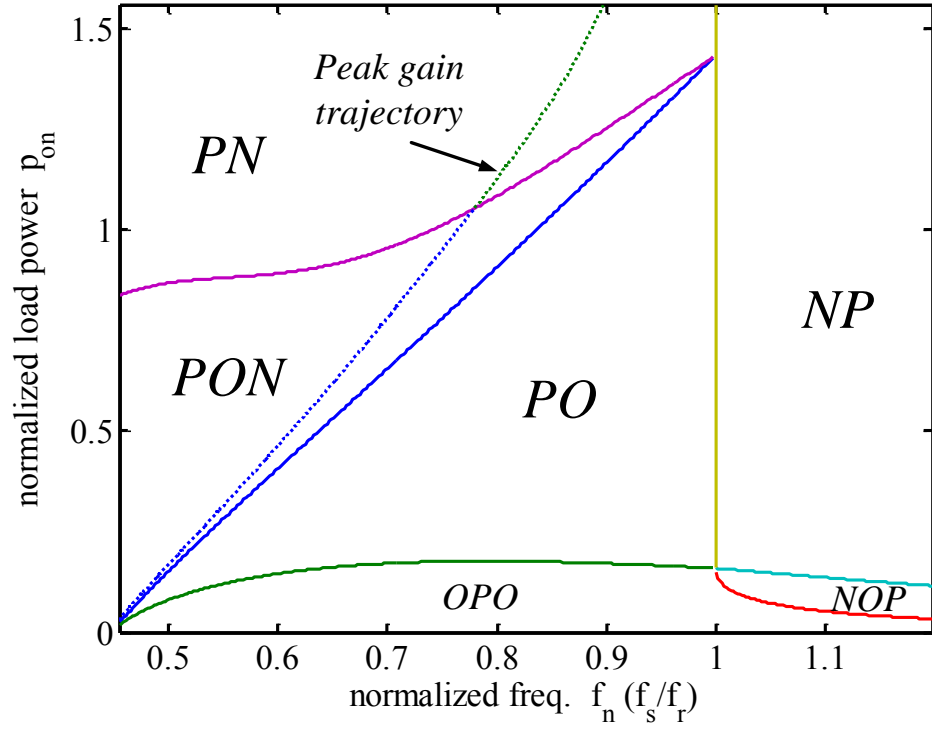
Figure 3.1 Peak gain trajectory (dash lines) on LLC mode distribution map (*m=5*)

3.3.2 Peak Gain in PON Mode

A gain curve with lighter load condition has a higher peak value and lower peak gain frequency, and therefore the peak point may move into PON mode. As aforementioned, the mode equations of PON have not closed-form solutions due to the nonlinearity brought by the discontinued stage O, and hence some approximate assumptions are made in this mode in order to calculate the peak gain.

Also, since PON and PN mode have the same start and end stage in the half cycle, the symmetry conditions (2.6) applied to both modes are the same. Therefore, after applying the peak gain condition (3.3), PON has the same peak expression as PN in (3.4), but the current parameters I_{rPn} and I_{rNn} have different expressions.

The current parameters I_{rPn} and I_{rNn} can be derived from peak gain condition (3.4) and boundary equations obtained by applying (2.6) – (2.9) to PON mode, and it gives that

$$
\begin{aligned}
I_{rPn} &= \sqrt{(I_{rOn}\sin\theta_{O0})^2 + (\sqrt{m}I_{rOn}\cos\theta_{O0} - 1)^2} \\
I_{rNn} &= \sqrt{I_{rOn}^2 - 1/(m-1)}
\end{aligned}
\tag{3.7}
$$

They can be represented by functions of I_{rOn} and θ_{O0}, but they have no further explicit forms. Hence, Matlab is used to find the numerical solutions of the peak gain equations for given m and f_n values. From the frequency-sweep results, it is observed that I_{rOn} is proportional to f_n, which decreases as f_n goes down. To simplify the calculation, we make the assumption that I_{rOn} is a linear function of f_n.

There are two peak gain points where I_{rOn} can be solved and used to determine the linear approximation function. One is at the zero load condition, whereas the other is at the boundary between PON and PN mode.

As the load is dropped to zero, stage O will span the whole switching cycle and thus θ_O equals π/f_n. However, it can still be treated as a special PON mode whose stage P and N have zero time duration ($\theta_P = \theta_N = 0$). The stage O constraint condition in (2.8) requires that $v_{mOn} = -1$ at the end of the stage, which is

$$\frac{m-1}{\sqrt{m}} I_{rOn} \cos(\theta_O / \sqrt{m} + \theta_{O0}) = -1 \tag{3.8}$$

Also, from the peak gain condition (3.3), the resonant current starts from zero at the beginning of the switching cycle, which indicates that the initial phase angle of the current, θ_{O0}, is also zero. Substituting this into (3.8) and applying the O mode symmetry condition (2.7), it can be solved that

$$\begin{aligned} I_{rOn0} &= \sqrt{m}/(m-1), \\ f_{n0} &= 1/\sqrt{m} \end{aligned} \tag{3.9}$$

where I_{rOn0}, f_{n0} are the resonant current magnitude and frequency at zero load. Hence, the peak gain point on zero load condition is settled.

Another point on the peak gain trajectory is at the boundary of PON and PN mode, which is also PN mode. Although there is no stage O in PN mode, the PON mode equations still applies by letting the duration of stage O equal to zero. The boundary stage O current magnitude I_{roNb} can therefore be solved as follows:

$$I_{rOnb} = \frac{1}{m-1} \sqrt{(\frac{\pi}{2 f_{nb}})^2 + m} \tag{3.10}$$

where f_{nb} denotes the boundary frequency of PN/PON. Note that f_{nb} is an unknown parameter. To solve f_{nb}, applying the boundary condition between PON and PN mode (2.16) and peak gain condition (3.3) to PN mode equations (2.12) yields that

$$\tan(\frac{\pi}{f_{nb}}) = \frac{m-1}{(2m-1)\frac{f_{nb}}{\pi} + \frac{\pi}{4f_{nb}}} \tag{3.11}$$

Unfortunately it is a transcendental equation of f_{nb} and thus has no explicit expression solution. However, it can be numerically estimated using curve-fitting technique. It is observed that f_{nb} tends to become smaller when m increases; as m approaches infinity, the limit of f_{nb} is 0.735; as m approaches infinity, the limit of f_{nb} is 1. Hence, the boundary frequency f_{nb} is evaluated as below:

$$f_{nb} = f_{nb\_min} + (1 - f_{nb\_min})/m^{1.11} \tag{3.12}$$

where $f_{nb\_min}=0.735$ is the lower limit of the frequency and the exponent of m, 1.11, is obtained from curve-fitting. The estimated result gives acceptable accuracy over a range of m. After knowing I_{roNb} and f_{nb}, the second point on the peak gain trajectory is determined.

Given two points' coordinates on a line, the line's equation can be uniquely determined. Therefore, the linear approximation function of the stage O current amplitude I_{rOn} can be expressed by the two-point form as

$$I_{rOn}(f_n) = (I_{rOn0} - I_{rOnb})\frac{f_n - f_{nb}}{f_{n0} - f_{nb}} + I_{rOnb} \tag{3.13}$$

The initial phase angle θ_{O0} of the resonant current at stage O cannot be approximated by the common linear or polynomial function, and the Newton-Raphson method is used. The Newton-Raphson method is a numerical root-finding algorithm for solving nonlinear one-variable equations. The equation of θ_{O0} can be derived after proper manipulation of the boundary conditions, which is

$$\cos(\beta)\theta_{O0} + \sin(\theta_{O0}) + \cos(\beta)(\frac{\pi}{f_n\sqrt{m}} - \beta) + \sin(\beta) = 0 \tag{3.14}$$

where β is the end phase angle of the current i_{rOn} in stage O. It can be expressed as a function of m and I_{rOn} which is derived from (3.8) as

$$\beta = \frac{\theta_O}{\sqrt{m}} + \theta_{O0} = \arccos\left(-\frac{\sqrt{m}}{(m-1)I_{rOn}}\right) \tag{3.15}$$

The Newton-Raphson method is an iterative calculation starting from an initial guess. The recurrence relation equation can be derived as

$$\theta_{O0k+1} = \theta_{O0k} - \frac{f(\theta_{O0k})}{f'(\theta_{O0k})} \tag{3.16}$$

To simplify the calculation, the first guess of the phase angle θ_{O0} is set to $\pi/2$ and the first iteration would give

$$\theta_{O01} = \frac{-1 - \cos(\beta)(\frac{\pi}{f_n\sqrt{m}} - \beta) - \sin(\beta)}{\cos(\beta)} \tag{3.17}$$

It is observed that two-time iterations can let the function converge to a close solution. The final expression for the phase angle θ_{O0} is given by

$$\theta_{O0} = \frac{\cos(\theta_{O01})\theta_{O01} - \sin(\theta_{O01}) - \cos(\beta)(\frac{\pi}{f_n\sqrt{m}} - \beta) - \sin(\beta)}{\cos(\theta_{O01}) + \cos(\beta)} \tag{3.18}$$

Hence, the peak gains in PON mode can be directly calculated by applying (3.18), (3.13) to (3.7) and then to (3.4). Regarding the load power at the peak gain point, it can be expressed as follows:

$$p_{on} = \frac{f_n}{\pi}\left[\frac{m-1}{2}(I_{rOn}\cos\theta_{O0})^2 - \sqrt{m}I_{rOn}\cos\theta_{O0} + \frac{m}{2(m-1)} \right.$$
$$\left. - \sqrt{I_{rOn}^2 - \frac{1}{m-1}} + \sqrt{(I_{rOn}\sin\theta_{O0})^2 + (\sqrt{m}I_{rOn}\cos\theta_{O0} - 1)^2}\right] \tag{3.19}$$

3.3.3 Approximation Results

To verify the effectiveness of the peak gain approximation, we calculate the peak gain for the LLC prototype built in Chapter Two, and the peak estimates is plotted on gain curve plot (Figure 2.21) with the experimental data as seen in Figure 3.2. The result shows that the estimated peak gain trajectory crosses the measured peak points closely.
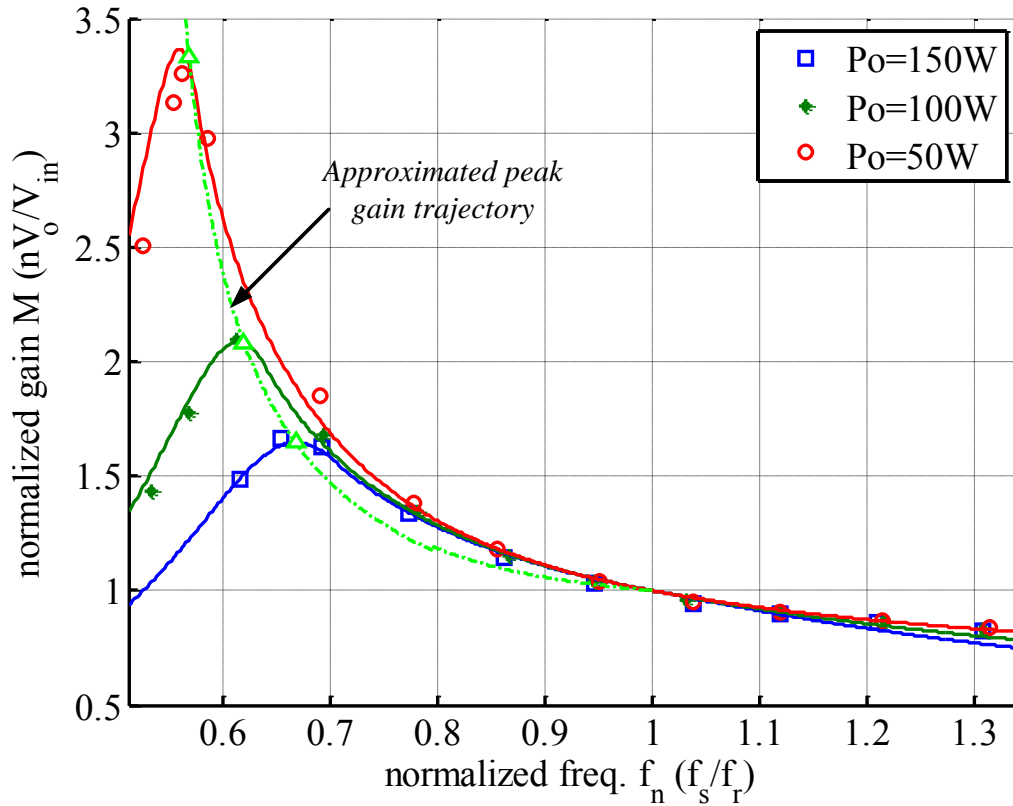
Figure 3.2 Gain curves obtained from mode analysis (solid lines), and experiment (markers), and estimated peak gain trajectory (dash-dot lines) with "Δ" markers showing the estimated peak gain points at corresponding loads.

To investigate how different m values affect the peak gain, we also use circuit simulation tools to observe the gain characteristic and compare with the approximation approach. Figure 3.3 shows a 3-D plot of peak gain trajectories and the peak gain-load and peak gain-frequency

relations are shown in the 2-D Figure 3.4. In both figures, peak gains for $m = 2,3,...,9$ from both the approximation method and the simulation results are plotted. Note that the simulation only shows the peak gain results in PON mode, since in PN mode the peak gain has an exact solution given by (3.4) and (3.5). It can be seen that the approximation matches the simulation. . From Figure 3.4, the corresponding frequency and load for given m and peak gain values can be easily obtained. Although the peak deviation becomes larger at a decreased frequency for large m, the approximation method has huge advantage over the simulation method for the convenience and less time consuming.

The following peak gain characteristics can be learned: the peak gain of the LLC decreases as the inductor ratio m increases; for heavy load condition, all peak gain trajectories converge towards to the resonant frequency (see Figure 3.3); for a lighter load condition, the converter can achieve higher peak gain at a lower frequency.
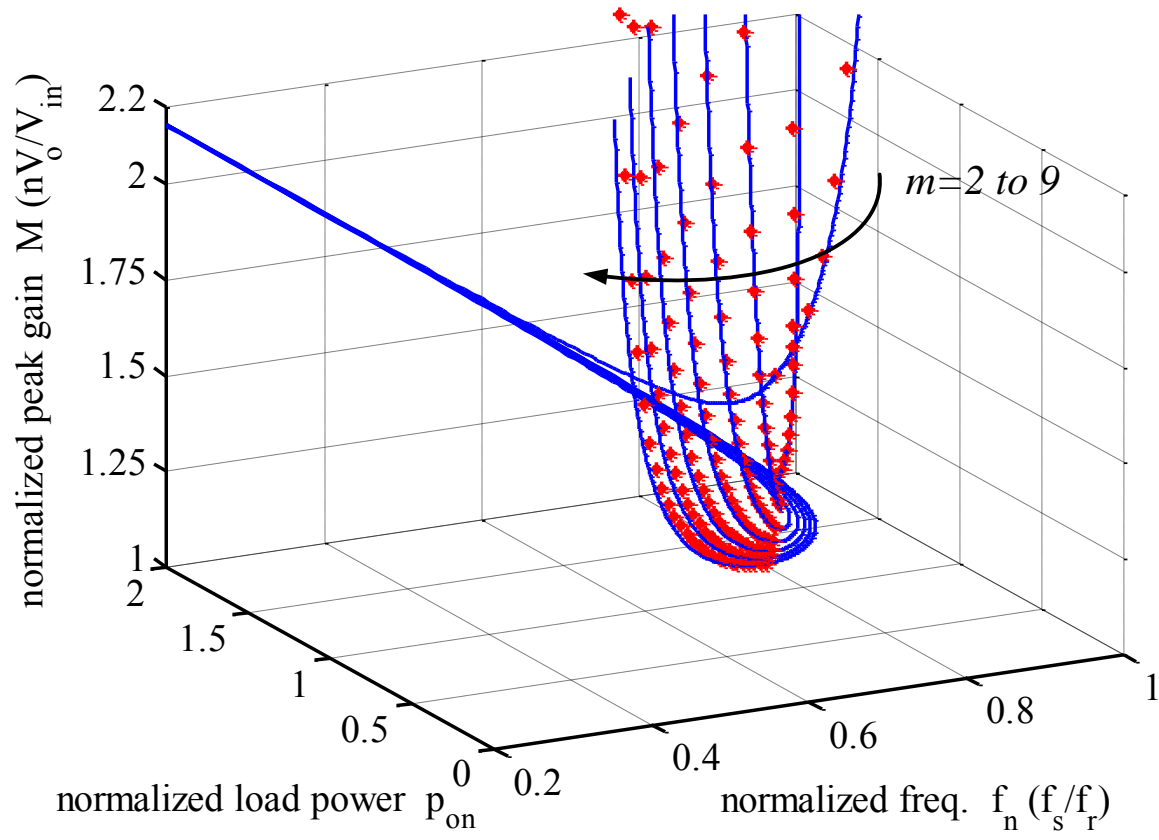
Figure 3.3 The 3-D peak gain trajectories for m from 2 to 9, where solid lines are obtained from the proposed approximation method and markers are from simulation result
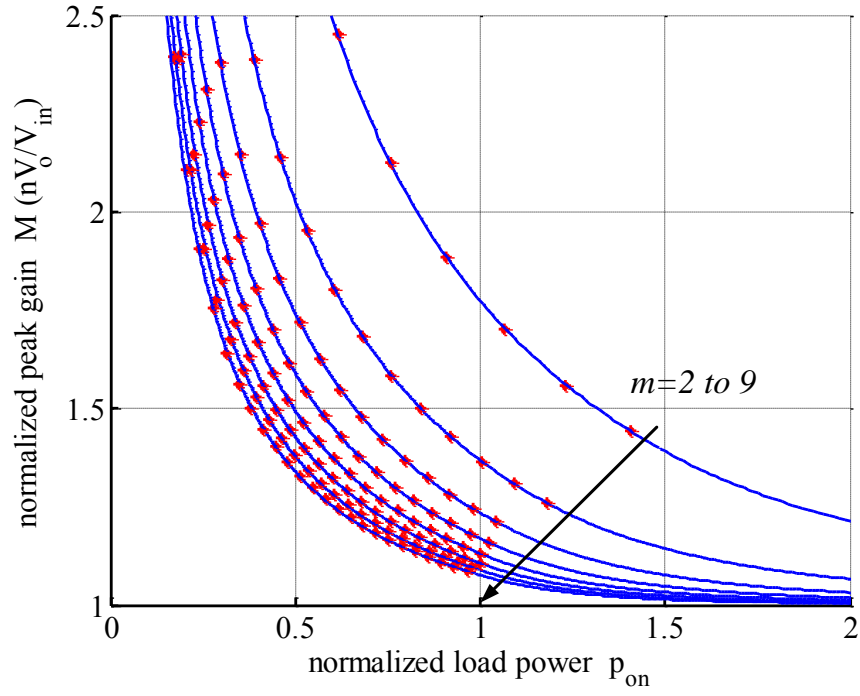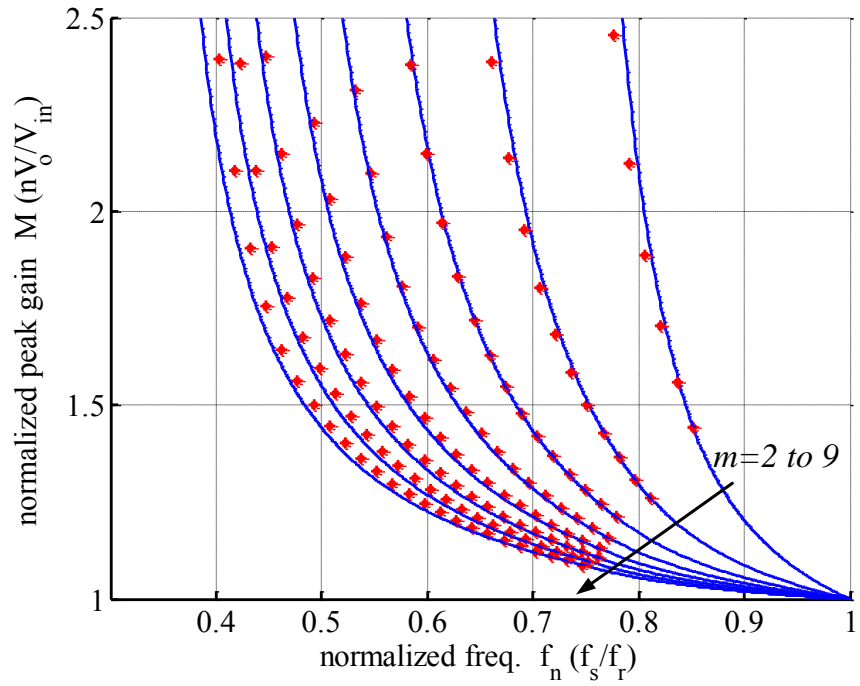
Figure 3.4 Comparison between proposed approximation method (solid lines) and simulation result (markers) under various m: (a) peak gain vs. load, (b) peak gain vs. frequency.

3.4 PO Mode Boundary Approximation

From mode analysis, it is known that PO mode is the preferable operation mode for the LLC converter for its merits like achieving ZVS, no reverse recovery issue of rectifiers and maintaining control loop stability. In the previous section, a peak gain approximation method is developed and it is said that the frequency at the peak points can be treated as the lower limit of the operating range. However it is based on the considerations that the converter should not enter ZCS zone and prevent instability caused by positive gain curve, the converter may still operate in PON or PN mode near the peak gain points. It would be useful for converter designers if there is a handy way to know the region of PO mode so that the LLC can be confined within this mode to achieve optimum performance. In this section, the mode boundary approximation is discussed.

From the mode distribution map shown in Figure 3.1, it can be seen that the boundary line between PO and PON mode on the load-frequency plot resembles a straight line. To consolidate this impression, more PO/PON boundaries are drawn in Figure 3.5, where each line is for a different inductors ratio m as it is the only factor that can change the mode borders in the normalized mode map analysis. The boundary lines started from a high load power at $f_n = 1$ is more in linear shape, and the boundary has a smaller load following the decrease of frequency, and, as the line ends towards zero load condition, it bends and compromises the linearity.
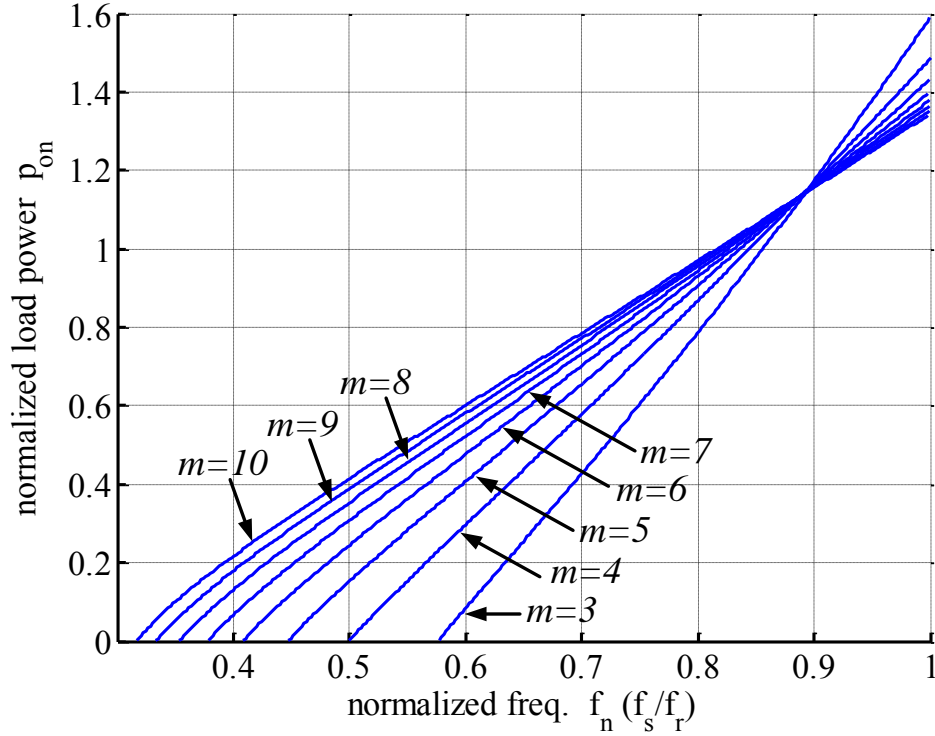
Figure 3.5 The PO and PON mode boundaries over different inductors ratio m

It needs the coordinates of two different points on a line to determine the line equation on a 2-D plane: for the PO/PON mode boundary, one is the border intersection point at $f_n = 1$ and the other is the intersection at $p_{on} = 0$. At the resonant frequency, PO, PON and PN mode all converge to one boundary point with $p_{on} = 2(2m - 1)/(m - 1)/\pi$, whose detailed analysis is presented in Chapter 2.3. At the zero load condition, the boundary intersection is also a convergence point of three modes, PO, PON and OPO mode. The PO/PON boundary mode is PO mode, whose boundary condition requires that the end value of v_m in stage O is equal to $-nV_o$, and the gain should be monotonically increasing as load decreasing. Ideally, at zero load, the gain should approach infinity, which can be expressed by the v_c continuity condition as follows

$$\sqrt{m}I_{rOn}\cos\left(\frac{\pi}{2f_n\sqrt{m}}+\theta_{O0}\right)\cos\left(\frac{\pi}{2f_n\sqrt{m}}\right)=\frac{1}{M}\bigg|_{M\to\infty}=0 \qquad (3.20)$$

From the i_r symmetry condition, it is given that

$$I_{rOn}\sin\left(\frac{\pi}{2f_n\sqrt{m}}+\theta_{O0}\right)\cos\left(\frac{\pi}{2f_n\sqrt{m}}\right)=0 \qquad (3.21)$$

Combining the above two equations, the feasible solution is that $f_n = 1/\sqrt{m}$. Note that it is the same frequency for peak gain point at no load, since they all share the same infinity gain condition.

Provided the coordinates of the two points, the slope of the boundary line is given as below:

$$k=\frac{2\sqrt{m}(2m-1)}{\pi(\sqrt{m}-1)(m-1)} \qquad (3.22)$$

Hence, the line equation can be expressed as

$$p_{on}=k(f_n-1)-\frac{2(2m-1)}{\pi(m-1)} \qquad (3.23)$$

The estimated PO/PON boundaries for different m are plotted on Figure 3.6. It can be seen that: the boundary $p_{on}(f_n)$ is convex downwards for small m ($m < 4$), and is concave upwards for large m ($m > 6$); for intermediate m ($4 < m < 6$), the boundary $p_{on}(f_n)$ is convex downwards in high frequency and concave upwards in low frequency.
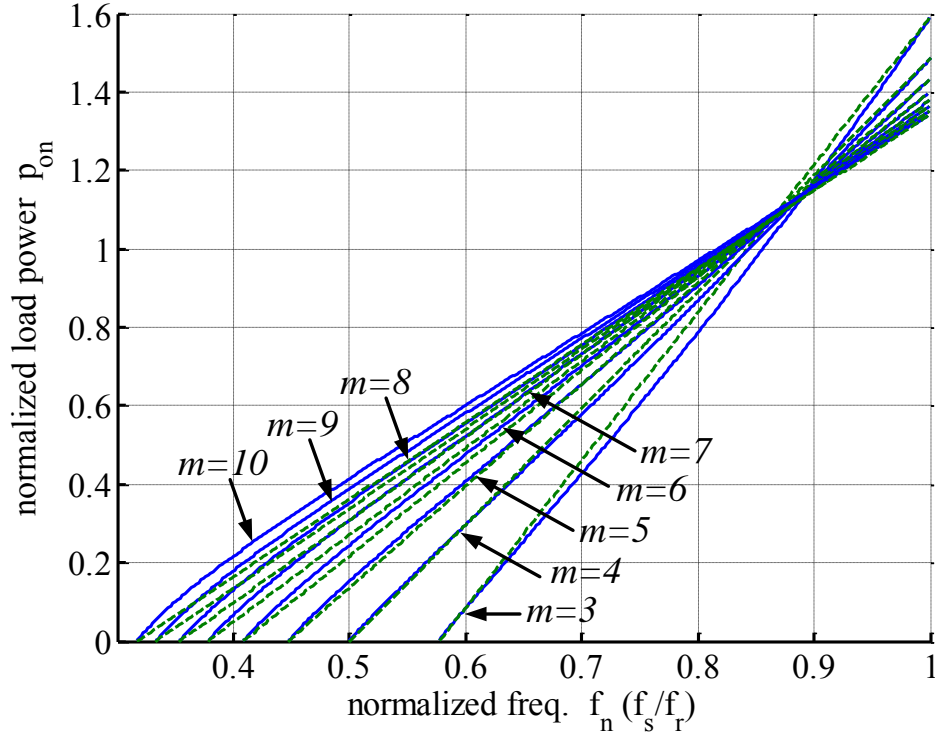
Figure 3.6 The PO and PON mode boundaries from mode model (solid lines) and approximation (dash lines) over different inductors ratio m

The error between the actual and the approximated boundary load is plotted in Figure 3.7. For a small m, the estimated load is higher than the actual load in the high frequency region, and smaller than the actual value in the low frequency region. But as m increases above 6, the error will always be positive, which means that the estimates are smaller than the actual values. In general, the load error is within 0.05 for $m = 3$ to 9. However, since the boundary load is falling at a decreased frequency, the percentage error in lower frequency region is much higher than in higher frequency region. Fortunately, the high error region is for light load and low frequency condition, which is usually avoided in LLC design to ensure the converter's operation in desirable ZVS region, this boundary approximation is valued more for its accurate prediction for normal load condition.
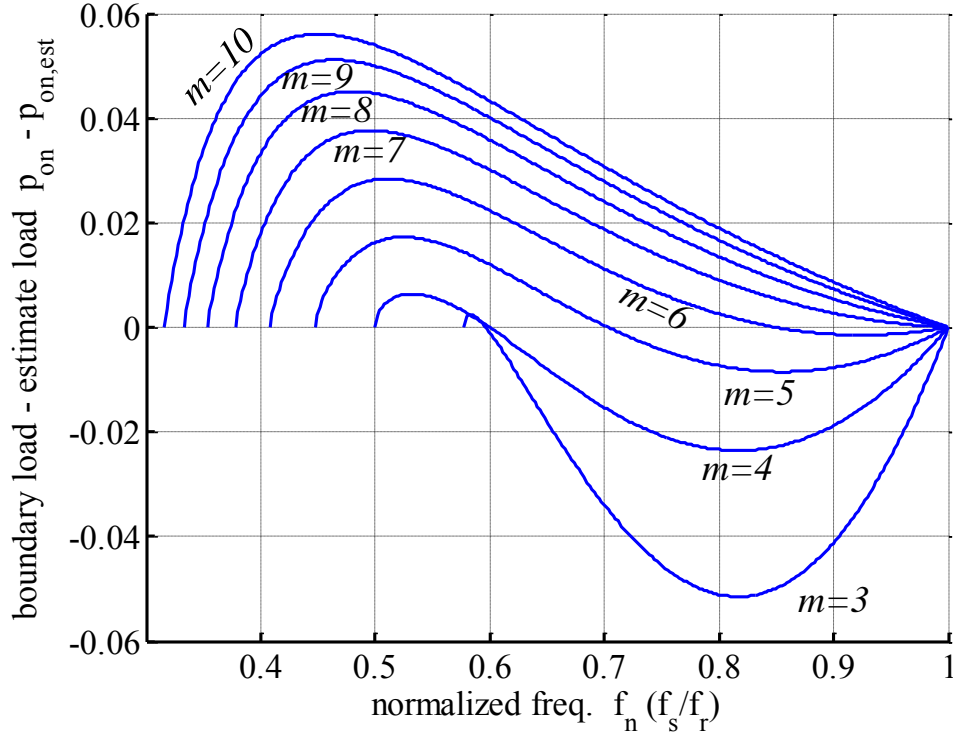
Figure 3.7 The PO and PON mode boundaries from mode model (solid lines) and approximation (dash lines) over different inductors ratio m

Also, the gain at the PO/PON mode boundary can be calculated from solving the corresponding mode equations, and the result is illustrated in Figure 3.8 with the peak gain trajectories. It can be seen that the peak gain point has lower frequency than the boundary at the same gain level, but the two gain curves of the same m go closer together at a decreased frequency.
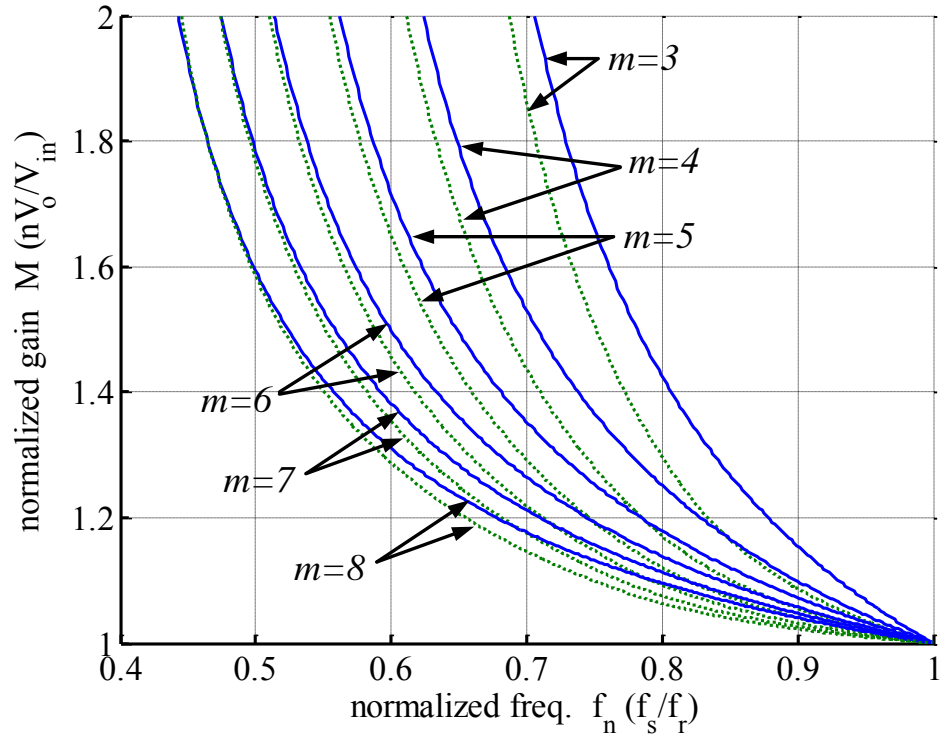
Figure 3.8 The PO and PON mode boundary gains (solid lines) and peak gain trajectories (dash lines) over different inductors ratio m

CHAPTER FOUR: DESIGN OPTIMIZATION OF THE LLC CONVERTER

4.1 Introduction

The LLC topology is similar to series resonant converter (SRC) but has three resonant components, L_m, L_r and C_r instead of two. The complex resonant circuit behavior and various operation modes of the LLC make it less intuitive and even difficult in selecting the resonant components and optimizing the L-C parameters in converter designs.

Several optimal design methodologies have been proposed to facilitate the LLC design. But they are either based on approximate models with limited accuracy or based on complex models which are cumbersome in practice use. Due to lack of convenient analysis method, previous design methods often rely on circuit simulation or graphical design tools. Another limitation of the existing design strategies is that some rely on pre-chosen circuit components like MOSFETs or operation parameters like dead time to finalize the design of the resonant tank. In this chapter, we develop an optimal design method based on the operation mode model, and the resonant tank parameters are normalized in this method to generalize the discussion.

The difficulty in the converter design is making the compromise between achieving wide gain range and high efficiency. The LLC analysis shows that for a certain load condition the gain-frequency curve has its peak point which is affected by the resonant components C_r, L_r, L_m values, or particularly the inductors ratio m if using normalized resonant frequency f_r. The peak gain rises higher for a smaller m. In other word, the input voltage range could be wider for a smaller m. With that said, it does not mean that the magnetizing inductor should be set as small as possible. During stage P and N, the magnetizing inductance determines the changing rate of the magnetizing current i_m: the linear waveform of i_m becomes steeper with a smaller m. It could

94

increase the power losses with the resonant currents affected by the parameter m. Therefore, the goal of the optimal design is to find the suitable circuit parameters satisfying the design specifications while pushing the converter power efficiency as high as possible.

In this chapter, a review of prior design methods are given; the relation between the circuit parameters and the resonant currents, which is related to the power losses, is analyzed and discussed; three optimal design methods is proposed to be applied to different application scenarios, and a design example is given and verified by experiments; the generalized LLC optimization is discussed to summarize the basics and principles in resonant tank design considerations.

4.2 Review on Prior LLC Design Methods

With the increase popularity of the LLC resonant converter in various applications, the demand of the design methodologies to meet the various design objectives and specifications and find the optimal converter configurations is rising in tandem. Many design approaches are developed aiming at this topology, all of which are based on a certain analytical method or model, either an exact model or an approximation method, to evaluate the performance and guide the design of the converter circuit. Since the analysis and estimation of the LLC are covered in the previous two chapters, the discussion here is mainly concentrated on the design considerations and the optimization principles of different methods, but not the difference between analysis tools. Also, it should be noted that some studies on improving the performance of the LLC converter, which are about the magnetic or conductive component integration or the rectifiers or switches driving schemes, are not included, and the optimization here refers to the resonant tank component configuration, the inductors and capacitor values setting.

95

In [69], the optimization target parameters are chosen as the inductors ratio L_n (related to m as $L_n = m + 1$) and the characteristic factor Q ($Q = \frac{\sqrt{L_r/C_r}}{n^2 R_{load}}$ is related to the load condition). If L_n and Q are determined, the LLC components can be calculated accordingly. The importance of obtaining the peak gain capability is emphasized, and the peak values are affected by L_n and Q. If the resonant frequency and load resistance are specified, the product of L_n and Q is proportional to the magnetizing inductor L_m. It is found that a larger L_m is desirable to achieve minimum conduction loss, but it is limited by the dead time and MOSFETs' junction capacitance in order to ensure soft switching. The max L_m can be determined by the switching frequency, the dead time and the MOSFET capacitance, and therefore the product of L_n and Q can be fixed. The peak gains that can be achieved for different L_n and Q combination are given graphically as shown in Figure through circuit simulation tools. According to the peak gain requirement and the determined L_m, the selecting range for the suitable L_n and Q combination can be plotted on the peak gain graph. Other design considerations need to be included to settle the final value of L_n and Q. The switching frequency range is narrowed for a decreased L_n, but a larger L_n can make the transformer design easier. Although this tradeoff problem of choosing L_n is raised, a clear selection criteria is not given in [69]. From its design procedure, the dead time and MOSFET capacitance is required by this approach as known parameters. However, the MOSFET selection in practical design is usually weighed together with the resonant tank configurations, and the dead time is an adjustable parameter. By relaxing these two parameters, more freedom is given to L-C value choosing so that a better design may be achievable.

In [70], the effect of different dead time setting on the power losses is analyzed, and an improved design procedure based on [69] is proposed. It is found that the conduction and

switching losses at the resonant operating point is only determined by the magnetizing inductor, and an optimal L_m value exists when considering the total losses and the overall efficiency of different load. As L_m is determined by the dead time, the optimal dead time can be calculated from the optimal L_m in reverse. The following design steps are the same as in [69].

4.3 Discussion on L-C Parameters and Resonant Tank Currents

The L-C parameter configuration of the resonant tank is closely related to the resonant and magnetizing current, and therefore connected to the conduction losses. By proper setting the inductors and capacitor values, the optimal set can be achieved under the minimal conduction losses circumstance. Therefore, it is vital to find out the relationship between L-C values and the currents.

From the mode analysis in Chapter 2, it is found that the LLC resonant current would be pure sinusoidal when the switching frequency is at the resonant point, which is in P mode; the mode equations in this mode have closed-form solutions, which give the expression of the magnitude of the resonant current I_{rPn} and the initial magnetizing current I_{mPn} as follows:

$$I_{rPn} = \frac{\pi}{2}\sqrt{p_{on}^2 + \frac{1}{(m-1)^2}} \tag{4.1}$$

$$I_{mPn} = -\frac{\pi}{2(m-1)} \tag{4.2}$$

Note that since the magnetizing current waveform is in triangle wave shape with zero DC offset for P mode, I_{mPn} is also the negative peak value of the triangle wave. The root mean square (RMS) of the currents i_r and i_m are therefore given by

$$I_{rRMSn} = \frac{\pi}{2\sqrt{2}} \sqrt{p_{on}^2 + \frac{1}{(m-1)^2}} \qquad (4.3)$$

$$I_{mRMSn} = \frac{\pi}{2\sqrt{3}(m-1)} \qquad (4.4)$$

The normalized RMS currents are related to the inductors ratio m and the normalized load power p_{on}. It appears that for a given load condition, the RMS currents will be lower if m increases, and so does the conductions loss. To de-normalize the current parameter, it should be multiplied by (nV_o/Z_r), where $Z_r=(L_r/C_r)^{0.5}$; regarding the load power, p_{on} can also be de-normalized in the similar manner. Then, the actual RMS currents become

$$I_{rRMS} = \frac{\pi}{2\sqrt{2}} \sqrt{\frac{P_o^2}{(nV_o)^2} + \frac{(nV_o)^2}{(m-1)^2 Z_r^2}} \qquad (4.5)$$

$$I_{mRMS} = \frac{\pi}{2\sqrt{3}(m-1)} \frac{nV_o}{Z_r} \qquad (4.6)$$

For a converter design, the output voltage is given as one of the specifications. Thus, the actual RMS currents are also connected to the transformer turns ratio n and the characteristic impedance Z_r.

When the converter is operating in other modes, there are no simple expressions for the RMS currents. Although the CCM, PN and NP mode, has closed-form solutions for the currents, the correlation between the currents and the circuit parameters is still implicit, not to mention in the DCM the closed-form solutions cannot be found for mode equations. Therefore, the study of the currents and the interrelated resonant tank configuration is carried out with recourse to the numerical tools. The precise current and voltage waveforms can be solved numerically from the mode equations using MATLAB, and hence the RMS of these waveforms can be calculated.

From the normalized current waveforms, the normalized RMS currents can be expressed as follows

$$I_{rRMSn} = \sqrt{\frac{f_n}{\pi} \int_0^{\pi/f_n} i_r{}^2 d\theta}$$

$$I_{mRMSn} = \sqrt{\frac{f_n}{\pi} \int_0^{\pi/f_n} i_m{}^2 d\theta}$$

(4.7)

The RMS currents for different load and frequency condition are plotted in Figure 4.1 for a fixed m (=5). It can be seen that: at the resonant point ($f_n = 1$) i_r's RMS is proportional to p_{on}; while the magnetizing current i_m has the same RMS value, which match the description of (4.3), (4.4); in above-resonance ($f_n > 1$) region, I_{rRMSn} is almost independent of the frequency change, while I_{mRMSn} decreases at an increased frequency but is independent of the p_{on} differences. The magnetizing current is less affected by the load change comparing to the resonant current, as i_m indicates the base level of the circulating current in the tank and is mainly determined by the clamped output voltage and the magnetizing inductance. In below-resonance ($f_n < 1$) region, I_{rRMSn} increases as the frequency decreases at first but may reach the peak and starts to decreases slowly, while I_{mRMSn} generally increases with the frequency decreasing but the changing rate varies for different load.
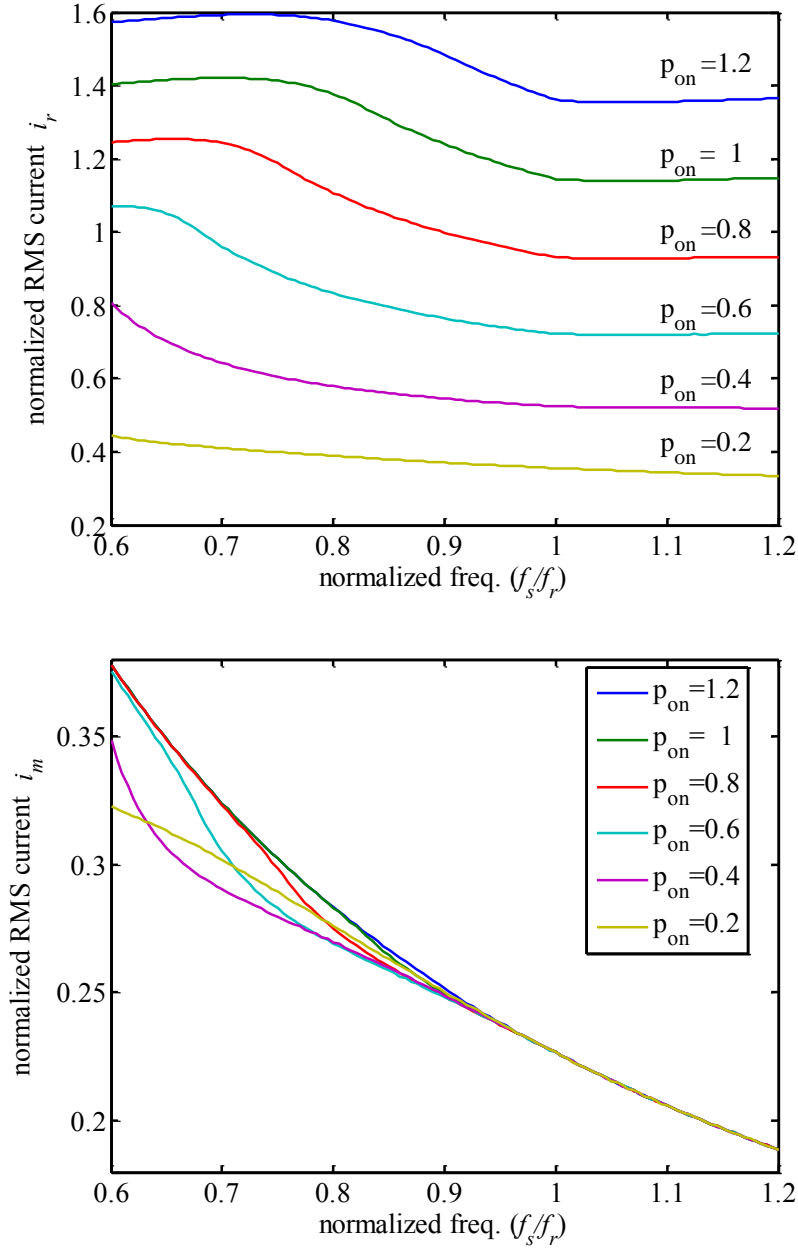
Figure 4.1 Normalized RMS currents under different frequency and load conditions (*m=5*)

In order to analyze how different tank parameters affect the power performance, the actual

RMS currents for different configurations should be compared under the same load power level.

Since the actual current equals the product of normalized current and based current ($I_{base} = $

V_{base}/Z_r), the actual current can be linked with the normalized load power (p_{on}) as the following expression:

$$I = I_n I_{base} = I_n \frac{V_{base}}{Z_r} = \frac{P_o}{V_{base}} \frac{I_n}{p_{on}}$$ (4.8)

where

$$Z_r = \frac{(V_{base})^2}{P_o} p_{on}$$ (4.9)

For the same load power and output voltage rating, P_o and V_{base} should remain constant. Therefore, the actual current can be directly reflected by I_n/p_{on}, and p_{on} is proportional to Z_r. The relation between I_n/p_{on} and f_n is shown in Figure 4.2. It can be observed that for both i_r and i_m, I_n/p_{on} over a range of frequency is generally smaller for an increased p_{on}. In other words, the actual RMS currents will decrease with larger tank impedance Z_r. For a certain load power and inductors ratio m, the LLC with a greater Z_r value is beneficial as the conduction loss will be lower.
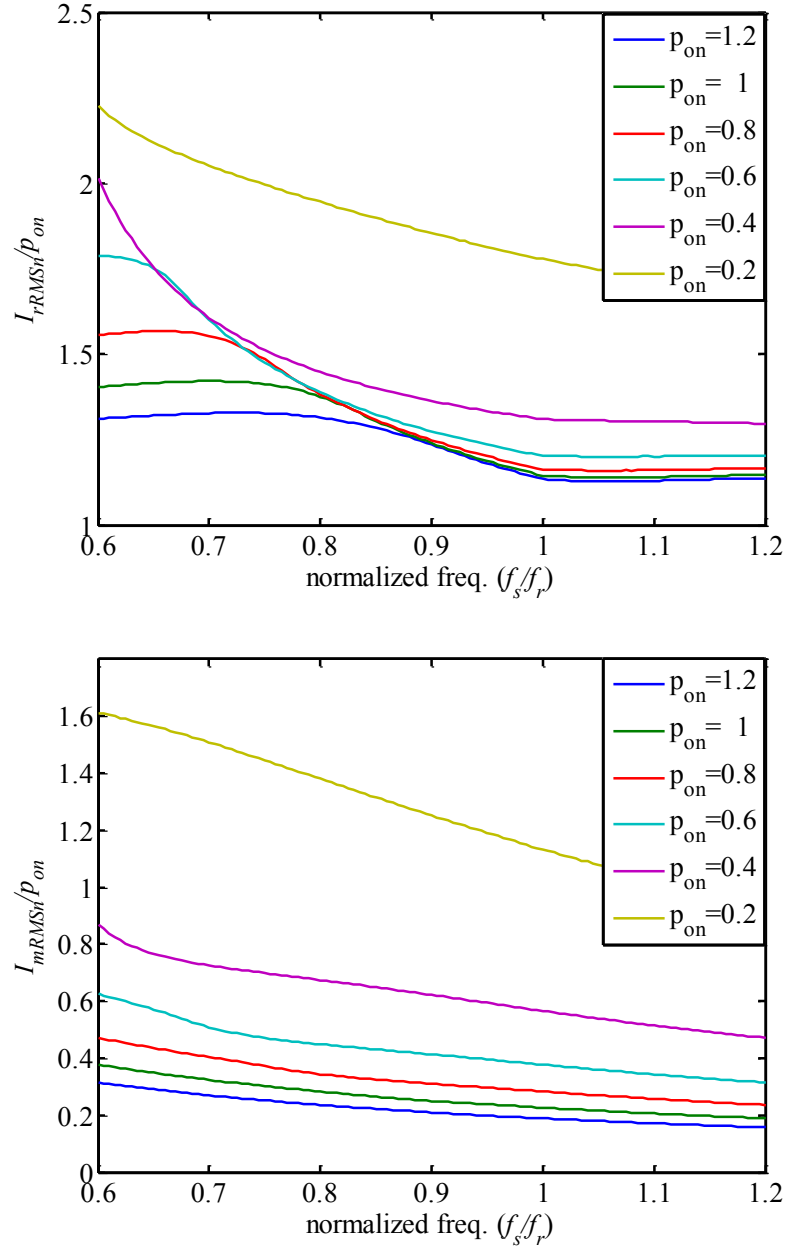
Figure 4.2 I_n/p_{on} under different frequency and load conditions

If we fix the normalized load power ($p_{on} = 0.6$) and let the inductors ratio m vary, another plot of the normalized RMS currents can be obtained as shown in Figure 4.3. Since p_{on} is fixed, the normalized currents here can indicate the actual current level. It can be seen that both

RMS currents, I_{rRMSn} and I_{mRMSn}, will decrease as m increases over the entire frequency changing range.
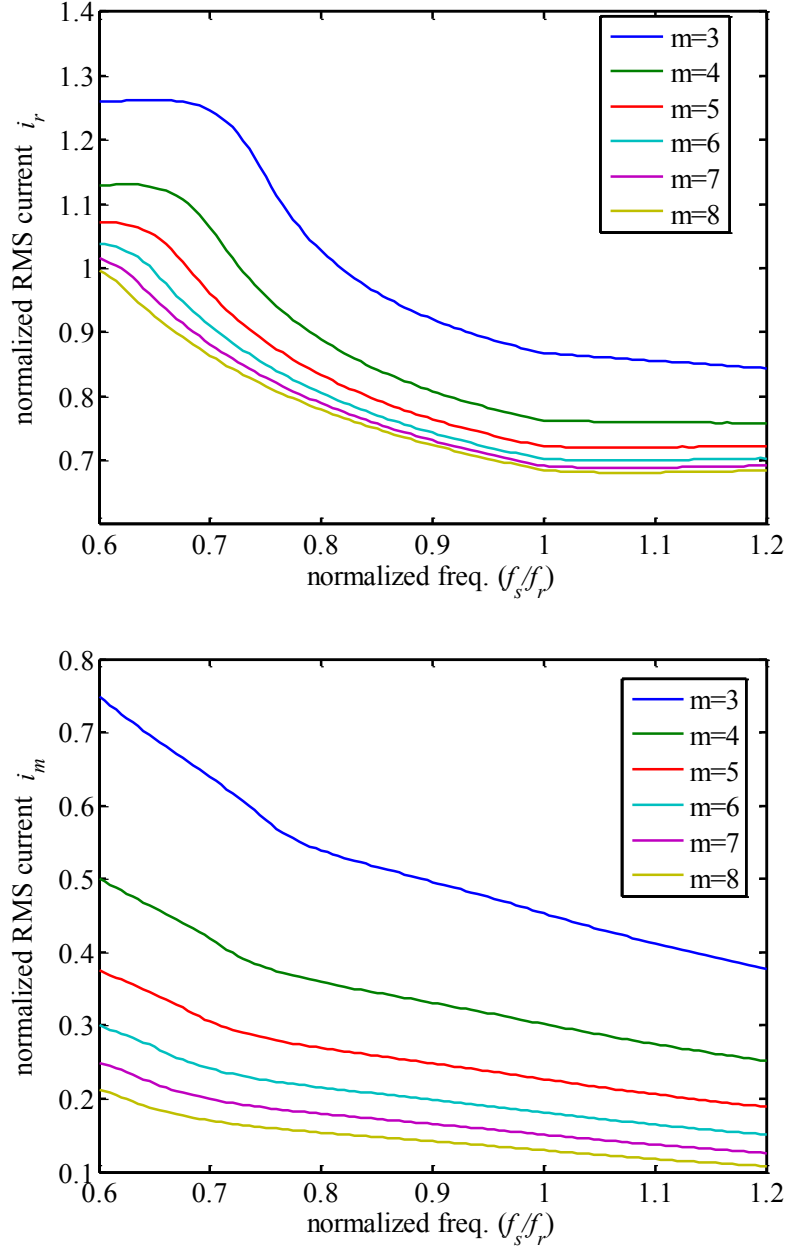
Figure 4.3 Normalized RMS currents under different frequency and m ($p_{on}=0.6$)

To further demonstrate the correlation of I_{rRMSn}, I_{mRMSn}, m and p_{on}, the 3-D shaded surfaces are built in Figure 4.4, in which the smooth surface (upper surface) is for operating at

103

$f_n = 0.8$ and the mesh surface (lower surface) is operating at $f_n = 1$. The topography of the RMS current surface goes low towards the growth direction of m and p_{on}, which is consistent with previous discussion.

From the above discussion, the resonant tank configuration and currents correlation is revealed. Roughly speaking, the RMS currents would be lower as well as the conduction losses if the inductors ratio *m* or the characteristic impedance Z_r is increased or the turns ratio *n* is decreased. In the LLC design, this relationship is very useful in guiding the L-C selecting to improve the power efficiency. However, the design specifications will put more constraints on the resonant tank setting like the input voltage range or the frequency variation range, and these restraints should be taken into account with the L-C and i_r, i_m relation to get the optimum design. The optimal design method will be present in the next section.
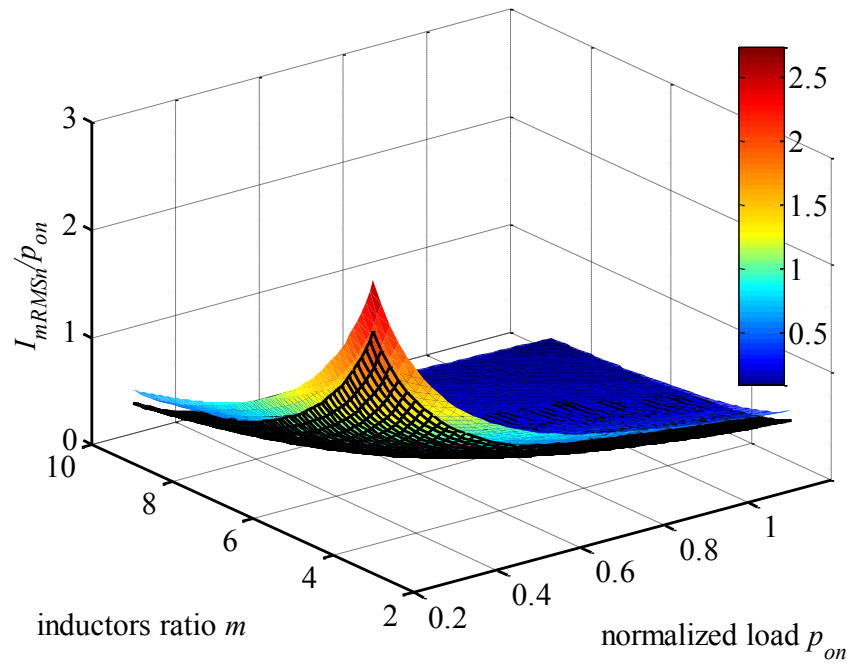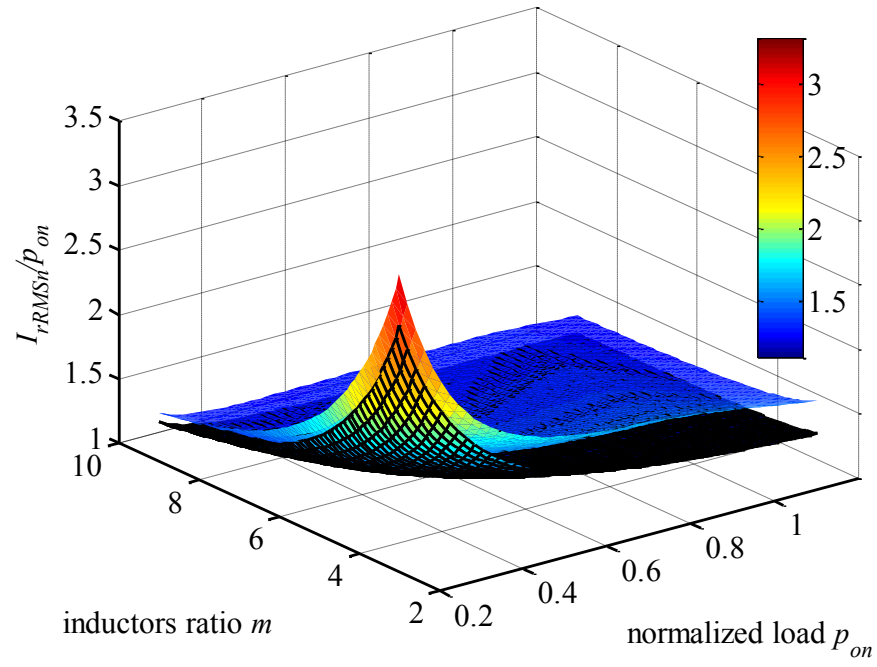
Figure 4.4 I_n/p_{on} for different m and p_{on} (upper surface $f_n=0.8$, lower surface $f_n=1$)

4.4 LLC Optimal Design Methods

As aforementioned, one major consideration of the LLC design is to maximize the efficiency while satisfying the gain requirement for the specified input voltage range or frequency range. For different application cases, the design strategy should be varied to fit the situation. In general, the design cases are divided into three scenarios: one is for the converter with a narrow input variation, one is for the converter with a wide input range and one is for the converter with large output current rating.

4.4.1 Optimal Design for Narrow V_{in} Range

If the input voltage variation is very narrow and the normal operation condition is set at the resonant frequency to maximize the efficiency, the circuit optimization efforts should be focused on minimizing RMS currents in P mode and thus the above expressions can be used to guide the design. For P mode, the gain M is load-independent and always equal to unity as long as the normalized load p_{on} is larger than $2/\pi/(m-1)$ (see Chapter 2.3). So the transformer turns ratio n is determined by $n=V_o/V_{in,norm}$, where $V_{in,norm}$ is the normal input voltage. In case the load condition is lighter than $2/\pi/(m-1)$ and the converter enters OPO mode and has higher gain, the switching frequency should be above f_r to adjust it. If the input voltage has a small disturbance and becomes smaller than the normal level, the operation frequency will go below f_r to let the converter have a higher gain. In this case, the LLC ought to operate in PO mode and prevent PN mode, as in PN mode the ZVS condition will be lost and the gain curve possibly will have a positive slope causing unstable control problem. To avoid PN, the normalized load power should

be lesser than $\frac{2(2m-1)}{\pi(m-1)}$ (see Chapter 2.3), which is the converging point of PO/PON/PN boundaries on P mode. This condition can be expressed in terms of the impedance Z_r that

$$Z_r < \frac{2}{\pi} \frac{2m-1}{m-1} \frac{(nV_o)^2}{P_{ofull}} \qquad (4.10)$$

Applying this inequality (4.10) to the RMS current functions (4.5), (4.6), it can be derived that

$$I_{rRMS} > \frac{\pi}{2\sqrt{2}} \sqrt{\frac{P_o^2}{(nV_o)^2} + \frac{\pi^2}{4(2m-1)^2} \frac{P_{ofull}^2}{(nV_o)^2}} > \frac{\pi}{2\sqrt{2}} \frac{P_o}{nV_o} \qquad (4.11)$$

$$I_{mRMS} > \frac{\pi}{4\sqrt{3}(2m-1)} \frac{P_{ofull}}{nV_o} \qquad (4.12)$$

It can be seen that for a sufficiently large inductors ratio m, both RMS currents will be closed to their minimum values. As m approaches infinity, the max impedance will be equal to $4(nV_o)^2/$ (πP_{ofull}). In other words, the inequality (4.10) always holds true for any m value by setting the impedance equal to $4(nV_o)^2/(\pi P_{ofull})$, and therefore it is the maximum impedance Z_r value. The impedance Z_r is constrained by this upper limit in order to give margin for PO mode, but it does not necessarily mean that setting Z_r close to this limit help reduce the RMS currents. Because the RMS currents are also affected by the inductors ratio m, for a smaller Z_r the potential room for m to grow might be larger and therefore is more beneficial in reducing the currents. Consequently, in order to get a more precise optimum setting of the resonant tank, addition efforts are needed using searching method to determine m and Z_r. In this case, the design will become a recursive approach.

To minimize the RMS currents, the product of $(m - 1)$ and Z_r should be maximized. For a certain design task, the load power rating and the output voltage are given in the specs, and from (4.8), Z_r can be indicated by p_{on} and the inequality (4.10) can be rewritten as follows:

$$p_{on} < \frac{2}{\pi} \frac{2m-1}{m-1} \tag{4.13}$$

Therefore, $(m - 1)p_{on}$ are chosen instead as the optimization target, which are the normalized parameters and can be directly applied to the operation mode model.

Although the input variation is small, it should be considered in the design procedure that the converter should be able to provide sufficiently large gain to cover the minimum V_{in} condition. It requires that the LLC operates below the resonant frequency; the minimum switching frequency is limited by the design specifications. Therefore, we take the gain and switching frequency drift from the normal operation point as known parameters, which are defined as below:

$$\Delta M = \frac{V_{in,norm}}{V_{in,\min}} - 1$$
$$\Delta f_n = 1 - f_{n\min} \tag{4.14}$$

The inductors ratio m cannot be arbitrarily large as the gain will decrease with the increase of m outside P mode region. Also, the gain has a tendency to decrease when the load rises if other conditions and circuit parameters are fixed. To provide the required ΔM with Δf_n, if we increase m, the corresponding p_{on} should be decreased. Therefore, there is an optimal point giving the maximum $(m - 1)p_{on}$.

For a predetermined m, the upper boundary of p_{on} is given in (4.13), which can be treated as a starting point. As m, p_{on} and the frequency range are known, the maximum gain achieved

within the frequency range can be calculated using the LLC mode equations and then be compared with the required gain offset. If the gain requirement is not met, reduce p_{on} and repeat the max M calculation until the maximum p_{on} is found. Eventually, the maximum p_{on} for this m is obtained. Then, change m and calculate the corresponding maximum p_{on}. Through comparing, the maximum $(m-1)p_{on}$ can be found.

After obtaining p_{on}, the characteristic impedance Z_r can be calculated by (4.9). For a certain design specifications, the desired normal operation frequency is set as the resonant frequency f_r. Then, the resonant inductor and capacitor value can be calculated from $L_r = \dfrac{Z_r}{2\pi f_r}$

$C_r = \dfrac{1}{2\pi f_r Z_r}$ and $L_m = (m-1)L_r$.

The above description can be summarized as an iterative design process, which is illustrated in Figure 4.5.
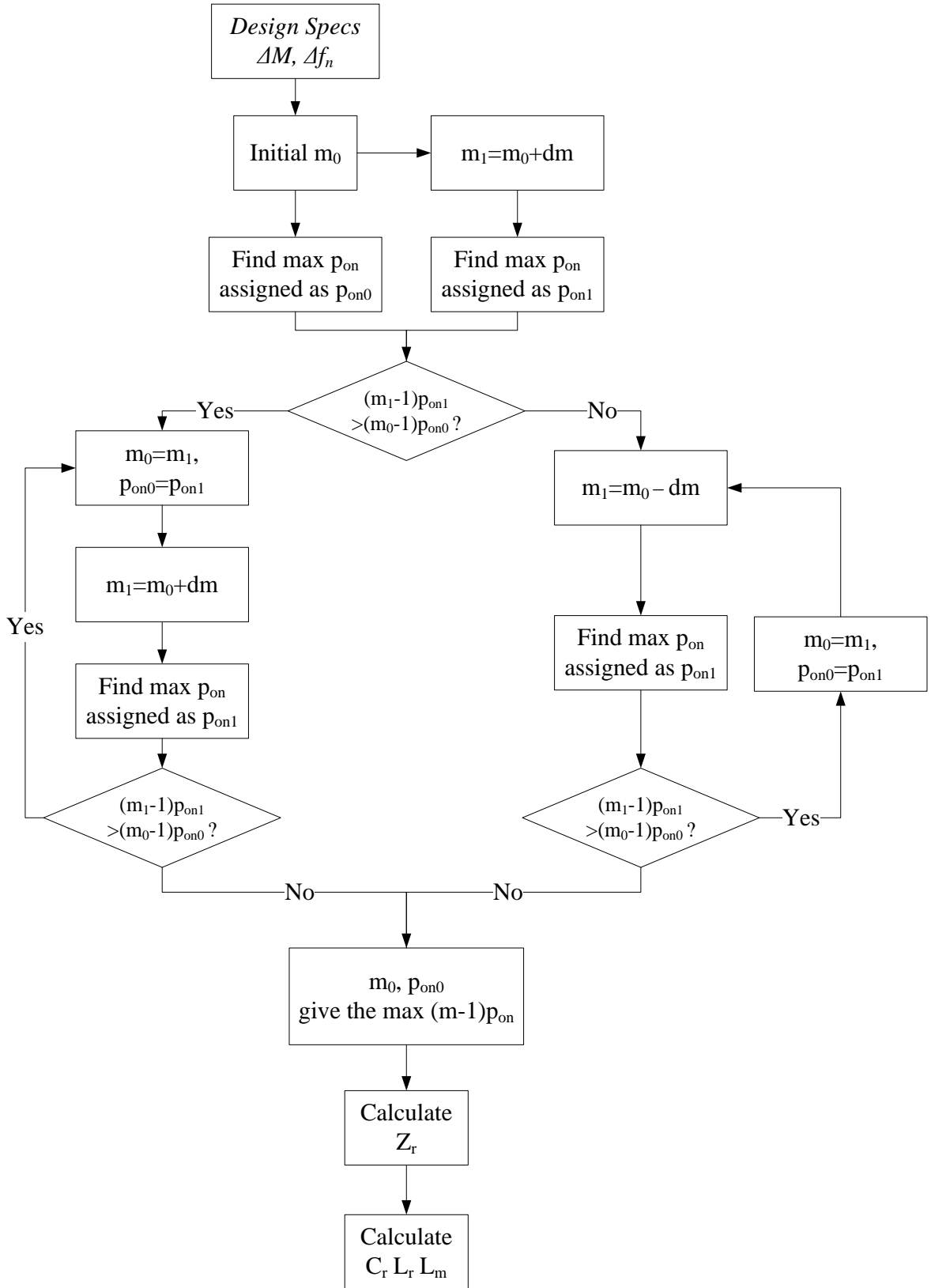
Figure 4.5 The Optimal design procedure to search max *(m-1)p_{on}* for narrow V_{in}

To study the parameters changing of this optimal design methodology, the optimal m and p_{on} for different ΔM and Δf_n are calculated by computer program and the results are plotted in Figure 4.6 and Figure 4.7. The gain drift ΔM is set to vary from 5% to 15%, and the frequency variation Δf_n is selected as 10%, 15%, 20% and 25%. As ΔM increases, $(m - 1)p_{on}$ goes down, where the dominant factor of the decrease is the declining inductors ratio m, while the fluctuation of p_{on} is relatively small. Increasing Δf_n gives a higher $(m - 1)p_{on}$, which is also majorly driven by the increment of m, although p_{on} decreases at an increased Δf_n. In summary, small input voltage variation and large permissible frequency range are preferable for minimizing the conduction loss.
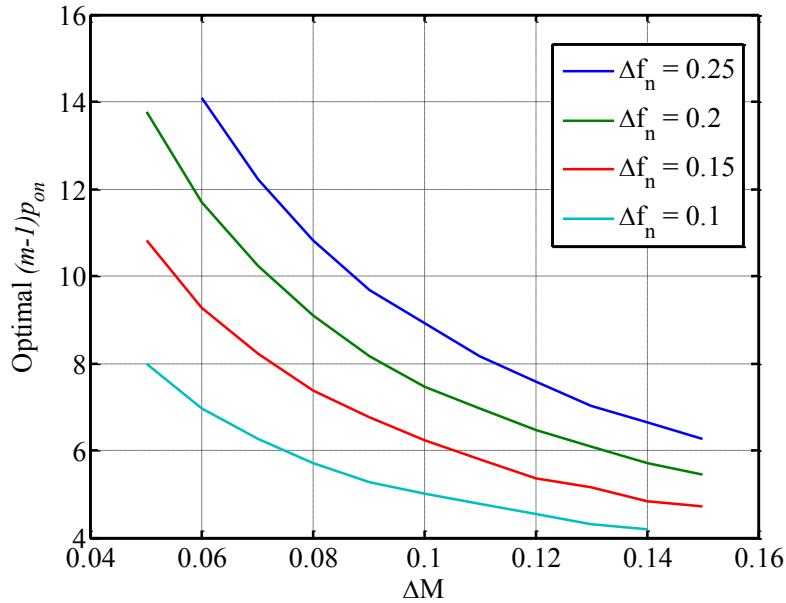
Figure 4.6 Maximum $(m\text{-}1)p_{on}$ for different gain and frequency drift
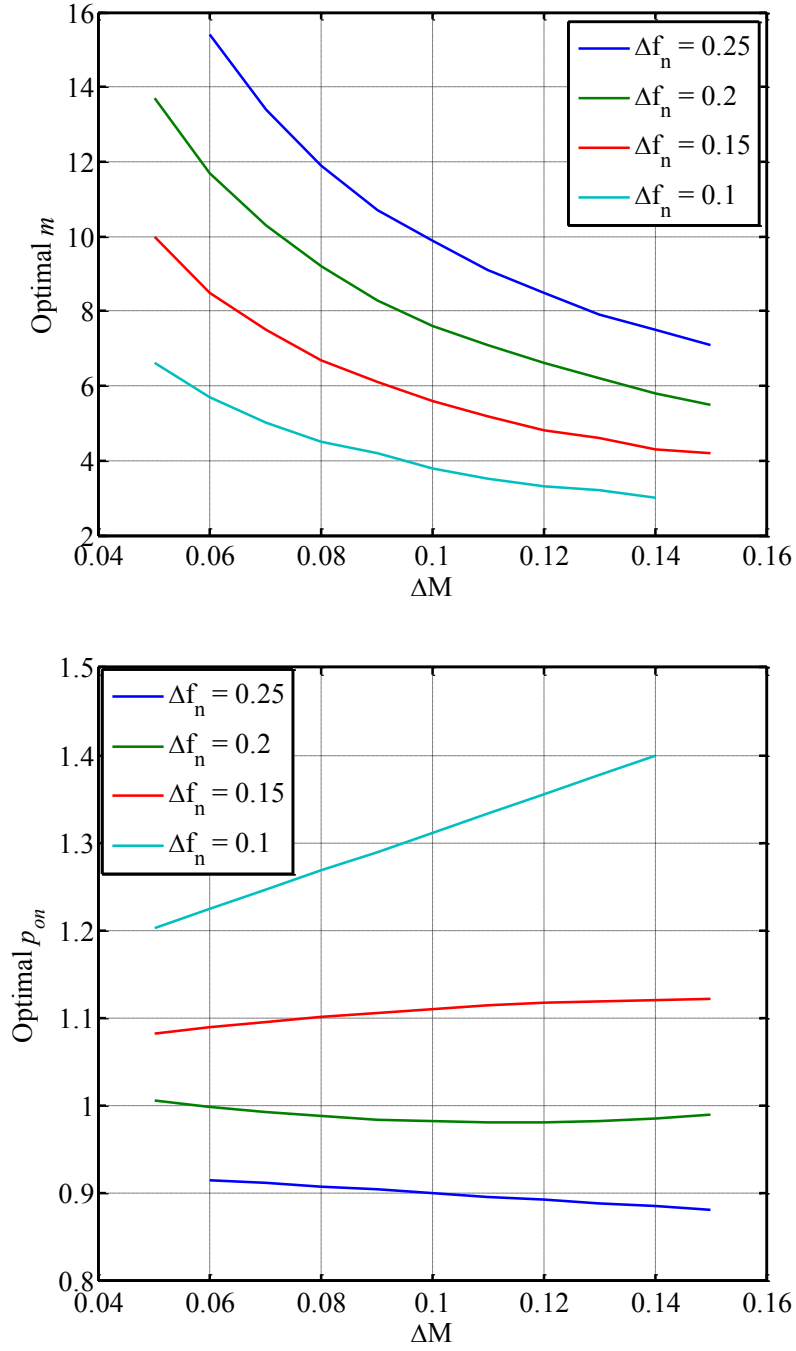
Figure 4.7 Optimal *m* and p_{on} for different gain and frequency drift

The above design method focuses on the optimizing the converter performance in P mode,

which is mainly about reducing the conduction losses at resonant frequency. It is suitable for the

applications that have stable input and only small disturbances occur on the input line voltage, and the converter operation is restricted in a narrow frequency variation range. If the input variation is large or there is no stable operation point, the optimization criterion here may not be suitable for the overall performance at different working conditions.

4.4.2 Optimal Design for Wide V_{in} Range

When the input voltage range is wide, the previous method is not suitable as it primarily focuses on optimizing the converter performance at resonant frequency, whereas meeting the required gain margin within the required frequency range is the main consideration for a wide V_{in}. As a result, the major operation region would be set in PO mode instead of P mode. The benefits of working in PO mode include getting a gain boost, achieving ZVS, maintaining control stability, having no reverse recovery losses for the rectifier. But the LLC may also enter PON or PN mode if the switching frequency is close to the peak gain point, or enter NP or NOP mode if the switching frequency moves above resonant frequency, or enter OPO mode in light load condition. Nevertheless, these modes should be limited in edge operation condition that rarely occurs or be avoided during the design process.

It is found from the previous analysis that the RMS magnetizing current at resonant frequency is inversely proportional to $(m - 1)Z_r/n$ if the output voltage V_o are specified. Although the resonant current does not directly link with $(m - 1)Z_r/n$ when the frequency is below f_r, it can still be used as a parameter to roughly indicate the RMS value of i_m or i_r, which will decrease if $(m - 1)Z_r/n$ increases. Hence, increasing it can reduce the circulating current and through resonant tank therefore reduce the conduction loss. However, the converter with a

bigger m value has lower voltage gain. There is a trade-off between minimizing the conduction loss and maintaining the desired gain range. The goal of the optimal design is to find the maximum $(m-1)Z_r/n$ under the gain and frequency range limitation.

For a specified operation frequency range above the peak gain point, the gain increases monotonically with the decrease of frequency or load. It means that at the minimum frequency the converter shows its max gain capability, whereas the converter reaches its lowest gain at the maximum frequency. From the design perspective, it requires that the converter is capable of dealing with the lowest V_{in} condition at the lowest frequency and the highest V_{in} condition at the highest frequency. As regarding to different load condition, the gain curve at full load has the lowest gain comparing to other lighter load condition for the same frequency, and if the gain requirement for min V_{in} is met under full load, the converter can regulate the output at any other load condition. In zero load condition the lower boundary of the gain given in Chapter 2.3 marks the highest gain comparing to other heavier load condition for the same frequency, and the zero-load boundary gain should be low enough for the max V_{in}.

In summary, the LLC design should meet the following two criteria: the gain at maximum frequency and zero load condition should be low enough for the maximum input voltage; the gain at minimum frequency and full load condition should be high enough for the minimum input. Therefore, the required max gain should be equal to the max gain at full load and f_{min} condition, and it can be expressed by the max and min V_{in} ratio as

$$M_{\max,req} = M_{\max,full} = \frac{V_{in\max}}{V_{in\min}} M_{\min,0} = \frac{V_{in\max}}{V_{in\min}} \frac{m-1}{m\cos[\pi/(2\sqrt{m}f_{n\max})]} \tag{4.15}$$

where $M_{max,full}$ is the max gain at full load and minimum f_n, and $M_{min,0}$ is the lower gain limit at zero load and max f_n.

114

After knowing the required gain range, we can find the resonant tank that gives the maximum allowable $(m - 1)Z_r$. Its maximum can be achieved by properly setting the peak gain point position of a normalized gain curve equal the required max gain defined by (4.15) at f_{nmin} and then letting the corresponding p_{on} of the curve equal to the normalized full load power. The reason for such peak gain placement is that the increase of inductors ratio m or load p_{on} results in a lower gain curve (Note that p_{on} is proportional to Z_r for a given V_o and P_{full} as referred to (4.9)). In other words, the peak gain will be lower than the required for a bigger $(m - 1)Z_r$. To explain this correlation, a partially enlarged gain plot is shown in Figure 4.8 as an example.
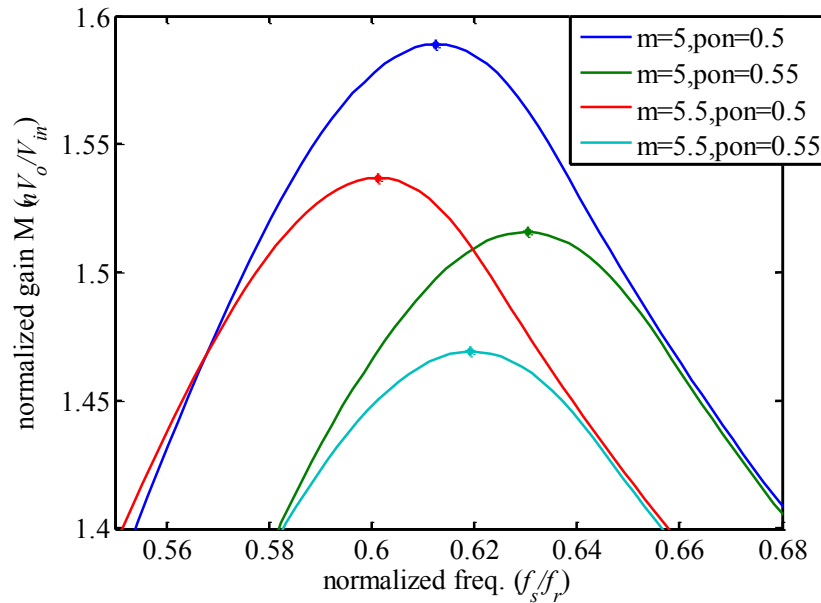
Figure 4.8 DC gain curves near the peak (marked with asterisks) for different m and p_{on}

In summary, the peak gain point placement method is portrayed in Figure 4.9.
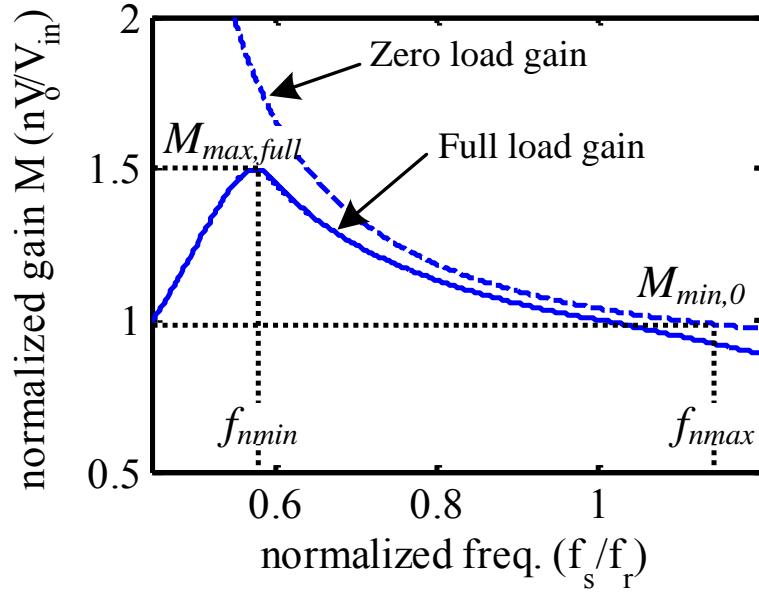
Figure 4.9 Peak gain point placement method for the optimal design

The peak gain point information can be extracted from the PON or PN mode equations and the peak gain condition, and furthermore the peak gain approximation method can apply here to facilitate the design procedure. The required max gain in (4.15) is a function of m, whereas the peak gain is also a function of m for a given f_{nmin}. Therefore, an equation of m can be obtained by letting $M_{max,req}$ equal M_{pk}, from which the inductors ratio m can be solved.

After determining m, the turns ratio n can be calculated by $n = M_{min,0}V_{inmax}/V_o$, or $n = M_{max,full}V_{inmin}/V_o$, which are equivalent given (4.15). The corresponding normalized load p_{on} at the peak gain can also be obtained from the peak-gain-and-load correlation, which is assigned as the normalized power for full load condition. With the obtained m and p_{on}, the resonant tank components' parameters are given as

$$L_r = \frac{(nV_o)^2}{2\pi f_r}\frac{p_{on}}{P_{full}}, \; C_r = \frac{1}{(2\pi f_r)^2 L_r}, \; L_m = (m-1)L_r \qquad (4.16)$$

116

This optimization procedure is illustrated in Figure 4.10, which can be seen that it is a straightforward flow without recursive loop. This peak gain setting method focuses on optimizing the converter configuration at full load condition. For a wide range of V_{in}, the gain range is one major concern in the converter design, and since the full load condition gives the lowest gain range, it can be considered as the worst case scenario. In addition, the converter's output current is also at its maximum level at full load, and causes more conduction losses. If the design meets all the specifications at full load within the assigned frequency region, the converter in all other conditions will qualify automatically. Also, by improving the efficiency of full load operation, the converter will benefit from the LLC configuration for other lesser load conditions.

Design Specs
V_{inmin}, V_{inmax},
f_{nmin}, f_{nmax}

Solve m from
$M_{pk}=M_{max,full}$

Calculate turns ratio
$n= M_{min,0}V_{inmax}/V_o$

Calculate the normalized
full load power p_{on}

Calculate Lr, Cr, Lm
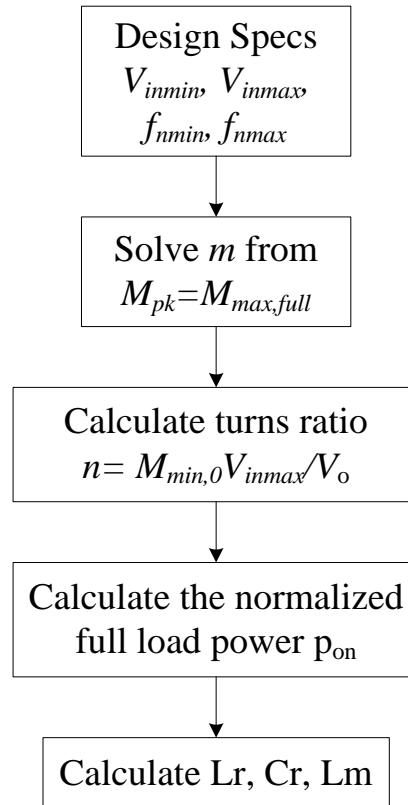
Figure 4.10 Peak gain placement design procedure

It can be seen from the design procedure that the converter enters PON or PN mode causing more power dissipation than PO mode when switching frequency is close to the minimum frequency and near the peak point, and enters NP or NOP mode causing reverse recovery issues when switching frequency is above resonant point. Although the max operating frequency can be limited below resonant frequency to avoid NP and NOP modes, the converter will not be able to benefit from the high power efficiency performance possessed by the resonant point (P mode) in max input voltage and normal load condition. It is because that one of the design criteria requires the zero load gain boundary at max frequency equal or larger than the required minimum gain, and, that is to say, the normal load gain will be lower than the required gain for minimum V_{in}. Consequently, the converter will lost its highest efficiency operating point, which is in P mode, by limiting the frequency below resonant frequency.

4.4.3 Optimal Design for No Reverse Recovery

The previous two optimal methods are mainly on conduction losses reduction but not much attention is put to eliminate the reverse recovery issue of the secondary side rectifiers. The LLC is well-known for letting rectifier commutate naturally, no sudden current disruption, but, actually, it is the merit of PO and OPO mode and other modes that are not ended or started in stage O for the half cycle still suffer from the recovery losses. The reverse recovery will not only cause addition power losses, but also introduce high current spike and voltage ringing on the rectifiers, which bring dangers to the circuit components and produce more noises. In voltage step-down and large output current applications, the reverse recovery accounts for more percentage in the total power losses, and it may have severe impact on the converter performance.

To completely eliminate the reverse recovery current, the converter should be restricted to only operate in PO mode or OPO mode, and therefore new design methodology is needed for this case.

In mode distribution analysis, the boundary between PO mode and NP/NOP mode is at the resonant frequency f_r, while the boundaries between PO and PON or PN are related not only to the frequency but also to the load condition. It can be seen from the mode distribution figure that PO and PN mode only contacts at one point on resonant frequency under heavy load condition, and the dividing point of PO and PON mode moves up closer to resonant frequency with the increase of the load power. Hence, if the dividing point of PO and PON for full load condition is set as the minimum allowable operating frequency, the rest load condition will be guaranteed within PO mode region, which is illustrated in Figure 4.11.
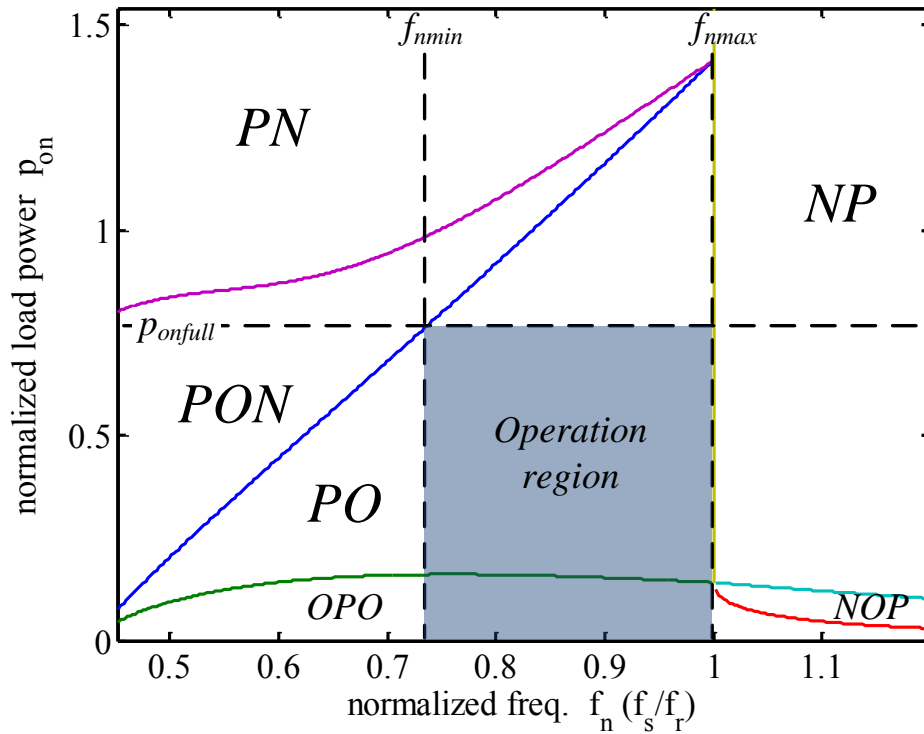
Figure 4.11 The PO-and-OPO-mode-only operation region on mode distribution map

Hence, the optimal method is mainly about setting the minimum frequency on full-load gain curve, which is somehow similar to the peak gain placement method. In Chapter 3.4, the approximation techniques for the mode boundary are studied and can be used here to assist the design procedure.

As the resonant tank configuration and current relation has been explored in the previous section, the LLC with higher inductors ratio m and larger impedance Z_r (or p_{on}) tends to have lower conduction losses. However, the trade-off is that the gain range is narrower with higher m and Z_r. This correlation is shown in the partially enlarged gain plot, Figure 4.12. It can be seen that increasing p_{on} (or Z_r) will reduce the PO/PON boundary gain and increase the boundary frequency, while increasing m will decrease the boundary gain and frequency.
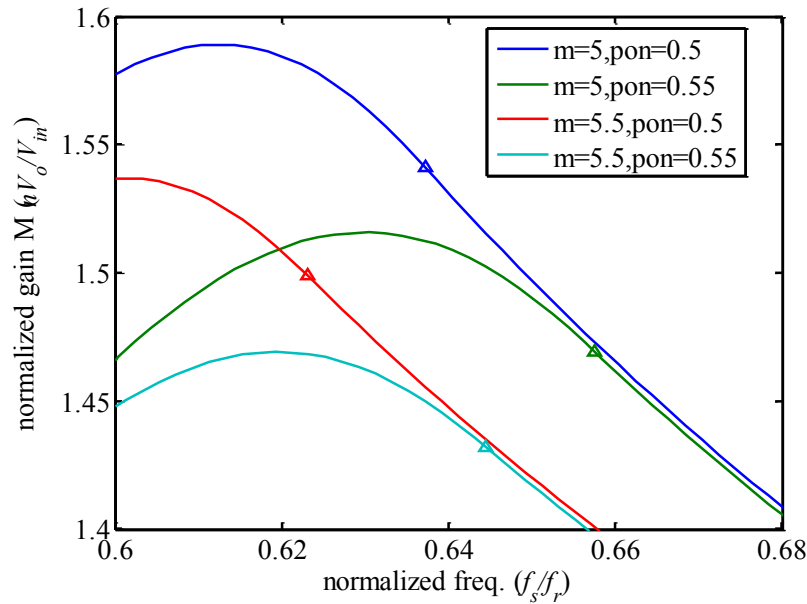
Figure 4.12 DC gain curves near the PO/PON boundary (marked with triangles) for different m and p_{on}

The two design criteria for converter gain in peak gain placement method are still valid in this case, and thus the required max gain should be equal to the gain at the PO/PON boundary for full load condition, which is

$$M_{max,req} = M_{b,full} = \frac{V_{in\,max}}{V_{in\,min}} M_{min,0} = \frac{V_{in\,max}}{V_{in\,min}} \frac{m-1}{m\cos[\pi/(2\sqrt{m}f_{n\,max})]} \tag{4.17}$$

Note that the normalized frequency f_{nmax} should be equal to 1, which is the resonant frequency.

The gain at the PO/PON boundary can be calculated by solving boundary PO mode equations, and by letting the boundary gain equal the required max gain in (4.17) the optimal inductors ratio m can be solved in a way similar to the peak gain placement design. The two boundary gain values can then be calculated, and the transformer turns ratio is therefore determined by $n= M_{min,0}V_{inmax}/V_o$, or $n=M_{b,full}V_{inmin}/V_o$. Since the normalized full load power p_{on} for the PO/PON dividing point can be obtained after knowing m and the actual full load rating is given in the design specifications, the characteristic impedance Z_r can be expressed as $Z_r = p_{on}(nV_o)^2/P_{full}$ and the LLC parameters is given by

$$L_r = \frac{Z_r}{2\pi f_r}, \quad C_r = \frac{1}{2\pi f_r Z_r}, \quad L_m = (m-1)\frac{Z_r}{2\pi f_r} \tag{4.18}$$

Note that it is equivalent to the approach taken in (4.16).

The flowchart of this design procedure is depicted in Figure 4.13. The operation region of the converter is almost all within PO mode, while a small portion for light load condition is inevitably extended into OPO mode, which has zero output current at every switching instant and hence will not introduce reverse recovery issue. Therefore, the output rectifiers will not be troubled by reverse-recovery effect. Under the premise of no reverse recovery, the design method finds the optimal set of the resonant tank components. It shares the similar imperfection with the

peak gain placement method that to regulate the minimum input voltage at close-to-zero load condition the converter makes the sacrifice that it will not be able to operate at resonant frequency for normal load.

```
┌─────────────────────┐
│    Design Specs     │
│  Vinmin, Vinmax,    │
│   fnmin, fnmax      │
└─────────────────────┘
           │
           ▼
┌─────────────────────┐
│    Solve m from     │
│  Mb,full=Mmax,full  │
└─────────────────────┘
           │
           ▼
┌─────────────────────┐
│ Calculate turns ratio│
│  n= Mmin,0Vinmax/Vo │
└─────────────────────┘
           │
           ▼
┌─────────────────────┐
│ Calculate the normalized│
│  full load power pon │
└─────────────────────┘
           │
           ▼
┌─────────────────────┐
│  Calculate Lr, Cr, Lm│
└─────────────────────┘
```
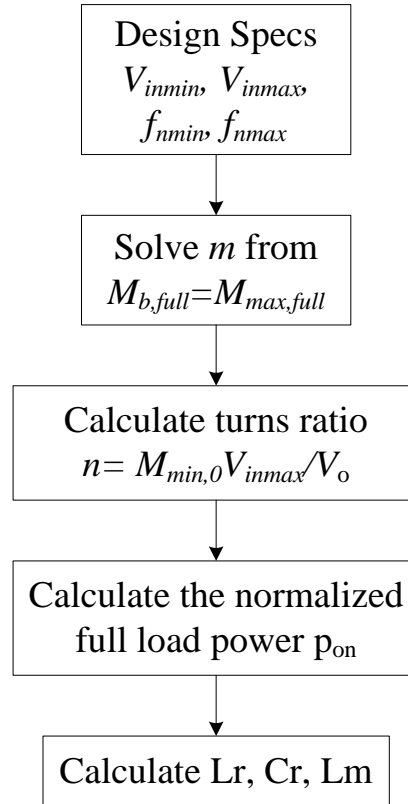
Figure 4.13 PO/PON boundary placement design procedure

4.5 Design Examples and Experiments

As an example, we designed a 400W, 400V output rating LLC converter prototype. The input voltage varies from 25V to 38V, the operating frequency range is from 80 kHz to 160 kHz and the resonant frequency is set to 140 kHz. The converter's specifications are listed in Table 4.1.

Table 4.1 LLC Prototype Design Specifications

Specifications	Values
Output voltage V_o	400V
Input voltage range V_{in}	25V – 38V
Rated load power P_{full}	400W
Frequency variation range	80kHz – 160kHz
Resonant frequency	140kHz

From the specs, the normalized frequency range is from 0.571 to 1.14 and $V_{inmax}/V_{inmin} = 1.52$. Following the peak gain placement design procedure, the inductors ratio is solved as $m=6.33$. The normalized peak gain M_{pk} at full load is equal to 1.5 and therefore the turns ratio can also be calculated by the following expression: $n=M_{max,full}V_{inmin}/V_o=0.0938$. The peak gain point for full load also give that $I_{rOn} =0.522$ and $\theta_{O0}=2.01$, and by substituting them into load power equation (3.19), the normalized full load power can be calculated as $p_{on}= 0.48$. Therefore, the resonant tank parameters can be obtained using (4.16) as follows: Lr = 1.91 uH, Cr=676 nF and Lm= 10.2 uH. The corresponding DC voltage gain characteristics of these resonant tank parameters are shown in Figure 4.14.
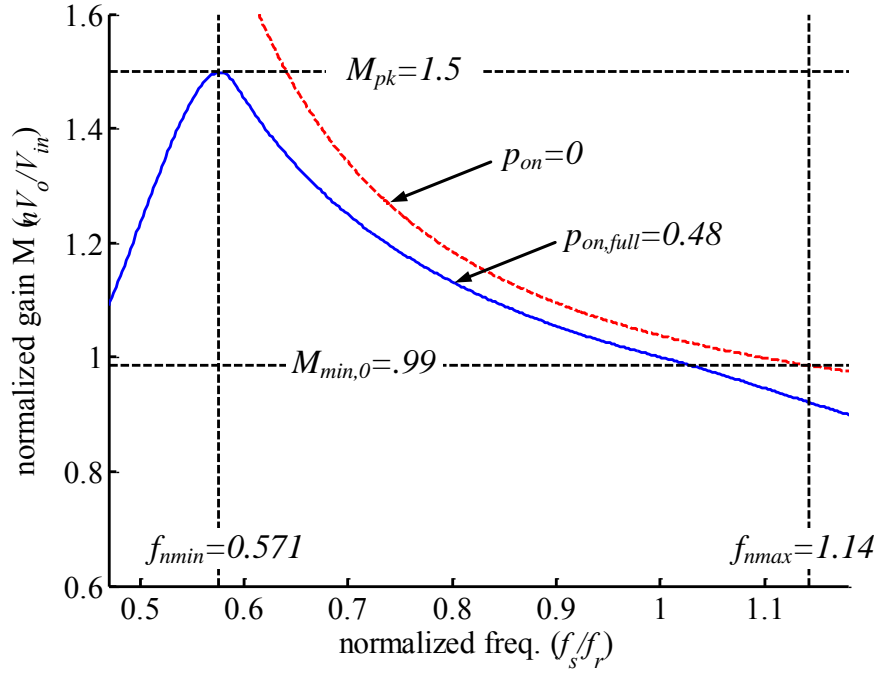
Figure 4.14 DC gain plot of the peak gain placement design using the prototype parameters

In building the prototype, the actual L-C parameters are selected as follows:

Table 4.2 LLC Resonant Tank Parameters of the Prototype

Parameters	Values
Resonant capacitor C_r	680nF
Resonant inductor L_r	1.9uH
Magnetizing inductor L_m	10uH
Transformer primary turns	5
Transformer secondary turns	55

The switching MOSFETs, rectifier diodes and other key circuit components of the converter circuit are listed in Table 4.3. A photo of the prototype is shown in Figure 4.15.

Table 4.3 LLC Prototype Circuit Components

Components	Part Number
Full-bridge MOSFET	STP160N75F3 $\times$ 4
Rectifier diodes	STTH3R06 $\times$ 4
Resonant capacitor C_r	WIMA film caps
Resonant inductor core	RM12 (3C95)
Transformer core	RM14 (3C95)
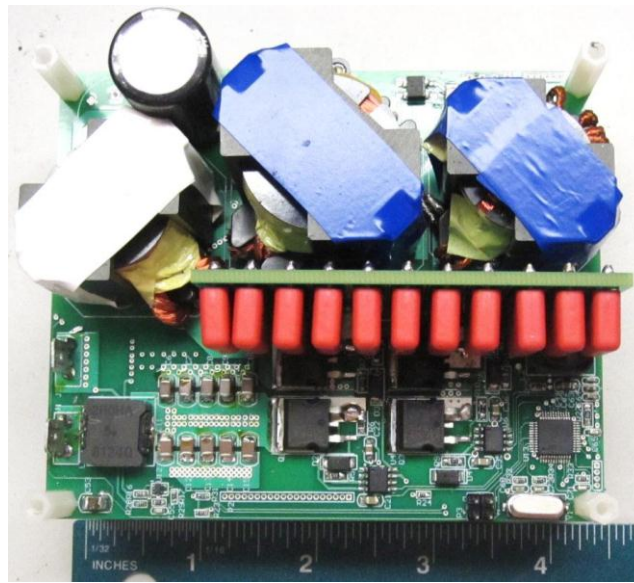
Figure 4.15 The LLC converter prototype photo

Some samples of the experimental waveforms in P mode and PO mode are shown in Figure 4.16, which are in line with the analysis results. The power efficiency is measured using power analyzer at different input voltage levels and load conditions, and the results are shown in Figure 4.17. Note that the driving loss is not included in the measured efficiency data, which is about 0.5W depending on the switching frequency. The efficiency for higher input voltage level is

higher for the same load power, since according to the law of power balance the input average current is reduced for an increased V_{in} and so does the conduction loss.

(a)

(b)
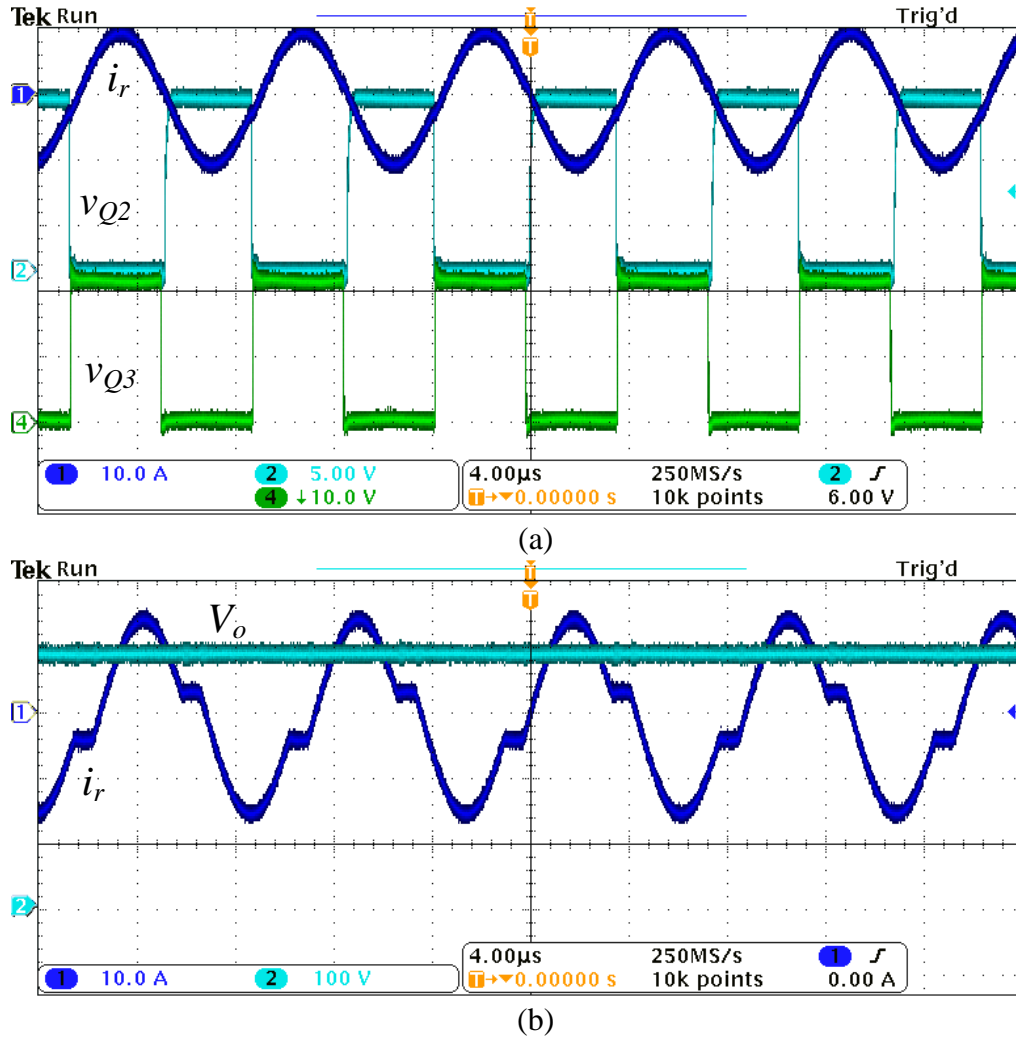
Figure 4.16 Experimental waveforms of the LLC converter prototype: (a) P mode; (b) PO mode
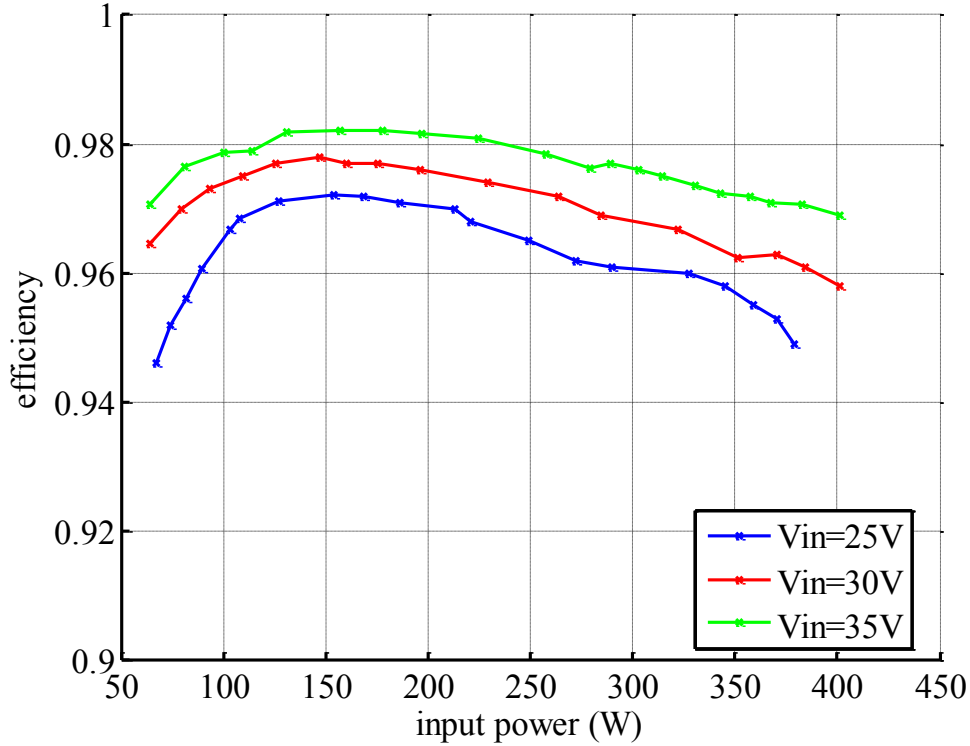
Figure 4.17 The LLC converter prototype efficiency at different input voltage

As a comparison, we design another group of parameters with a pre-set smaller resonant

capacitance $C_r=470nF$. Thus, L_r is also determined as the resonant frequency is fixed. To make it

a fair comparison, the magnetizing inductor should not be assigned randomly. Instead, the

searching method is used: we swept the magnetizing inductance value and verified it by circuit

simulation software to see if it met the max gain requirement in order to find the max L_m. Since

$L_m = (m-1)L_r = (m-1)Z_r/\omega_r$, the maximization of L_m is the same as increasing $(m-1)Z_r$

as far as possible, which is the optimal target of the peak gain placement design methodology. All

other circuit components remain the same. The new LLC resonant tank parameters are compared

with the proposed optimal parameters in Table 4.4.

Table 4.4 LLC Resonant Tank Parameter Comparison

	Proposed Optimal Parameters	Reduced Cr Parameters
Resonant capacitor C_r	680nF	470nF
Resonant inductor L_r	1.9uH	2.75uH
Magnetizing inductor L_m	10uH	7.67uH

The efficiency curves of the two designs are plotted in Figure 4.18, Figure 4.19 and Figure 4.20. Although the two designs have comparable efficiency in low input voltage condition, the LLC converter with optimal parameters outperforms the reduced C_r one in high V_{in} region. At heavy load the efficiency curves for the two parameter set are converged, while the performance advantages for optimal design are mostly shown in the medium and light load conditions. It is because the magnetizing current i_m is mainly determined by L_m and less affected by the load power, and i_m is the dominant portion accounting for the conduction loss at light load. Since the optimal LLC resonant tank has a higher L_m, the efficiency improvement appears in light load region. It can be seen that the LLC with optimal parameters has generally higher efficiency than the other design; especially in mid- and low-load region. The peak efficiency of the LLC prototype achieves above 98%.
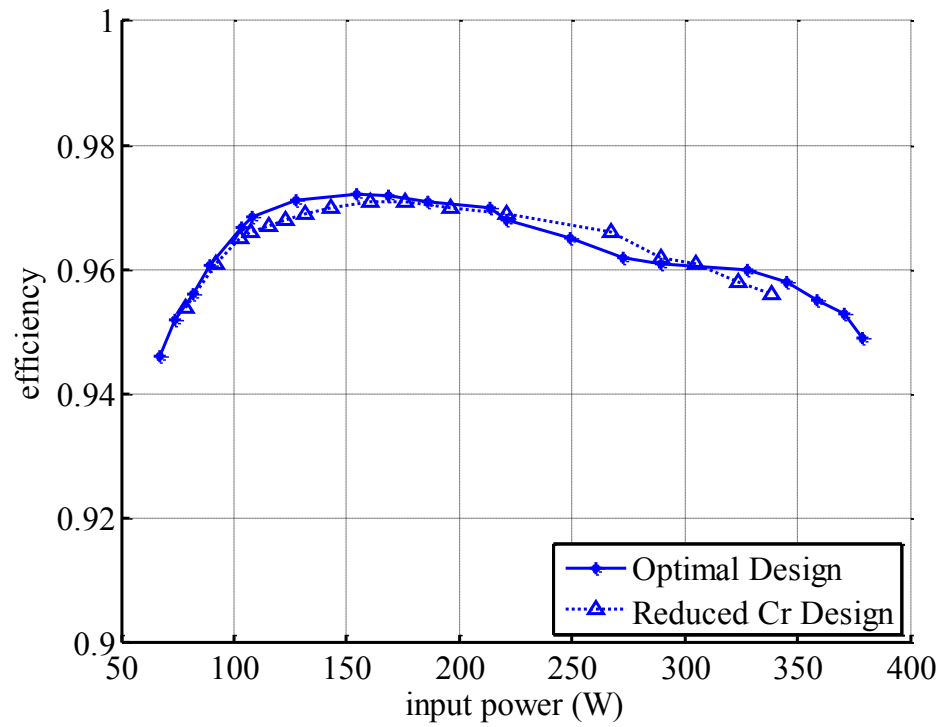
Figure 4.18 Efficiency comparison at $V_{in}=25V$
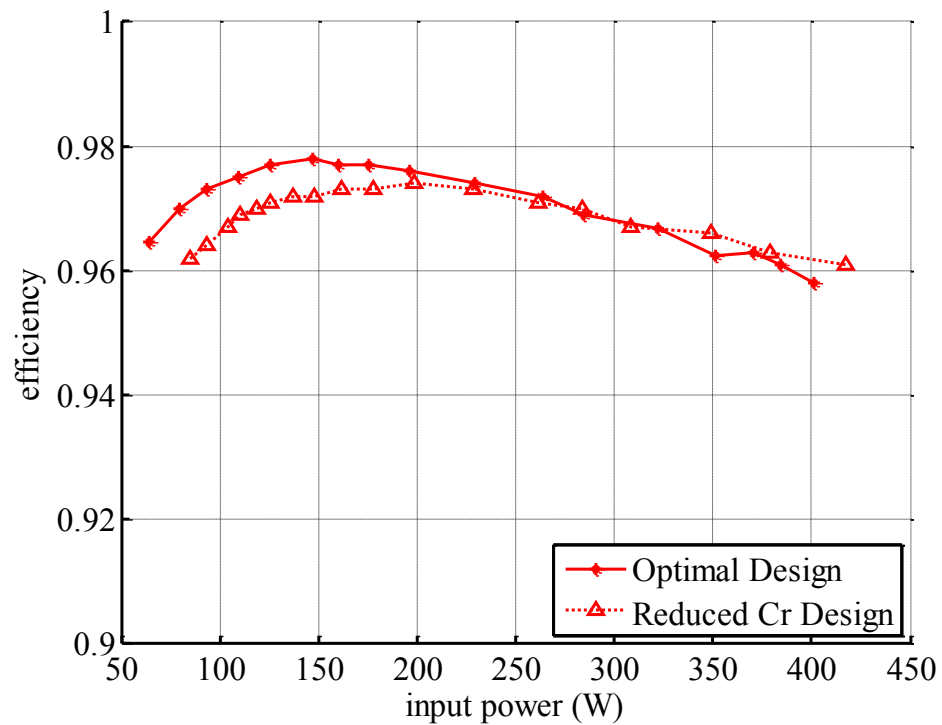
Figure 4.19 Efficiency comparison at $V_{in}=30V$

129
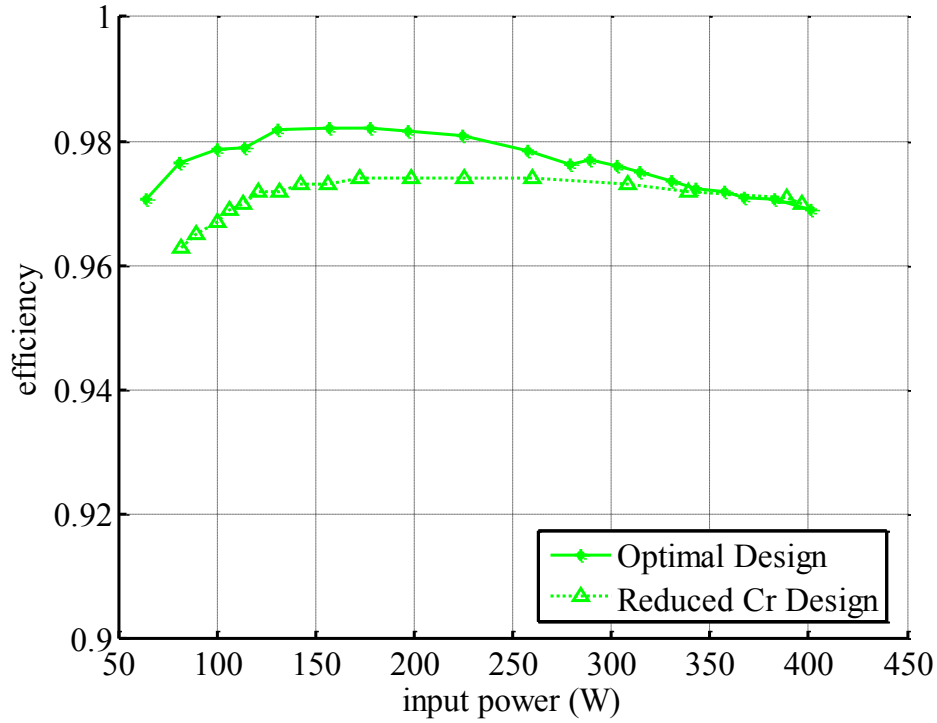
Figure 4.20 Efficiency comparison at $V_{in}=35V$

4.6 Generalized Discussion of the LLC Optimization

The LLC converter optimization is based on the specific design case in the several proposed design methods. To let the design proceed, some design specifications are required to be provided in advance, such as the minimum and maximum input voltage, the switching frequency variation range, the output voltage and the load power rating, etc. For a sound converter design, it should be able to meet these specifications and provide good efficiency. However, the actual design subjects to many constraints such as the selection of MOSFETs, diodes, capacitors, the core material and structure, and the driver scheme, etc. Even given the same resonant tank parameters, the converter's performance could still be vastly different affected by the actual choice of devices and components. From this perspective, there is no universal rule or guideline applied to every LLC resonant converter application. Still, from previous analysis all LLC

130

converters share some same operation characteristics that can be employed in the general design considerations. In previous section, the currents in the LLC tank are investigated, which is directly connected to the conduction losses as it is equal to the product of the conductive resistance and the RMS current square. Though the conductive resistance may be varied, it is universally beneficial for the converter to reduce the resonant current as much as possible. Since the previous presented operation mode is based on normalized variables, the generalized LLC converter optimization is to use the normalized variables and parameters rather than specified values and to find the optimized normalized resonant tank configurations. After a simple de-normalization process, the generalized result is applicable to a specific design case. Therefore, this generalization can be used as a reference in converter design or performance validation.

The specifications appeared in previous optimal design methods include: the full power rating, the output voltage, the minimum and maximum input voltage, the resonant frequency and the switching frequency variation range. These design specifications should be replaced by normalized parameters for the sake of generalization.

In the normalized specs the full power rating and the output voltage is omitted, as they only appear in the defined base coefficient during the operation mode analysis, and therefore are not necessary to be taken into account during the generalized design but to be included later in the de-normalization procedure.

The minimum and maximum input voltage can be represent by one normalized parameter, the gain margin GM, which is defined as the ratio of the maximum gain and minimum gain, and it is obvious that

131

$$GM = \frac{M_{\max}}{M_{\min}} = \frac{V_{in,\max}}{V_{in,\min}} \tag{4.19}$$

Similarly, the frequency range can be represented by the frequency margin FM, which is defined as follows:

$$FM = \frac{f_{n\min}}{f_{n\max}} = \frac{f_{s\min}}{f_{s\max}} \tag{4.20}$$

In order to utilize the peak gain placement method, the required max gain $M_{max,req}$ and the normalized minimum and maximum frequencies, f_{nmin} and f_{nmax}, should be provided, and only knowing GM and FM is not enough. From (4.15), $M_{max,req}$ is a function of GM, m and f_{nmax}, and m is part of the optimization targets. Therefore, the only missing parameter is the resonant frequency f_r.

The resonant frequency should be set near the upper boundary of the switching frequency. It is because that the preferable operation mode PO mode locates below the resonant frequency. In previous design approaches, the max frequency limit is either set at the resonant frequency or in the vicinity of it to exploit the advantages of PO mode. Another property of the resonant point operation is that the gain is unity for a wide range of load conditions if the converter is in P mode. To solve the resonant frequency, we set the converter to work at the resonance at the maximum input voltage. Hence the transformer turns ratio should be set accordingly as $n = V_{in,max}/V_o$. However, in light load to zero load condition, the gain will exceed one as the converter enters OPO mode. To regulate the input voltage at light load, the converter should be operated at a frequency above the resonance, at which the zero load gain limit equals to one. Then the actual max frequency can be derived as

132

$$M_{min,0} = \frac{m-1}{m\cos[\pi/(2\sqrt{m}f_{n\max})]} = 1 \;\Rightarrow\; f_{n\max} = \frac{\pi}{2\sqrt{m}\cos^{-1}[(m-1)/m]} \tag{4.21}$$

The max frequency increases with the increase of m, which is shown in Figure 4.9. For an m below 10, the increment on the resonant frequency does not exceed 10%. As m approaches infinity, the limit of the max frequency is

$$\lim_{m\to\infty} f_{n\max} = \frac{\pi}{2\sqrt{2}} \approx 1.11 \tag{4.22}$$

This is still relatively small. Therefore, by allowing about 10% frequency increase above the resonance, the converter can utilize the unity gain point to regulate $V_{in,max}$.
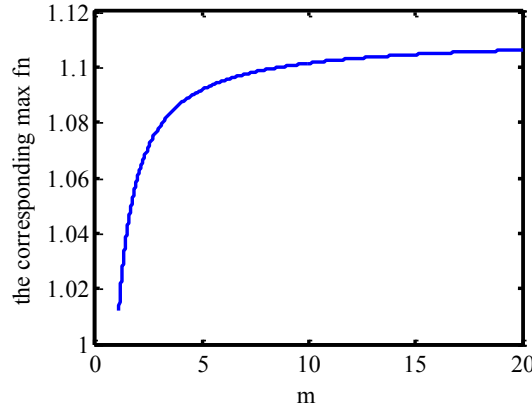
Figure 4.21 The actual max switching frequency variation with different m

Reversely the resonant frequency can be determined by the max switching frequency as follows

$$f_r = 2\sqrt{m}\cos^{-1}\left(\frac{m-1}{m}\right)\frac{f_{s\max}}{\pi} \tag{4.23}$$

and the normalized minimum frequency is given by

$$f_{n\min} = \frac{\pi}{2\sqrt{m}\cos^{-1}[(m-1)/m]}FM \tag{4.24}$$

which is a function of m. Also, the required max gain is given by

$$M_{max,req} = \frac{V_{in,\max}}{V_{in,\min}} M_{\min,0} = GM \qquad (4.25)$$

Hence, following the peak gain placement method, the optimal m and p_{on} can be found that the converter reaches its peak gain defined by (4.25) at the frequency defined by (4.24).

The specifications and the parameters involved in the LLC design are summarized in Table 4.4, in which the middle two columns only contain normalized parameters.

Table 4.5 Normalized and De-normalized LLC Design Parameters

Actual Design Specs	Normalized Specs	Optimization Targets	De-normalized Tank Parameters
V_o P_{full} $V_{in,min}, V_{in,max}$ $f_{s,min}, f_{s,max}$	$GM = \dfrac{V_{in,max}}{V_{in,min}}$ $FM = \dfrac{f_{s,min}}{f_{s,max}}$	m p_{on}	$n = V_{in,max}/V_o$ $f_r = 2\sqrt{m}\cos^{-1}\left(\dfrac{m-1}{m}\right)\dfrac{f_{s,max}}{\pi}$ $L_r = \dfrac{(nV_o)^2}{2\pi f_r}\dfrac{p_{on}}{P_{full}}$ $C_r = \dfrac{1}{(2\pi f_r)^2 L_r}$ $L_m = (m-1)L_r$

Figure 4.22 shows the optimal m and p_{on} under different gain and frequency margins. The optimization target $(m-1)p_{on}$ becomes larger if GM or FM decreases. In other words, if the converter design is for a narrower range of input voltage and allows wider frequency variation, the converter can achieve higher power efficiency.

Using the same specs of the design example given in the previous section, the margins are given as $GM = 1.52$, $FM = 0.5$, and the optimal parameters are solved as $m = 6.94$, $p_{on} = 0.44$. The de-normalized converter parameters are: $n = 1:10.5$, $f_r = 146kHz$, $L_r = 1.72\mu H$,

$C_r = 691nF$, $L_m = 10.8\mu H$. It is very close to the actual parameters used in the prototype, but the resonant frequency is slightly larger and $(m-1)p_{on}$ is slightly smaller than the prototype. However, it allows the converter to work at the resonant frequency for the max input condition which offers high efficient performance for this single frequency point operation.

From the above discussion, it can be seen that the LLC design procedure can be abstracted to an equation solving problem, in which GM and FM are the known variables and m and p_{on} are the unknowns. It is independent of a specific design case, but can apply to actual design after parameter de-normalization.
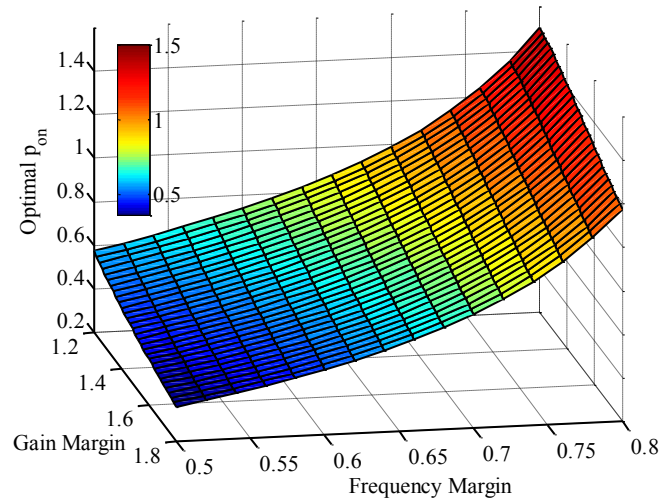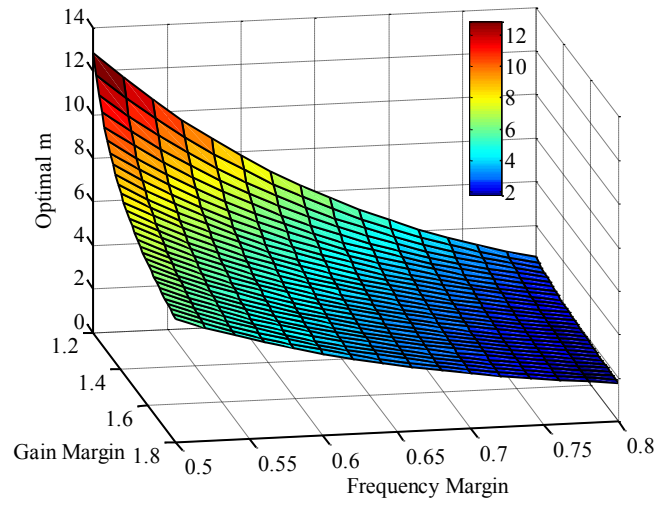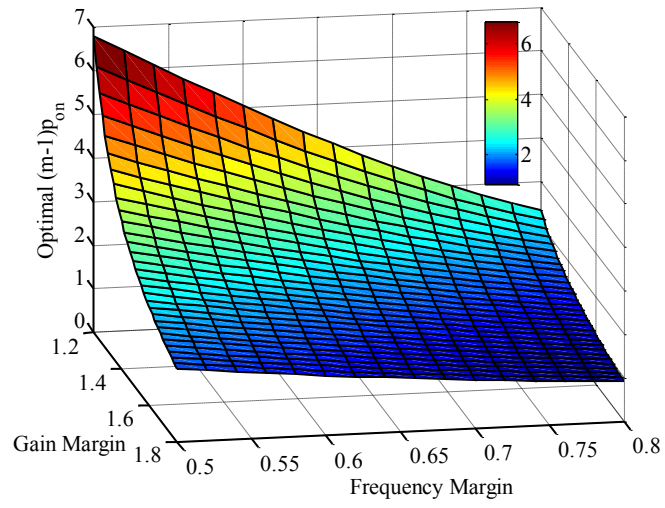
Figure 4.22 The optimal m and p_{on} under different gain and frequency margins

136

CHAPTER FIVE: GENERILIZED ANALYSIS OF RESONANT CONVERTER

5.1 Introduction

In Chapter Two, the operation mode model of the LLC resonant converter is built and studied. The exact solutions of the current and voltage waveforms can be extracted from the mode equations. Although the mode equations are nonlinear and transcendental and it is difficult or even impossible to derive the closed-form solutions, the numerical solution can still be found with the help of numerical computing software such as MATLAB. Some of the analysis method and principles are applicable to other resonant converter topologies, and therefore a generalized procedure can be developed to derive the resonant functions, list the simultaneous equations, set the mode boundaries. Following the standardized procedure, the corresponding program can be coded using numerical tools to solve the operation modes and DC characteristics. In this chapter, a generalized analysis procedure, aiming to facilitate the numerical calculation process, is presented and discussed, and several resonant converter examples are given to demonstrate the use of the method.

5.2 Resonant Converter Circuit Generalization

The structure of a resonant converter, introduced in Chapter 1.1, can be divided into three power processing and converting stages: switch network input stage, resonant stage, and rectification and filter output stage. The resonant tank is the key link in the power conversion and

all the discussion and analysis are focused on this stage. Equivalent signal sources are found to replace the input and output stage in order to simplify the discussion on the middle resonant stage.

Although there are different configurations for the switch network input stage, such as half bridge, full bridge, the function of this stage is to produce a voltage excitation for the resonance. Assuming that the variable frequency control is employed, the input stage can be represented by a square-waveform voltage signal generator. Since the duty cycle is equal to 50%, the steady-state operating waveforms of a half cycle are in symmetry with the other half in opposite polarity. The investigation on a half cycle is adequate to understand the operation of the entire time domain. Hence, the input stage can be further simplified to a constant DC voltage source during the half switching period.

The output stage configuration can be grouped into two types according to the output filter: voltage source output (VSO) and current source output (CSO), as the output capacitor/inductor low-pass filter is supposed to have a sufficient large capacitance/inductance that it act like a DC voltage/current source during the half switching cycle. Based on the conduction status of the rectifiers, there are three possible conditions for the output stage in a half cycle. It is similar to the LLC converter that they are named as stage P, stage N and stage O as shown in Figure 5.1. Note that, for current source output, the output is equivalent to a short-circuit connection during stage O, while voltage source output is showing open-circuit in stage O. The appearance or duration of these stages varies for different resonant tanks and operation conditions.
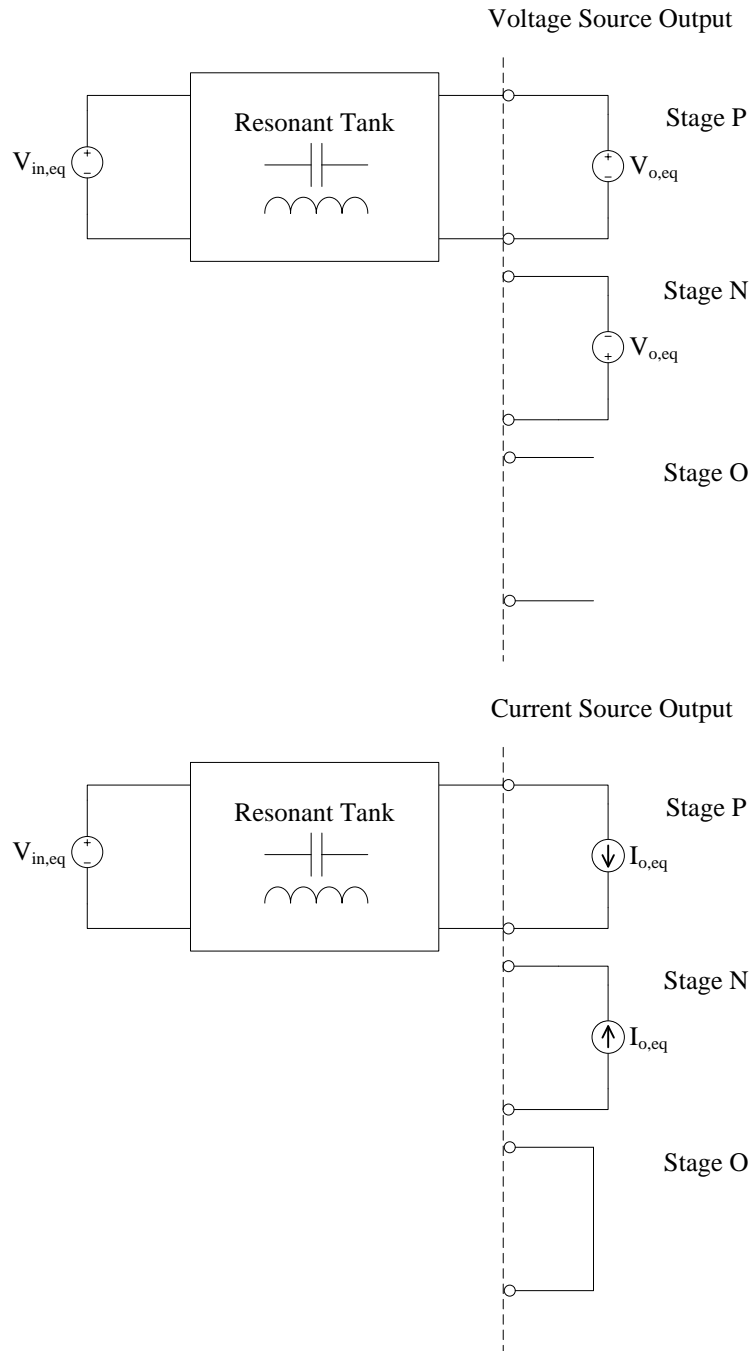
Figure 5.1 Equivalent circuit for different resonant stages

To simplify and generalize the analysis, all variables and parameters are normalized. The equivalent circuit of stage P is assigned as the reference circuit to define the base coefficients for normalization.

The base resonant frequency is set equal to the resonant frequency of the tank in stage P, and the base impedance is the characteristic tank impedance.

For voltage source output, the base voltage is defined as the equivalent supply voltage $V_{o,eq}$. For current source output, it is assumed that the converter regulates the output voltage at a constant value, and the output current is strictly proportional to the load condition. We define the base voltage as the quotient of the load power divided by the equivalent supply current $I_{o,eq}$, which should be a constant under the above assumption. The base current is then obtained as the quotient of the base voltage divided by the base impedance, and the base power is the product of the base voltage and the base current.

By applying the base coefficients into the equivalent circuit, the actual values are replaced by the normalized values. If the normalized gain M is defined as the base voltage divided by the equivalent input source voltage, then the input voltage can be represented as $1/M$. For voltage source output, the normalized output is 1. For current voltage source output, the normalized output current is derived as

$$\frac{I_{o,eq}}{I_{base}} = \frac{P_o}{V_{base} I_{base}} = p_{on} \tag{5.1}$$

which is equal to the normalized load.

The L-C components are also represented by the normalized parameters. If the normalized current and voltage are used to describe the capacitor's V-I relationship, it is given by

$$i_{Cn} = \frac{i_C}{I_{base}} = \frac{C}{I_{base}} \frac{dv_C}{dt} = \frac{CV_{base}}{I_{base}} \frac{d\theta}{dt} \frac{dv_{Cn}}{d\theta} = \left(Z_{base} \omega_{base} C \right) \frac{dv_{Cn}}{d\theta} \tag{5.2}$$

140

where subscript n denotes the normalized variable, ω_{base} is the base resonant frequency of the tank, and the phase angle $\theta = \omega_{base}t$ is used to replace the time variable. Note that for different stage the resonant tank topology could be different, and the stage resonant frequency ω_{tk} could differ from ω_{base}. The normalized capacitance is $Z_{base}\omega_{base}C$, which is a dimensionless quantity. Similarly, the inductor has the following V-I relationship:

$$v_{Ln} = \left(\frac{\omega_{base}L}{Z_{base}}\right)\frac{di_{Ln}}{d\theta} \tag{5.3}$$

and the normalized inductance is $\omega_{base}L/Z_{base}$.

Several normalized resonant tank circuitries are shown in Figure 5.2, Figure 5.3 and Figure 5.4.

$$L_m = (m-1)L_r \quad \omega_{base} = \frac{1}{\sqrt{L_rC_r}}, Z_{base} = \sqrt{\frac{L_r}{C_r}}$$
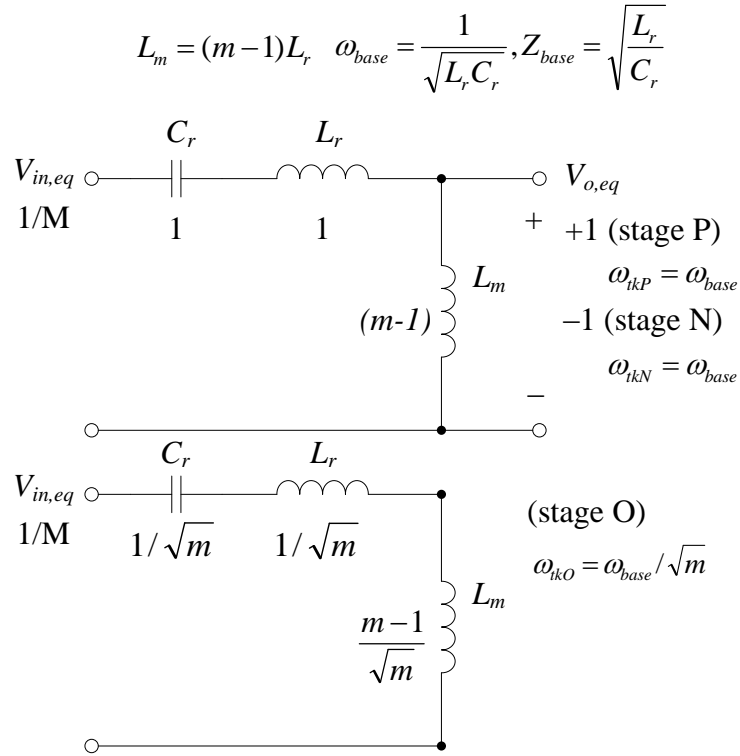
Figure 5.2 Normalized resonant tank circuit of the LLC

141

$$L_m = (m-1)L_r \quad \omega_{base} = \sqrt{\frac{m}{m-1}} \frac{1}{\sqrt{L_r C_r}}, Z_{base} = \sqrt{\frac{m-1}{m}} \sqrt{\frac{L_r}{C_r}}$$
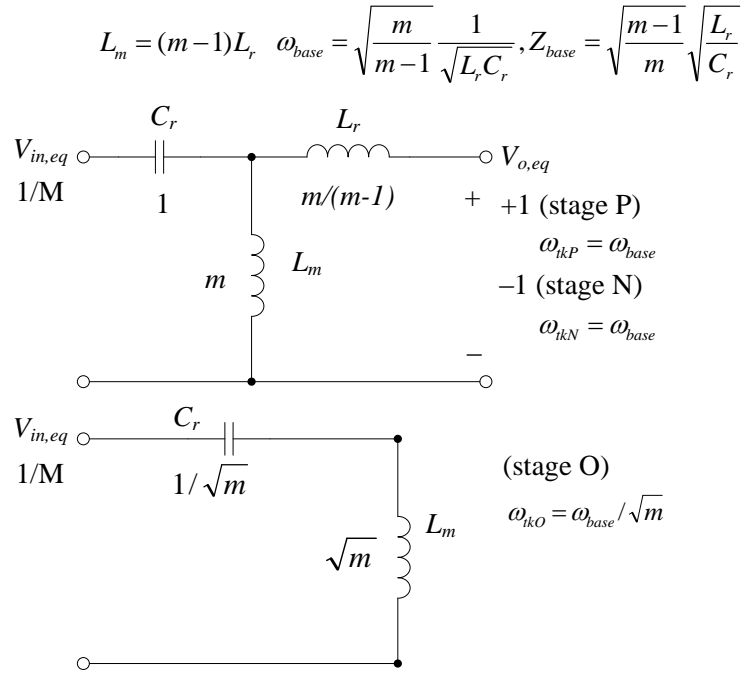
Figure 5.3 Normalized resonant tank circuit of the CLL

$$C_p = (m-1)C_r \quad \omega_{base} = \sqrt{\frac{m}{m-1}} \frac{1}{\sqrt{L_r C_r}}, Z_{base} = \sqrt{\frac{m}{m-1}} \sqrt{\frac{L_r}{C_r}}$$
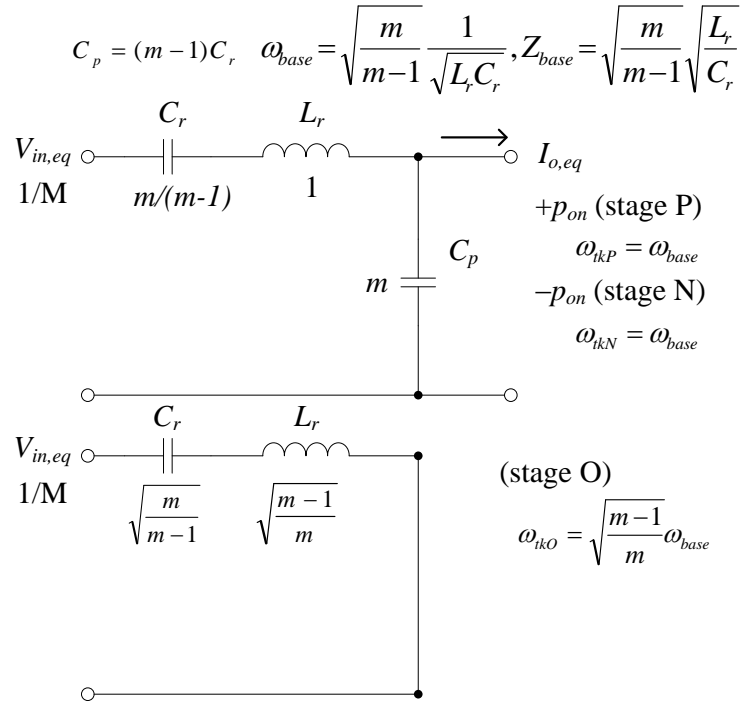
Figure 5.4 Normalized resonant tank circuit of the LCC

5.3 Resonant Variable Functions

The capacitor voltage and the inductor current are selected as the resonant variables. If all L-C components in the resonant tank are ideal and lossless, the currents and voltage functions are the mixture of sinusoidal and linear signals. In general, a normalized resonant variable can be expressed as

$$x_{an} = X_{an} \sin\left(\frac{\omega_a}{\omega_{base}} \theta + \theta_{a0} \right) + X_{asn}\theta + X_{a0n} \tag{5.4}$$

In this resonant variable function, the subscript a denotes the corresponding resonant component; there is a coefficient modifier (ω_a/ω_{base}) for θ, since different stages can have different resonant frequency; X_{an}, X_{asn}, X_{0n}, θ_{a0} are the dimensionless parameters for the sinusoid magnitude, linear changing rate, initial value and the initial phase angle of the resonant variable respectively.

Choosing the capacitor voltage and the inductor current as the resonant variables is sufficient to describe all the resonant tank behavior. It is because that the current of a capacitor can be expressed by the derivative of its voltage, and the voltage of an inductor can be expressed by the derivative of its current. Also, a capacitor current it can be expressed by a sum of inductor currents and the output current (if current source output), while an inductor voltage is a sum of capacitor voltages, the input voltage and output (if current source output). For a resonant tank topology, the differential equations of the resonant variables can be summarized in matrix form as follows:

$$\frac{d}{d\theta} X = AX + B \tag{5.5}$$

where X is the variable vector, A and B are the coefficient matrices, and they look like:

$$X = [x_1, x_2 \ldots, x_k]^T$$

$$A = \begin{bmatrix} 0 & a_{12} & a_{13} & \cdots & & a_{1k} \\ a_{21} & 0 & a_{23} & \cdots & & a_{2k} \\ a_{31} & a_{32} & 0 & & & \vdots \\ \vdots & \vdots & & \ddots & & a_{(k-1)k} \\ a_{k1} & a_{k2} & \cdots & a_{k(k-1)} & & 0 \end{bmatrix}$$

$$B = [b_1, b_2 \ldots, b_k]^T$$

From the above relation, the ith order derivatives can be obtained as

$$\frac{d^i}{d\theta^i}X = A\frac{d^{(i-1)}}{d\theta^{i-1}}X + B \tag{5.6}$$

If we treat these derivatives as resonant variables, the new variable vector for total k resonant components from 0 to $(k-1)$th order derivatives is reconstructed as follows:

$$X' = \left[X^T, \frac{dX^T}{d\theta}, \cdots, \left(\frac{d^i}{d\theta^i}X^T \right), \cdots, \left(\frac{d^{k-1}}{d\theta^{k-1}}X^T \right) \right]_{k^2 \times 1}^T \tag{5.7}$$

Therefore, a new matrix equation is derived as

$$A'X' + B' = 0 \tag{5.8}$$

in which

$$A' = \begin{bmatrix} A & -I & & & \\ & A & -I & & \\ & & \ddots & \ddots & \\ & & & A & -I \end{bmatrix}_{k(k-1) \times k^2} \tag{5.9}$$

$$B' = \begin{bmatrix} B \\ O_{k(k-2) \times 1} \end{bmatrix}_{k(k-1) \times 1} \tag{5.10}$$

and I is the identity matrix with the size of $k \times k$, $O_{k(k-2) \times 1}$ is the zero matrix with the size of $k(k-2) \times 1$.

If we assume x_1 has the expression (5.4), then any high order derivative of x_1 is also obtained. Therefore, x_1 and its high order derivatives can be treated as known parameters. If we only consider the 0 to $(k-2)$th order derivatives of the rest resonant variables as the unknowns, the variable vector is then given by

$$X'' = \left[X_r^T, \frac{dX_r^T}{d\theta}, \cdots, \left(\frac{d^i}{d\theta^i} X_r^T \right), \cdots, \left(\frac{d^{k-1}}{d\theta^{k-1}} X_r^T \right) \right]^T_{(k-1)^2 \times 1} \tag{5.11}$$

where $X_r = [x_2, x_3, \ldots, x_k]^T$; the number of the unknown variables becomes $(k-1)^2$. To solve the new variable vector, another new coefficient matrix A'' is constructed from A' by eliminating rows $[k(k-2)+2,\ k(k-2)+3, \ldots, k(k-1)]$, columns $[1, k+1, 2k+1, \ldots, k(k-1)+1]$, and columns $[k(k-1)+2, k(k-1)+3, \ldots, k^2]$, and after the elimination the size of A' reduce to $(k-1)^2 \times (k-1)^2$, which is a square matrix.

$$\begin{bmatrix} 0 & a_{12} & a_{13} & -1 & 0 & 0 & 0 & 0 & 0 \\ a_{21} & 0 & a_{23} & 0 & -1 & 0 & 0 & 0 & 0 \\ a_{31} & a_{32} & 0 & 0 & 0 & -1 & 0 & 0 & 0 \\ 0 & 0 & 0 & 0 & a_{12} & a_{13} & -1 & 0 & 0 \\ 0 & 0 & 0 & a_{21} & 0 & a_{23} & 0 & -1 & 0 \\ 0 & 0 & 0 & a_{31} & a_{32} & 0 & 0 & 0 & -1 \end{bmatrix}$$

Figure 5.5 From A'' to A', eliminate the matrix elements circled in red ($k=3$)

The constant matrix B' is reconstructed by including x_1 and its derivatives, and the new matrix B'' is given by

145

$$B'' = \begin{bmatrix} B \\ O \end{bmatrix}_{(k-1)^2 \times 1} + \begin{bmatrix} \left[-\dfrac{dx_1}{d\theta}, \quad a_{21}x_1, \quad a_{31}x_1, \quad \cdots \quad a_{k1}x_1 \right]^T \\ \left[-\dfrac{d^2x_1}{d\theta^2}, \quad a_{21}\dfrac{dx_1}{d\theta}, \quad a_{31}\dfrac{dx_1}{d\theta}, \quad \cdots \quad a_{k1}\dfrac{dx_1}{d\theta} \right]^T \\ \vdots \\ \left[-\dfrac{d^{k-2}x_1}{d\theta^{k-2}}, \quad a_{21}\dfrac{d^{k-3}x_1}{d\theta^{k-3}}, \quad a_{31}\dfrac{d^{k-3}x_1}{d\theta^{k-3}}, \quad \cdots \quad a_{k1}\dfrac{d^{k-3}x_1}{d\theta^{k-3}} \right]^T \\ -\dfrac{d^{k-1}x_1}{d\theta^{k-1}} \end{bmatrix}_{(k-1)^2 \times 1} \tag{5.12}$$

For $k = 3$, $B'' = \left[b_1 - \dfrac{dx_1}{d\theta}, b_2 + a_{21}x_1, b_3 + a_{31}x_1, -\dfrac{d^2x_1}{d\theta^2} \right]^T$.

After obtaining the two matrices, we can solve X'' as follows:

$$X'' = -(A'')^{-1} B'' \tag{5.13}$$

If the matrix A'' is not invertible, another resonant variable should be chosen as the known variable, and we can then repeat the above procedure by properly readjusting the order of the $x_1, \ldots, x_k$ variables. Since the operation functions of a resonant tank do exist, an invertible A'' is assuredly achievable.

The above variable solving process can be summarized as an iterative process, as shown in Figure 5.6, which can be implemented by a computer program.
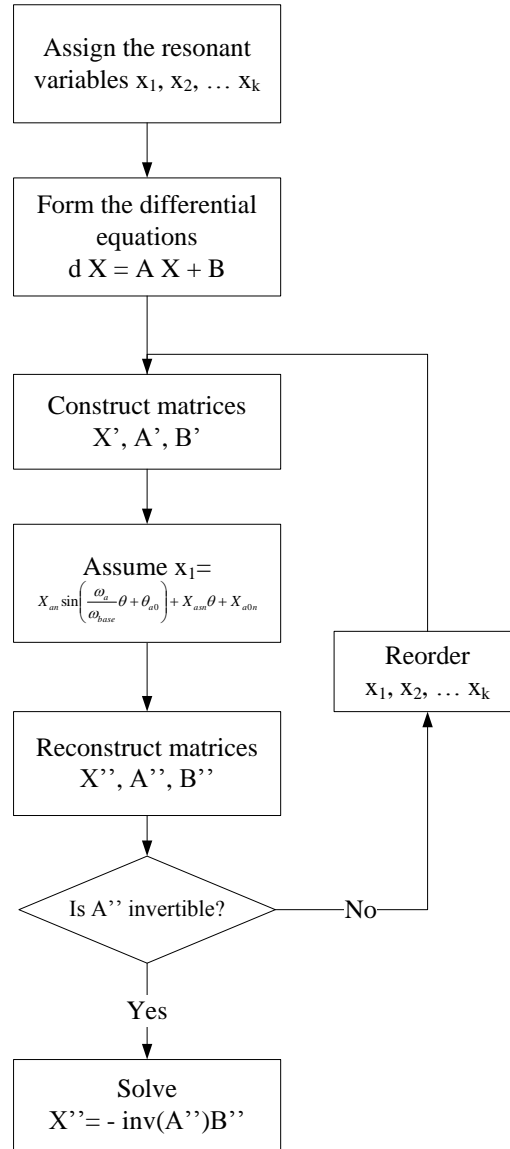
Figure 5.6 Resonant variables solving procedure

It can be seen that each resonant variable is a linear combination of expression (5.4) and its derivative functions. In other words, for a given tank topology and resonant stage, there are at most four unknown parameters X_{an}, X_{asn}, X_{0n}, θ_{a0} for all resonant variable functions. The high order derivatives of a variable are directly given in equations (5.5), while they can also be derived from the low order derivatives. By comparing the coefficients of the derivative expressions obtained from these two approaches, the parameters X_{asn} and X_{0n} may be solvable so that the

147

number of the unknowns can be further reduced. Note that for some resonant converter topologies, the resonant tank can be divided into sub-tanks, such as the LCLC tank topology as seen in Figure 5.7. The above process still applies to each sub-tank, and consequently there are more unknown parameters.
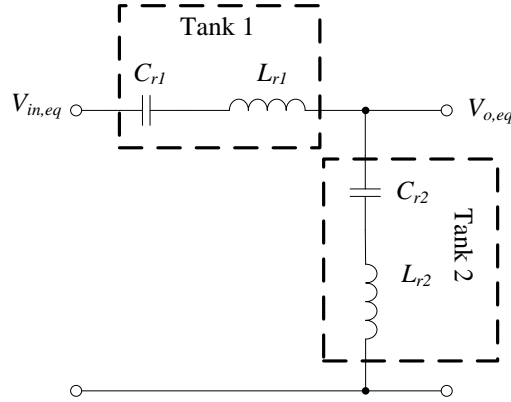
Figure 5.7 The LCLC resonant tank divided into 2 sub-tanks

5.4 Resonant Stage Boundary and Transition Conditions

To solve the resonant variable functions for each resonant stage, the boundary conditions of the operation mode should be found to establish equations. In general, the boundary conditions can be summarized into three categories, which are the symmetry conditions, the continuity conditions and the stage constraint conditions.

The symmetry conditions state that the starting and ending value of a resonant variable for the half switching cycle have the same absolute value but opposite polarity.

The continuity conditions are that resonant variables remain continuous at the transition of two resonant stages.

The stage constraint conditions vary from stage to stage. The stage constraints are placed on the resonant tank output voltage, denoted as v_{tkn}, and the tank output current, denoted as i_{tkn}. Although v_{tkn} and i_{tkn} are not the designated resonant variables, they can be represented by the linear combinations of the resonant variables. For voltage-source-type output, the tank output is either clamped by the output voltage or in open circuit. In stage P, it requires that $v_{tkn} = 1, i_{tkn} > 0$; in stage N, it requires that $v_{tkn} = -1, i_{tkn} < 0$; in stage O, it requires that $|v_{tkn}| < 1, i_{tkn} = 0$. For current-source-type output, the tank output is either forced to provide constant output current or shorted. In stage P, it requires that $v_{tkn} > 0, i_{tkn} = p_{on}$; in stage N, it requires that $v_{tkn} < 0, i_{tkn} = -p_{on}$; in stage O, it requires that $v_{tkn} = 0, |i_{tkn}| < p_{on}$.

The boundary conditions are summarized in Table 5.1.

Table 5.1 The Operation Mode Boundary Conditions of Resonant Converters

		Voltage Source Output	Current Source Output
Symmetry Conditions		$x_{iA}(0) = -x_{iB}(\theta_B), \qquad i = 1,2,\dots,k$	
Continuity Conditions		$x_{iC}(\theta_C) = x_{iD}(\theta_D), \qquad i = 1,2,\dots,k$	
Stage Constraints	Stage P	$i_{tkn,P} \geq 0,$ $i_{tkn,P}(\theta_P) = 0$	$v_{tkn,P} \geq 0,$ $v_{tkn,P}(\theta_P) = 0$
	Stage N	$i_{tkn,N} \leq 0,$ $i_{tkn,N}(\theta_N) = 0$	$v_{tkn,N} \leq 0,$ $v_{tkn,N}(\theta_N) = 0$
	Stage O	$|v_{tkn,O}| \leq 1,$ $v_{tkn,O}(\theta_O)$ $= \begin{cases} 1 \ \ if \ followed \ by \ stage \ P \\ -1 \ \ if \ followed \ by \ stage \ N \end{cases}$	$|i_{tkn,O}| \leq p_{on},$ $i_{tkn,O}(\theta_O)$ $= \begin{cases} p_{on} \ \ if \ followed \ by \ stage \ P \\ -p_{on} \ \ if \ followed \ by \ stage \ N \end{cases}$

*Note: x_i denotes the ith resonant variables; assume that subscript A denotes the starting stage, B denotes the ending stage, and C, D are two adjacent stages

Based on the above three conditions, if the L-C values of the resonant tank are given and the following normalized parameters are known: the gain M, the switching frequency f_n and the load p_{on}, sufficient simultaneous equations can be established to solve the resonant variable function's parameters for each stage. The durations of each stage can also be solved noting that the sum phase angle of every stage is equal to π/f_n.

In addition, there are output current and voltage balance conditions for voltage and current source output configurations respectively. The output current balance condition requires that the average $|i_{tkn}|$ over the half cycle is equal to p_{on} for voltage source output, while the voltage balance condition states that the average $|v_{tkn}|$ equals 1 for current source output. Since in stage O for either output types the resonant tank is cut off from the output load, only stage P and N are related to the balance condition. The current balance condition is given by

$$p_{on} = \frac{f_n}{\pi}\left[\int_{stageP} i_{tkn}d\theta - \int_{stageN} i_{tkn}d\theta\right] \tag{5.14}$$

The voltage balance condition is given by

$$1 = \frac{f_n}{\pi}\left[\int_{stageP} v_{tkn}d\theta - \int_{stageN} v_{tkn}d\theta\right] \tag{5.15}$$

With the added balance condition, one of the three parameters, M, f_n and p_{on}, can be solved if the other two are specified.

In numerical analysis software, iterative algorithms are typically employed to find the solutions; the limitation is not about the time-consuming issue provided today's fast computing capacity, but is that the algorithm, usually local optimized, only gives one root of the nonlinear equation, which may be mathematically correct but not physically valid to fit in the circuit

150

principle. Therefore, it is important to know the restrictions of each equation variables in order to select the proper starting values for the equation solving functions. In the LLC analysis, the operation mode boundaries are investigated and the ranges of frequency, gain and load for each mode are obtained. The same principle can be applied to the generalized analysis for mode boundary study.

From the stage constraints, some of the stage changing conditions can be found. For instance, the condition $i_{tkn} = 0$ marks the end of stage P for voltage source output. However, whether the converter will enter stage N or O is unable to determine provided only this condition. Actually, it can be seen that the stage shift from P to N, P to O, N to P and N to O for the two output types all have the same transition condition. To figure out the following stage after P or N, the boundary mode condition should be taking into consideration. As stage O is usually to act as a transition stage between stage P and N, for the resonant tank operating from stage P to O then to N, letting the period of stage O reduce to zero will give the boundary mode for stage changing from P to N, which is

$$v_{tkn,O}(\theta_O)\big|_{\theta_O \to 0} = -1 \tag{5.16}$$

where the subscript O denotes stage O, and θ_O is the time interval of stage O. From the continuity conditions, the boundary mode condition can be expressed in terms of the ending values of stage P variables as follows:

$$v_{tkn,O}(\theta_O)\big|_{\theta_O \to 0} = \sum_{i=1}^{k} c_i v_{i,O}(0) + d = \sum_{i=1}^{k} c_i v_{i,P}(\theta_P) + d = -1 \tag{5.17}$$

151

where $c_i, i = 1,2, \dots k$ and d is the variables' coefficients in the $v_{tkn,O}$ expression. So, if $\sum_{i=1}^{k} c_i v_{i,P}(\theta_P) + d \le -1$, the converter will enter stage N directly after stage P; otherwise, the converter will enter stage O first.

Also, the boundary mode condition can be alternatively expressed in terms of the starting values of stage N variables as

$$\sum_{i=1}^{k} c_i v_{i,N}(0) + d = -1 \tag{5.18}$$

This condition can be used to judge the preceding stage of stage N: if $\sum_{i=1}^{k} c_i v_{i,N}(0) + d \le -1$, the preceding stage is stage P; otherwise, it is stage O.

Taking the PON and PN boundary mode condition of the LLC resonant converter as an example, the expression of $v_{tkn,O}$ is given as

$$v_{tkn,O} = v_{mOn} = \frac{m-1}{m}\left(\frac{1}{M} - v_{COn}\right) \tag{5.19}$$

and therefore the boundary condition is

$$\frac{m-1}{m}\left(\frac{1}{M} - v_{CPn}(\theta_P)\right) = -1$$
$$\Rightarrow I_{rPn}\cos(\theta_P + \theta_{P0}) = -\frac{2m-1}{m-1} \text{ or } I_{rNn}\cos(\theta_{N0}) = -\frac{1}{m-1} \tag{5.20}$$

which is the same with the result derived in Chapter 2.3.

In the similar way, the other boundary mode conditions can also be derived, and the stage transition conditions for two output types are listed in Table 5.2 and Table 5.3.

Table 5.2 The Resonant Stage Transition Conditions for Voltage Source Output

From / To	Stage P	Stage N	Stage O
Stage P	-	$i_{tkn} = 0,$ $\sum_{i=1}^{k} c_i v_{i,N}(\theta_N) + d \geq 1$	$v_{tkn} = 1$
Stage N	$i_{tkn} = 0,$ $\sum_{i=1}^{k} c_i v_{i,P}(\theta_P) + d \leq -1$	-	$v_{tkn} = -1$
Stage O	$i_{tkn} = 0,$ $\sum_{i=1}^{k} c_i v_{i,P}(\theta_P) + d > -1$	$i_{tkn} = 0,$ $\sum_{i=1}^{k} c_i v_{i,N}(\theta_N) + d < 1$	-

*Note: c_i and d satisfy that $v_{tkn,O} = \sum_{i=1}^{k} c_i v_{i,O} + d$

Table 5.3 The Resonant Stage Transition Conditions for Current Source Output

From / To	Stage P	Stage N	Stage O
Stage P	-	$v_{tkn} = 0,$ $\sum_{i=1}^{k} g_i i_{i,N}(\theta_N) + h \geq p_{on}$	$i_{tkn} = p_{on}$
Stage N	$v_{tkn} = 0,$ $\sum_{i=1}^{k} g_i i_{i,P}(\theta_P) + h \leq -p_{on}$	-	$i_{tkn} = -p_{on}$
Stage O	$v_{tkn} = 0,$ $\sum_{i=1}^{k} g_i i_{i,P}(\theta_P) + h > -p_{on}$	$v_{tkn} = 0,$ $\sum_{i=1}^{k} g_i i_{i,N}(\theta_N) + h < p_{on}$	-

*Note: g_i and h satisfy that $i_{tkn,O} = \sum_{i=1}^{k} g_i i_{i,O} + h$

With the mode boundary condition, only one of the three parameters, M, f_n and p_{on} is needed to solve the rest two. In other words, the border lines between operation modes can be drawn, and the gain range and load range of a mode are identified.

5.5 Generalized Analysis Procedure

Based on the studies in previous sections, a resonant converter topology can be represented by normalized L-C resonant stage circuits, the current and voltage variables can be derived and expressed by normalized parameters and these variables along with the DC characteristics of the converter can be solved from the boundary conditions of operation modes using numerical computing tools. It is a generalized procedure for resonant converter analysis, of which the flowchart is given in Figure 5.8.

```
                  ┌─────────────────────┐
                  │  Find the equivalent │
                  │   circuits for each  │
                  │    resonant stage    │
                  └─────────────────────┘
                            │
                            ▼
                  ┌─────────────────────┐
                  │  Normalize circuit   │
                  │     parameters       │
                  └─────────────────────┘
                            │
                            ▼
                  ┌─────────────────────┐
                  │   Assign resonant    │
                  │      variables       │
                  └─────────────────────┘
                            │
                            ▼
                  ┌─────────────────────┐
                  │   Derive variable    │
                  │     functions        │
                  └─────────────────────┘
                            │
                            ▼
                  ┌─────────────────────┐
                  │  Find the operation  │
                  │        modes         │
                  └─────────────────────┘
                      │            │
                      ▼            ▼
            ┌──────────────┐  ┌──────────────────┐
            │              │  │ Build mode        │
            │ Build        │  │ boundary          │
            │ boundary     │  │ conditions        │
            │ conditions   │  └──────────────────┘
            │ for each     │          │
            │ mode         │          ▼
            └──────────────┘  ┌──────────────────┐
                   │          │ Solve mode        │
                   │          │ boundaries        │
                   │          └──────────────────┘
                   │                  │
                   └────────┬─────────┘
                            ▼
                  ┌─────────────────────┐
                  │ Solve resonant       │
                  │ variables            │
                  │ and DC gain          │
                  └─────────────────────┘
```
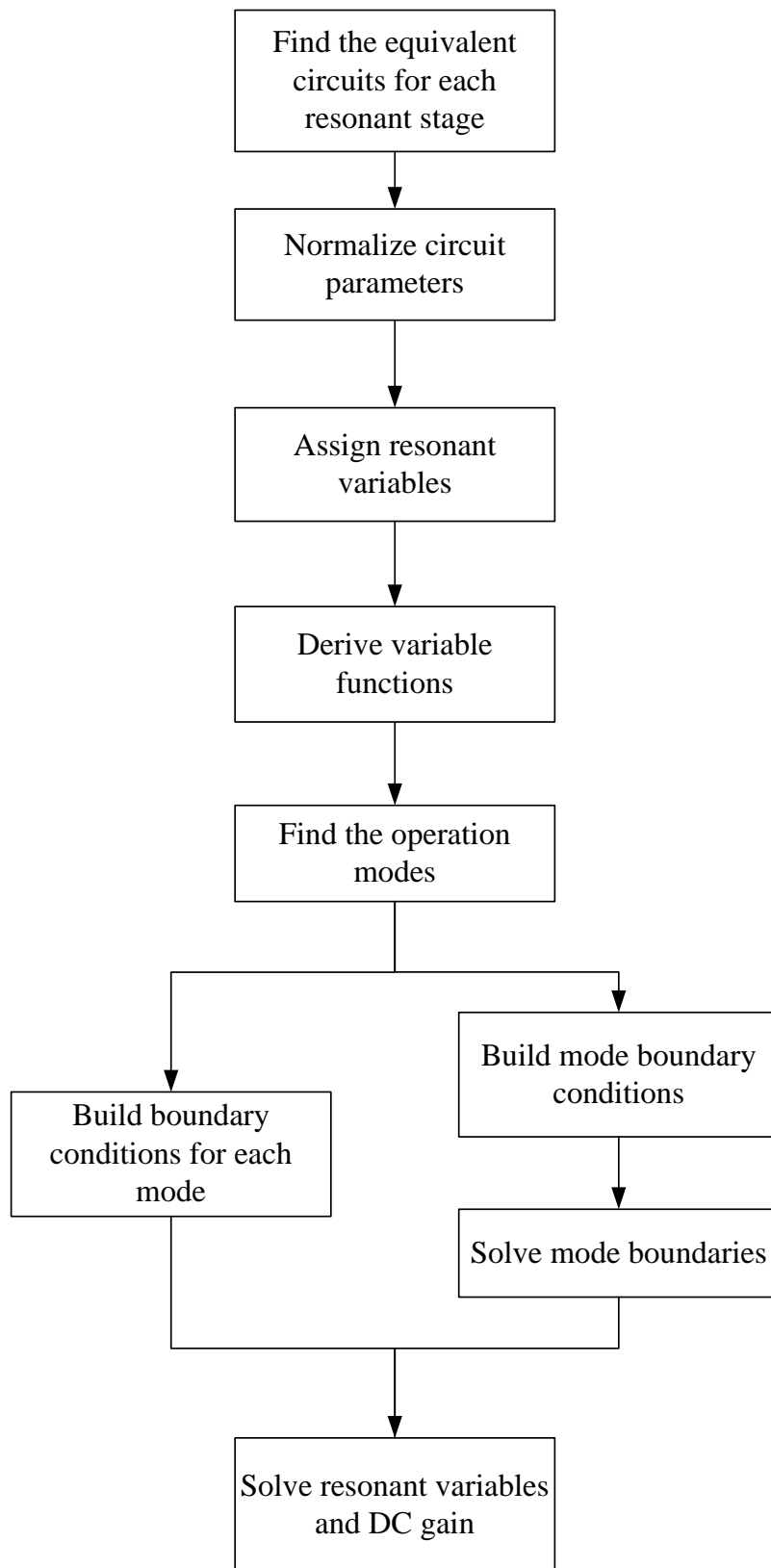
Figure 5.8 Generalized analysis procedure of a resonant converter

5.6 Resonant Tank Analysis Examples

5.6.1 Parallel Resonant Converter Analysis

The equivalent resonant tank circuit with normalized parameters is shown in Figure 5.9. The capacitor voltage and inductor current are selected as the resonant variables. As seen in Figure 5.9, the inductor is clamped to $1/M$ in stage O and the current is increasing linearly without resonance.

$$\omega_{base} = \frac{1}{\sqrt{L_r C_r}}, Z_{base} = \sqrt{\frac{L_r}{C_r}}$$
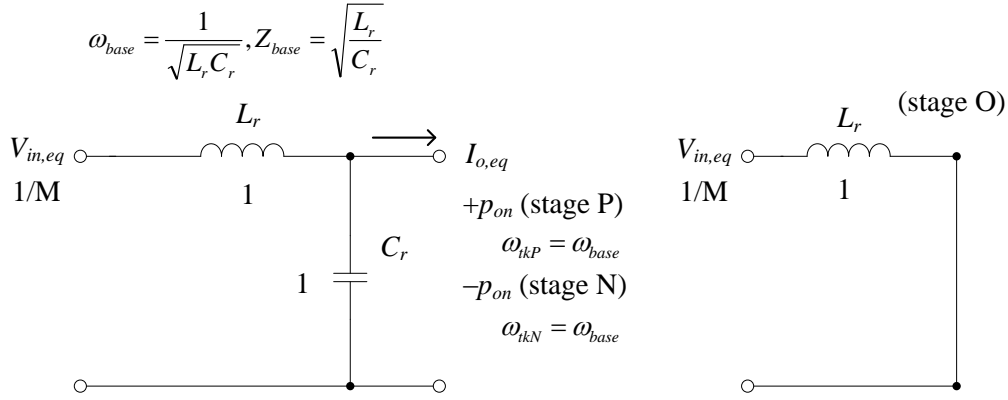
Figure 5.9 Normalized resonant tank circuit of the PRC

For stage P, the differential equations about the resonant variables are as follows:

$$\frac{d}{d\theta}\begin{bmatrix} i_{rPn} \\ v_{rPn} \end{bmatrix} = \begin{bmatrix} 0 & -1 \\ -1 & 0 \end{bmatrix}\begin{bmatrix} i_{rPn} \\ v_{rPn} \end{bmatrix} + \begin{bmatrix} 1/M \\ p_{on} \end{bmatrix} \tag{5.21}$$

Assume the current expression is as follows:

$$i_{rPn} = I_{Pn}\sin(\theta + \theta_{P0}) + I_{Psn}\theta + I_{P0n} \tag{5.22}$$

Substitute (5.22) into (5.21) and it can be solved that:

$$i_{rPn} = I_{Pn} \sin(\theta + \theta_{P0}) + I_{Psn}\theta + I_{P0n}$$

$$v_{rPn} = I_{Pn} \cos(\theta + \theta_{P0}) + I_{Psn} + \frac{1}{M}$$

(5.23)

Take the derivatives of (5.23) and compare the coefficients with (5.21) and it gives that

$$I_{Psn} = 0$$

$$I_{P0n} = p_{on}$$

(5.24)

Therefore, the variable functions are obtained:

$$i_{rPn} = I_{Pn} \sin(\theta + \theta_{P0}) + p_{on}$$

$$v_{rPn} = I_{Pn} \cos(\theta + \theta_{P0}) + \frac{1}{M}$$

(5.25)

Similarly, the variable functions for stage N are derived as follows:

$$i_{rNn} = I_{Nn} \sin(\theta + \theta_{P0}) - p_{on}$$

$$v_{rNn} = I_{Nn} \cos(\theta + \theta_{P0}) + \frac{1}{M}$$

(5.26)

For stage O, the variable functions are as follows:

$$i_{rOn} = \frac{1}{M}\theta + I_{O0n}$$

$$v_{rOn} = 0$$

(5.27)

From mode analysis, the PRC has two operation modes, NP mode and NOP mode. The boundary conditions for the two modes are listed in Table 5.4.

Table 5.4 The boundary conditions of PRC in NP and NOP mode

	NP mode	NOP mode
Symmetry Conditions	$i_{rNn}(0) = -i_{rPn}(\theta_P)$ $v_{rNn}(0) = -v_{rPn}(\theta_P)$	
Continuity Conditions	$i_{rNn}(\theta_N) = i_{rPn}(0)$ $v_{rNn}(\theta_N) = v_{rPn}(0)$	$i_{rNn}(\theta_N) = i_{rOn}(0)$ $v_{rNn}(\theta_N) = v_{rOn}(0)$ $i_{rOn}(\theta_O) = i_{rPn}(0)$ $v_{rOn}(\theta_O) = v_{rPn}(0)$
Stage Constraints	$v_{rNn} \leq 0$ $v_{rNn}(\theta_N) = 0$ $v_{rPn} \geq 0$ $v_{rPn}(0) = 0$	$v_{rNn} \leq 0$ $v_{rNn}(\theta_N) = 0$ $i_{rOn}(\theta_O) = p_{on}$ $v_{rPn} \geq 0$ $v_{rPn}(0) = 0$

As in stage O the tank output current is $i_{tkn,O} = i_{rOn}$, the NP/NOP boundary mode condition can be read from Table 2.2 as

$$i_{rNn}(\theta_N) = p_{on} \tag{5.28}$$

Hence, with the boundary mode condition (5.28), the voltage balance condition (5.15) and the NP mode conditions in Table 5.4, the NP/NOP mode boundary can be solved and it is illustrated in Figure 5.10. NOP mode, as a DCM, occupies the heavy load and low gain region, while NP mode, the CCM, is in light load and high gain region.
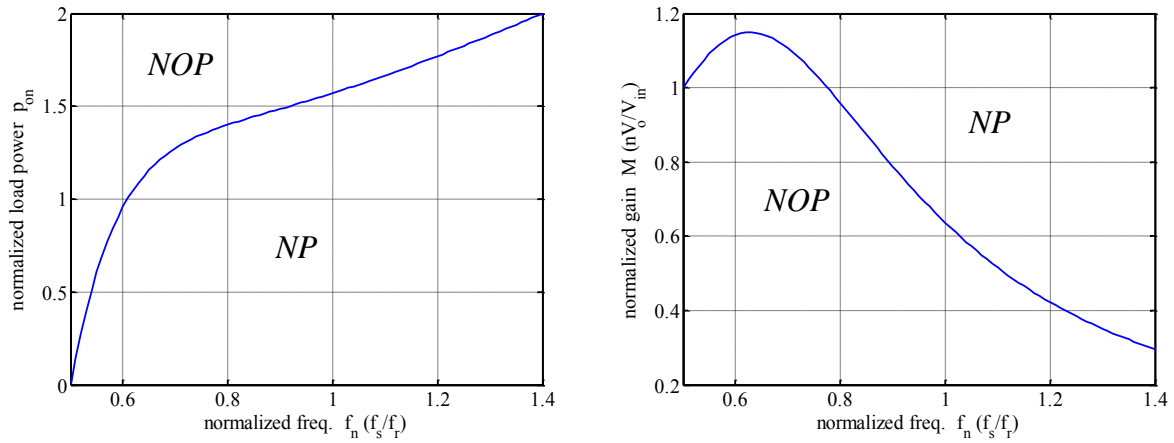
Figure 5.10 The distribution of NP and NOP mode of PRC

The operation waveforms of the two modes are shown in Figure 5.11 and Figure 5.12. The transition between stages can be clearly observed from the waveforms. In stage N, v_C is less than 0, and when it reaches 0, the stage ends; if the end value of i_r is greater than p_{on}, the converter will enter stage P, otherwise the converter will enter stage O. In stage O, v_C remains 0 and i_r increases linearly; stage O ends if i_r reaches p_{on}.

Figure 5.11 The PRC operating waveforms in NOP mode ($f_n=0.5, p_{on}=2.2$)

159

Figure 5.12 The PRC operating waveforms in NP mode ($f_n=1, p_{on}=1$)

The voltage gain characteristics can be seen in Figure 5.13.
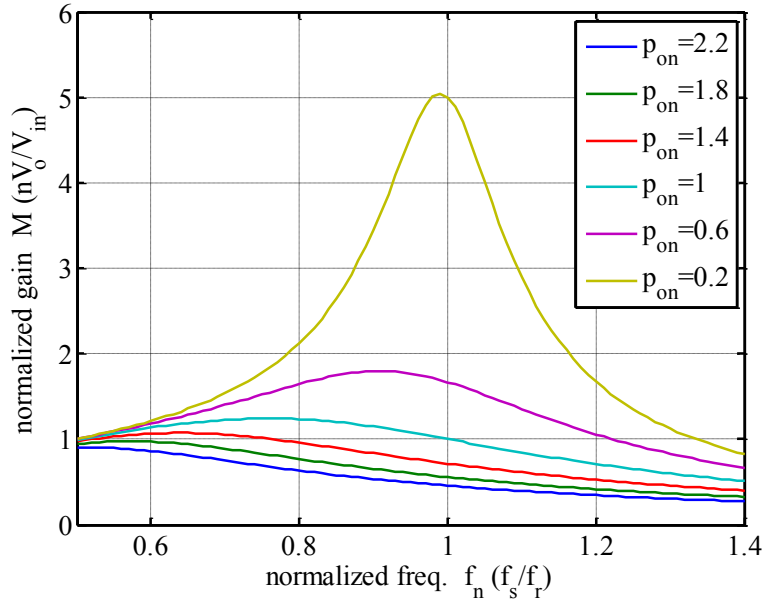
Figure 5.13 The PRC DC gain characteristics under different load conditions

5.6.2 LCC Resonant Converter Analysis

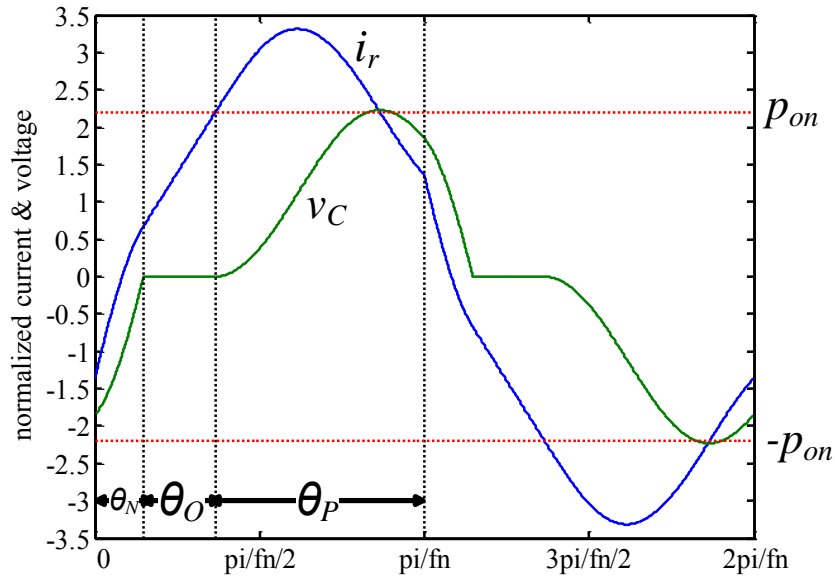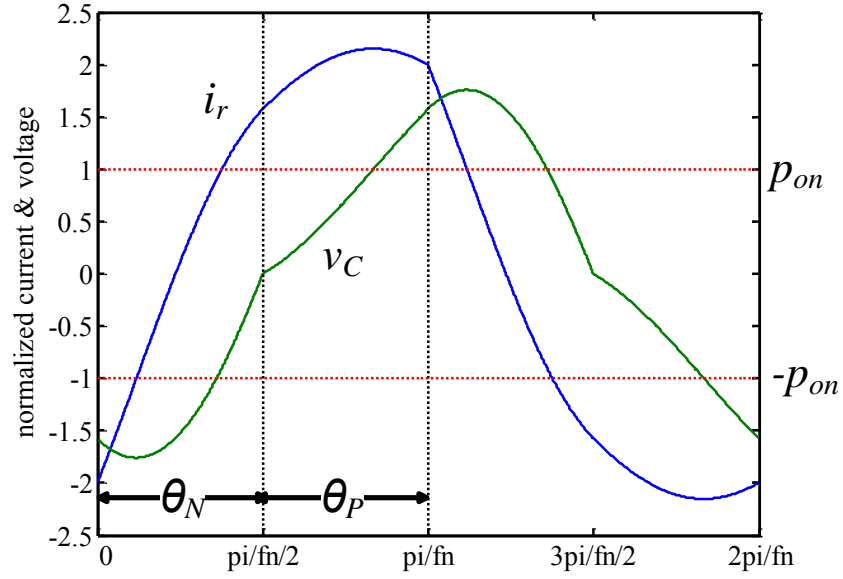The equivalent resonant stage circuit with normalized parameters of the LCC converter is illustrated in Figure.

$$C_m = (m-1)C_r \quad \omega_{base} = \sqrt{\frac{m}{m-1}}\frac{1}{\sqrt{L_r C_r}}, Z_{base} = \sqrt{\frac{m}{m-1}}\sqrt{\frac{L_r}{C_r}}$$
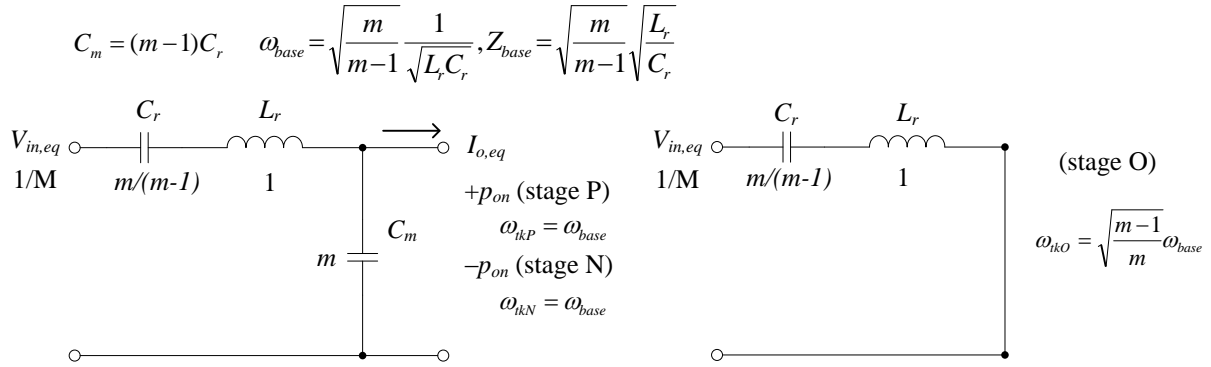
Figure 5.14 Normalized resonant tank circuit of the LCC

For stage P, the differential equations about the resonant variables are given by:

$$\frac{d}{d\theta}\begin{bmatrix} v_{rPn} \\ v_{mPn} \\ i_{LPn} \end{bmatrix} = \begin{bmatrix} 0 & 0 & \dfrac{m-1}{m} \\ 0 & 0 & \dfrac{1}{m} \\ -1 & -1 & 0 \end{bmatrix}\begin{bmatrix} v_{rPn} \\ v_{mPn} \\ i_{LPn} \end{bmatrix} + \begin{bmatrix} 0 \\ -\dfrac{p_{on}}{m} \\ \dfrac{1}{M} \end{bmatrix} \tag{5.29}$$

Assume that v_{rPn} is expressed as

$$v_{rPn} = V_{Pn}\sin(\theta + \theta_{P0}) + V_{Psn}\theta + V_{P0n} \tag{5.30}$$

The coefficient matrices are constructed as follows:

$$A'' = \begin{bmatrix} 0 & \dfrac{m-1}{m} & 0 & 0 \\[2ex] 0 & \dfrac{1}{m} & -1 & 0 \\[2ex] -1 & 0 & 0 & -1 \\[2ex] 0 & 0 & 0 & \dfrac{m-1}{m} \end{bmatrix} \tag{5.31}$$

$$B'' = \left[-\frac{dv_{rPn}}{d\theta}, \quad -\frac{p_{on}}{m}, \quad \frac{1}{M} - v_{rPn}, \quad -\frac{d^2 v_{rPn}}{d\theta^2} \right]^T$$

The resonant variables can be solved as

$$\begin{bmatrix} v_{mPn} \\[2ex] i_{LPn} \\[2ex] \dfrac{dv_{mPn}}{d\theta} \\[2ex] \dfrac{di_{LPn}}{d\theta} \end{bmatrix} = -(A'')^{-1} B'' = \begin{bmatrix} -v_{rPn} - \dfrac{m}{m-1}\dfrac{d^2 v_{rPn}}{d\theta^2} + \dfrac{1}{M} \\[2ex] \dfrac{m}{m-1}\dfrac{dv_{rPn}}{d\theta} \\[2ex] \dfrac{1}{m-1}\dfrac{dv_{rPn}}{d\theta} - \dfrac{p_{on}}{m} \\[2ex] \dfrac{m}{m-1}\dfrac{d^2 v_{rPn}}{d\theta^2} \end{bmatrix} \tag{5.32}$$

By substituting (5.30) into (5.32), the parameter V_{Psn} can be solved as $V_{Psn} = \frac{m-1}{m^2} p_{on}$, and the

resonant variable functions are:

$$v_{rPn} = V_{Pn}\sin(\theta + \theta_{P0}) + \frac{m-1}{m^2} p_{on}\theta + V_{P0n}$$

$$v_{mPn} = \frac{1}{m-1}V_{Pn}\sin(\theta + \theta_{P0}) - \frac{m-1}{m^2} p_{on}\theta - V_{P0n} + \frac{1}{M} \tag{5.33}$$

$$i_{LPn} = \frac{m}{m-1}V_{Pn}\cos(\theta + \theta_{P0}) + \frac{p_{on}}{m}$$

Similarly, the resonant variables in stage N can be expressed as

$$v_{rNn} = V_{Nn} \sin(\theta + \theta_{N0}) - \frac{m-1}{m^2} p_{on}\theta + V_{N0n}$$

$$v_{mNn} = \frac{1}{m-1} V_{Nn} \sin(\theta + \theta_{N0}) + \frac{m-1}{m^2} p_{on}\theta - V_{N0n} + \frac{1}{M} \quad (5.34)$$

$$i_{LNn} = \frac{m}{m-1} V_{Nn} \cos(\theta + \theta_{N0}) - \frac{p_{on}}{m}$$

For stage O, it can be solved that

$$v_{rOn} = V_{rOn} \sin\left(\sqrt{\frac{m-1}{m}}\theta + \theta_{O0}\right) - \frac{1}{M}$$

$$v_{mNn} = 0 \quad (5.35)$$

$$i_{LOn} = \sqrt{\frac{m}{m-1}} V_{rOn} \cos\left(\sqrt{\frac{m-1}{m}}\theta + \theta_{O0}\right)$$

The LCC also has NP and NOP modes in high frequency operation region, which are similar to the PRC. The boundary conditions for these two modes are summarized in Table 5.5

Table 5.5 The boundary conditions of LCC in NP and NOP mode

	NP mode	NOP mode
Symmetry Conditions	$v_{rNn}(0) = -v_{rPn}(\theta_P)$ $v_{mNn}(0) = -v_{mPn}(\theta_P)$ $i_{LNn}(0) = -i_{LPn}(\theta_P)$	
Continuity Conditions	$v_{rNn}(\theta_N) = v_{rPn}(0)$ $v_{mNn}(\theta_N) = v_{mPn}(0)$ $i_{LNn}(\theta_N) = i_{LPn}(0)$	$v_{rNn}(\theta_N) = v_{rOn}(0)$ $v_{mNn}(\theta_N) = v_{mOn}(0)$ $i_{LNn}(\theta_N) = i_{LOn}(0)$ $v_{rOn}(\theta_O) = v_{rPn}(0)$ $v_{mOn}(\theta_O) = v_{mPn}(0)$ $i_{LOn}(\theta_O) = i_{LPn}(0)$
Stage Constraints	$v_{mNn} \leq 0, v_{mNn}(\theta_N) = 0$ $v_{mPn} \geq 0, v_{mPn}(0) = 0$	$v_{mNn} \leq 0, v_{mNn}(\theta_N) = 0$ $i_{LOn} \leq p_{on}, i_{LOn}(\theta_O) = p_{on}$ $v_{mPn} \geq 0, v_{mPn}(0) = 0$

The voltage balance condition can be expressed as

$$\frac{f_n}{\pi}\left(\int_0^{\theta_P} v_{mPn}(\theta)d\theta - \int_0^{\theta_N} v_{mNn}(\theta)d\theta\right) = 1 \tag{5.36}$$

Also, the tank output current in stage O is $i_{tkn,O} = i_{LOn}$ as the capacitor C_m is shorted, and hence the NP/NOP boundary mode condition is given as

$$i_{LNn}(\theta_N) = p_{on} \tag{5.37}$$

The boundary NP mode can be solved using equations (5.36) – (5.37) and the NP mode conditions in Table 5.4. The border lines between NP and NOP for different m is shown in Figure 5.15. Similar to the mode distribution of the PRC, NOP mode is in the heavier load and lower gain region, and NP mode is in lighter load and higher gain area. It can be seen that the border line locates in a higher position in the load power plot for a higher m. Note that every NP/NOP boundary has a minimum frequency limit as shown in Figure 5.15, and it varies under different m. It is because that the span of stage P increases at a decreased frequency and eventually it will dominate the entire half cycle at the minimum frequency. Beyond this frequency lower limit, there are other operation modes, which are in ZCS region and are not discussed here.
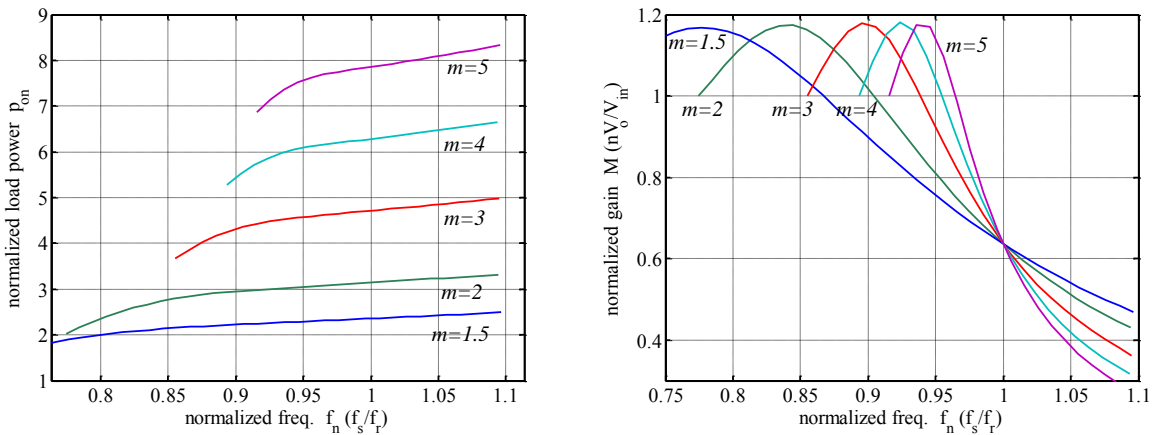
Figure 5.15 The boundaries of NP and NOP mode under different m for LCC

The typical operation waveforms of the two modes are shown in Figure 5.16 and Figure 5.17. The transition condition between stages can be clearly observed from v_m and i_L waveforms. They resemble v_r and i_r waveforms of the PRC. However, for LCC i_L increases sinusoidally in stage O, while for PRC i_r is linear.
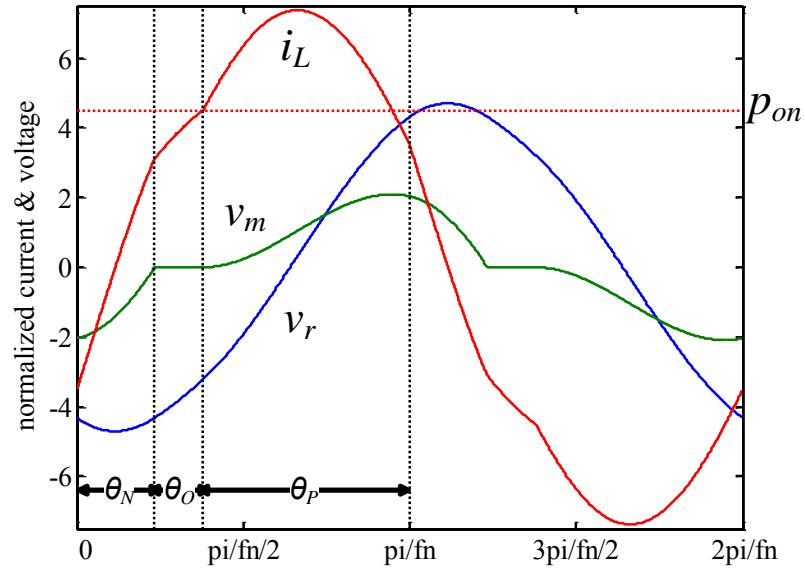
Figure 5.16 The LCC operating waveforms in NOP mode ($m=2, f_n=0.8, p_{on}=4.5$)
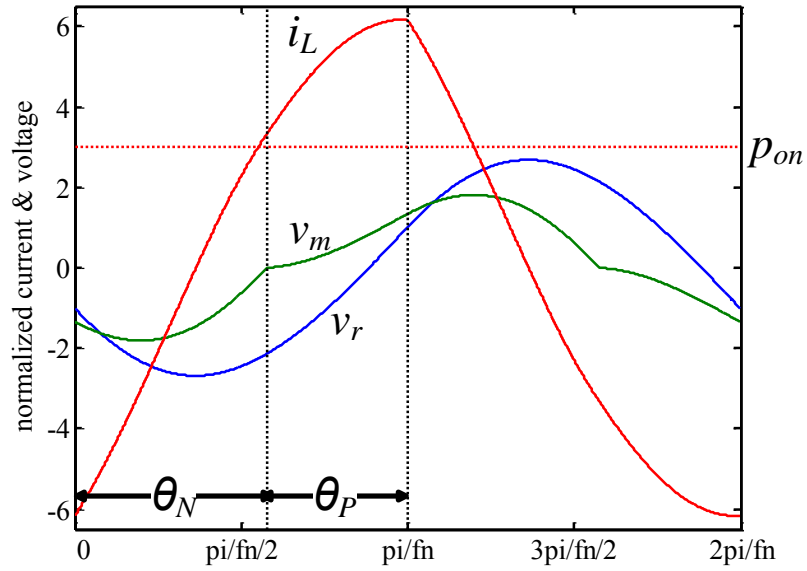
Figure 5.17 The LCC operating waveforms in NP mode ($m=2$, $f_n=1.1$, $p_{on}=3$)

A typical DC gain characteristics plot of the LCC is shown in Figure 5.18Figure 5.13.
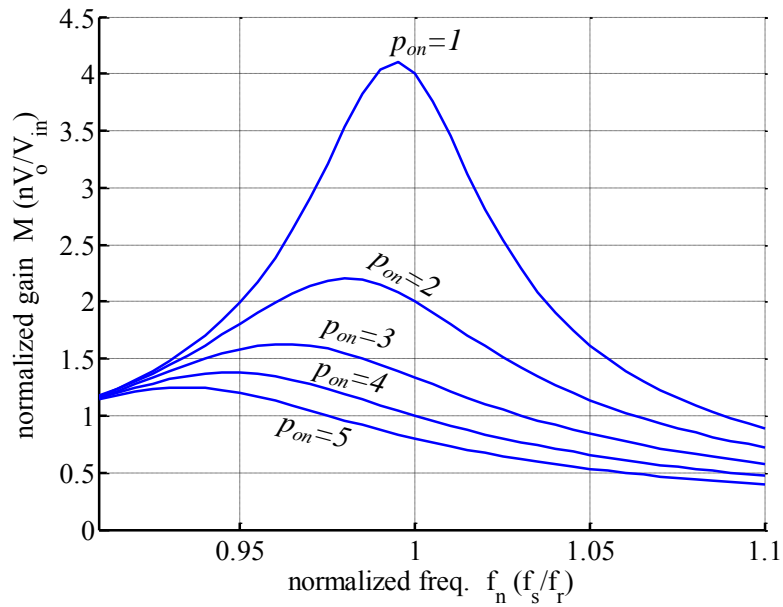
Figure 5.18 The LCC DC gain characteristics under different load conditions ($m=4$)

5.6.3 CLL Resonant Converter Analysis

The CLL resonant converter has the same resonant elements of the LLC, but different T-shaped tank, as seen in Figure 5.19[71-73]. Actually Figure 5.19 shows one way of transformer coupling, and there are alternative connection methods[71], such as putting L_r in the primary side. However, they will affect the analysis of the resonant tank.
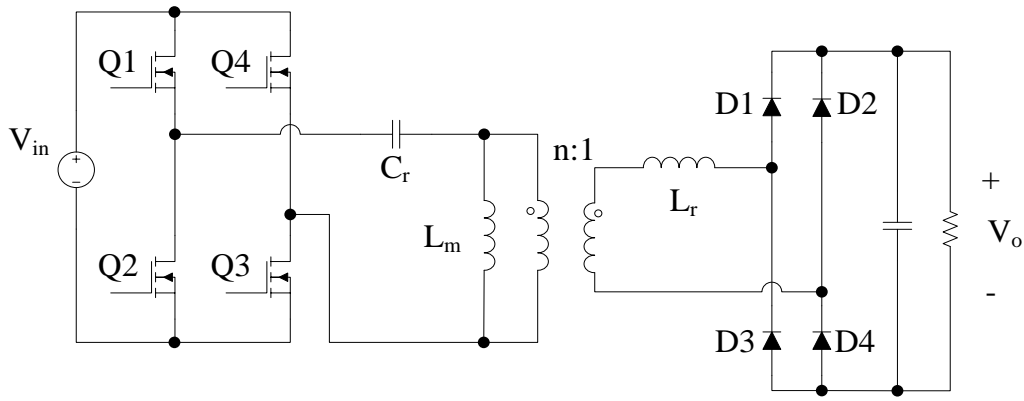
Figure 5.19 The full-bridge CLL resonant DC-DC converter

The equivalent resonant stage circuit with normalized parameters of the CLL converter is illustrated in Figure 5.20.

$$L_m = (m-1)L_r \qquad \omega_{base} = \sqrt{\frac{m}{m-1}} \frac{1}{\sqrt{L_r C_r}}, Z_{base} = \sqrt{\frac{m-1}{m}} \sqrt{\frac{L_r}{C_r}}$$
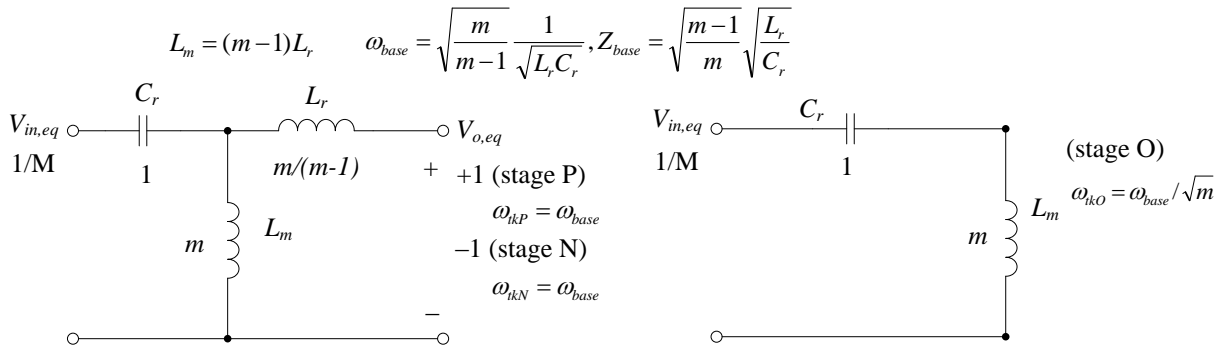
Figure 5.20 Normalized resonant tank circuit of the CLL

For stage P, the differential equations about the resonant variables are given by:

167

$$\frac{d}{d\theta}\begin{bmatrix} i_{rPn} \\ i_{mPn} \\ v_{CPn} \end{bmatrix} = \begin{bmatrix} 0 & 0 & -\dfrac{m-1}{m} \\ 0 & 0 & -\dfrac{1}{m} \\ 1 & 1 & 0 \end{bmatrix}\begin{bmatrix} i_{rPn} \\ i_{mPn} \\ v_{CPn} \end{bmatrix} + \begin{bmatrix} \dfrac{m-1}{m}\left(\dfrac{1}{M}-1\right) \\ \dfrac{1}{mM} \\ 0 \end{bmatrix}$$

(5.38)

Assume that i_{rPn} is expressed as

$$i_{rPn} = I_{Pn}\sin(\theta + \theta_{P0}) + I_{Psn}\theta + I_{P0n}$$

(5.39)

The coefficient matrices are constructed as follows:

$$A'' = \begin{bmatrix} 0 & -\dfrac{m-1}{m} & 0 & 0 \\ 0 & -\dfrac{1}{m} & -1 & 0 \\ 1 & 0 & 0 & -1 \\ 0 & 0 & 0 & -\dfrac{m-1}{m} \end{bmatrix}$$

(5.40)

$$B'' = \left[\dfrac{m-1}{m}\left(\dfrac{1}{M}-1\right) - \dfrac{di_{rPn}}{d\theta}, \quad \dfrac{1}{mM}, \quad i_{rPn}, \quad -\dfrac{d^2 i_{rPn}}{d\theta^2}\right]^T$$

The resonant variables can be solved as

$$\begin{bmatrix} i_{mPn} \\ v_{CPn} \\ \dfrac{di_{mPn}}{d\theta} \\ \dfrac{dv_{CPn}}{d\theta} \end{bmatrix} = -(A'')^{-1}B'' = \begin{bmatrix} -i_{rPn} - \dfrac{m}{m-1}\dfrac{d^2 i_{rPn}}{d\theta^2} \\ -\dfrac{m}{m-1}\dfrac{di_{rPn}}{d\theta} + \dfrac{1}{M} - 1 \\ \dfrac{1}{m-1}\dfrac{di_{rPn}}{d\theta} + \dfrac{1}{m} \\ -\dfrac{m}{m-1}\dfrac{d^2 i_{rPn}}{d\theta^2} \end{bmatrix}$$

(5.41)

By substituting (5.39) into (5.41), the parameter I_{Psn} can be solved as $I_{Psn} = -\dfrac{m-1}{m^2}$, and the

resonant variable functions are:

$$i_{rPn} = I_{Pn} \sin(\theta + \theta_{P0}) - \frac{m-1}{m^2}\theta + I_{P0n}$$

$$i_{mPn} = \frac{1}{m-1}I_{Pn} \sin(\theta + \theta_{P0}) + \frac{m-1}{m^2}\theta - I_{P0n} \qquad (5.42)$$

$$v_{CPn} = -\frac{m}{m-1}I_{Pn} \cos(\theta + \theta_{P0}) + \frac{1}{M} - \frac{m-1}{m}$$

Similarly, the resonant variables in stage N can be expressed as

$$i_{rNn} = I_{Nn} \sin(\theta + \theta_{N0}) + \frac{m-1}{m^2}\theta + I_{N0n}$$

$$i_{mNn} = \frac{1}{m-1}I_{Nn} \sin(\theta + \theta_{N0}) - \frac{m-1}{m^2}\theta - I_{N0n} \qquad (5.43)$$

$$v_{CNn} = -\frac{m}{m-1}I_{Nn} \cos(\theta + \theta_{N0}) + \frac{1}{M} + \frac{m-1}{m}$$

For stage O, it can be solved that

$$i_{rOn} = 0$$

$$i_{mOn} = I_{On} \sin(\theta/\sqrt{m} + \theta_{O0})$$

$$v_{COn} = -\sqrt{m}I_{On} \cos(\theta/\sqrt{m} + \theta_{O0}) + 1/M \qquad (5.44)$$

The operation mode division of the CLL is similar to the LLC's, which can be divided into six major modes as PO, PON, PN, OPO, NP and NOP. The stage constraint conditions for each mode are listed in Table 5.6. The symmetry and continuity conditions are about matching the corresponding resonant values at the start or end of the stage and are not enumerated here.

Table 5.6 The stage constraint conditions of CLL

Stage Constraints		Applied Operation Modes
Stage P	$i_{rPn}(\theta_P) = 0$	PO, PON, PN, OPO
	$i_{rPn}(0) = 0$	OPO, NP, NOP
Stage O	$v_{COn}(\theta_o) = \dfrac{1}{M} - 1$	OPO, NOP
	$v_{COn}(\theta_o) = \dfrac{1}{M} + 1$	PON
Stage N	$i_{rNn}(\theta_N) = 0$	NP, NOP
	$i_{rNn}(0) = 0$	PON, PN

The power balance condition of CLL is given by

$$p_{on} = \frac{f_n}{\pi}\left(\int_0^{\theta_P} i_{rPn}(\theta)d\theta - \int_0^{\theta_N} i_{rNn}(\theta)d\theta \right) \tag{5.45}$$

as the tank output current i_{tkn} is actually the resonant inductor current i_{rn}.

The naming of the CLL boundary modes is also identical to the LLC, and the boundary mode conditions are listed in Table 5.7.

Table 5.7 The boundary mode conditions of CLL

Boundary Modes	Boundary Modes Conditions
PO/PON boundary PO mode	$v_{COn}(\theta_o) = \dfrac{1}{M} + 1$
PO/OPO boundary PO mode	$v_{CPn}(0) = \dfrac{1}{M} - 1$
PN/PON boundary PN mode	$v_{CPn}(\theta_P) = \dfrac{1}{M} + 1$
NP/NOP boundary NP mode	$v_{CPn}(0) = \dfrac{1}{M} - 1$
NOP/OPO boundary OP mode	$v_{COn}(\theta_o) = \dfrac{1}{M} - 1$

By applying the boundary mode conditions along with other stage conditions of the corresponding mode in Table 5.6 and the symmetry and continuity conditions, sufficient simultaneous equations can be found to solve the resonant variables and DC characteristics of the boundary modes. Note that the boundary OP mode is not part of the six major modes and its stage constraint is given as $i_{rPn}(0) = 0$. The mode boundaries and distribution are shown in Figure 5.21, which is very similar to the LLC's mode distribution.
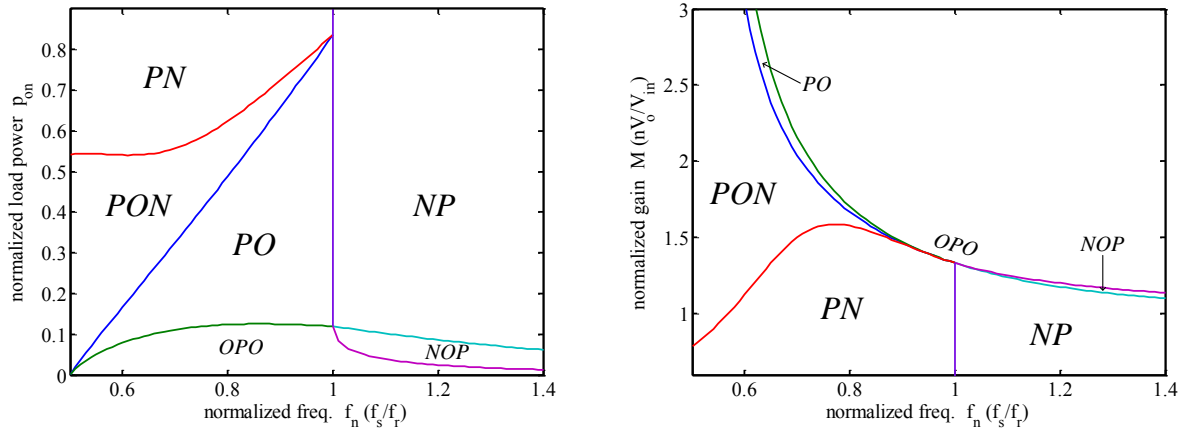
Figure 5.21 The mode boundaries and distribution of the CLL ($m=4$)

The CLL operation waveforms for different modes are shown in Figure 5.22 - Figure 5.27. In the waveform plots, the stage transition constraint conditions are marked. Stage P or N ends if i_r reaches zero; stage O ends if v_C crosses $1/M \pm 1$. The CLL and LLC have similar capacitor voltage v_C waveforms, and also the resonant current i_r in the CLL resembles the output current i_o of the LLC. However, CLL's magnetizing current i_m is quite different, which, unlike LLC's i_m, has no pure linear stage, as the transformer is never directly clamped by the output voltage.
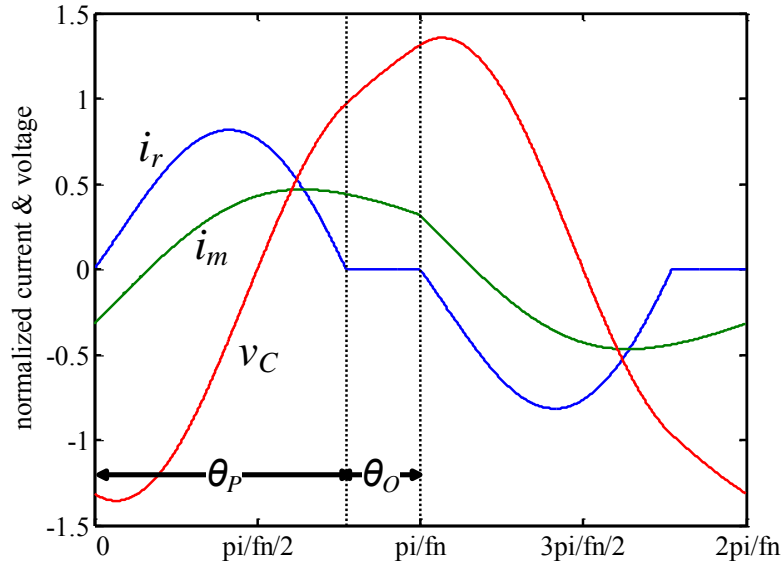
Figure 5.22 The CLL operating waveforms in PO mode ($m=4$, $f_n=0.8$, $p_{on}=0.4$)
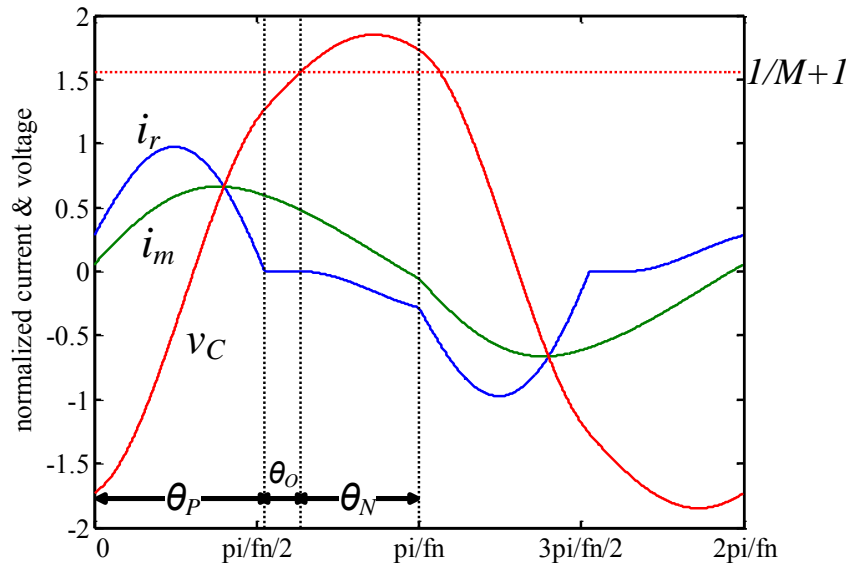
Figure 5.23 The CLL operating waveforms in PON mode ($m=4$, $f_n=0.65$, $p_{on}=0.4$)
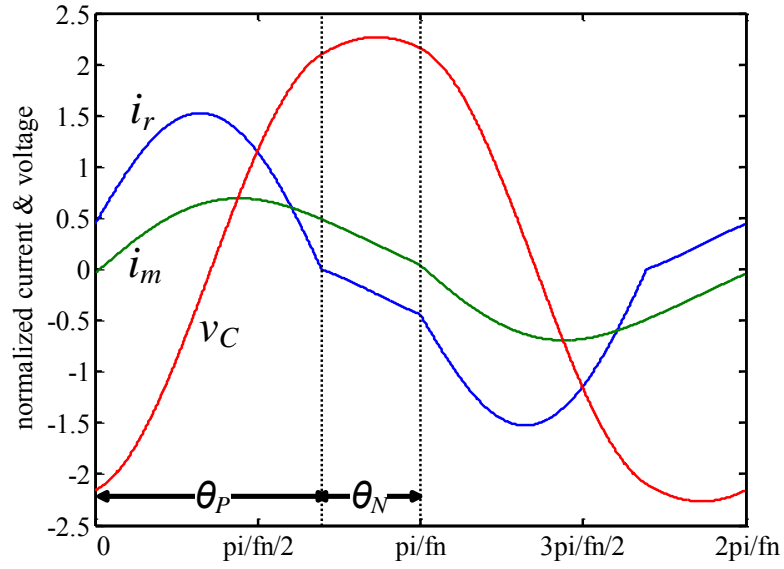
Figure 5.24 The CLL operating waveforms in PN mode ($m=4$, $f_n=0.8$, $p_{on}=0.8$)
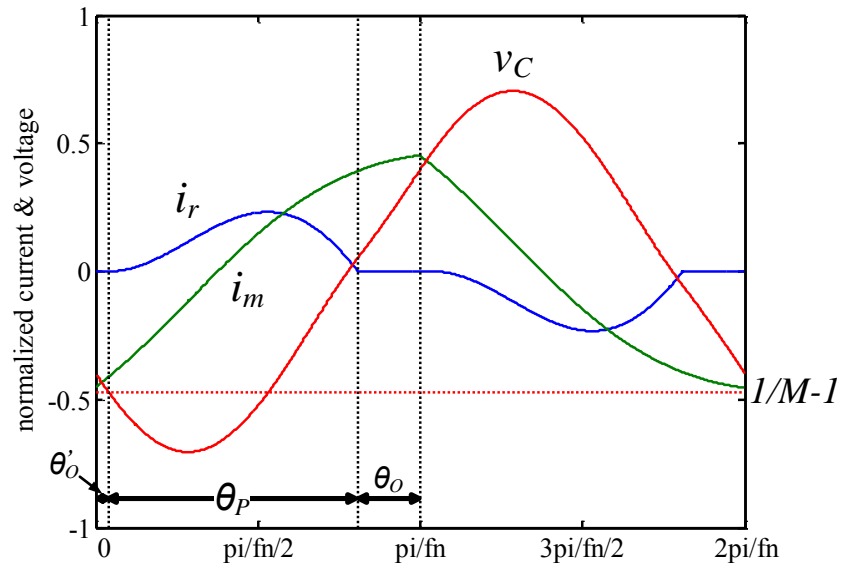
Figure 5.25 The CLL operating waveforms in OPO mode ($m=4$, $f_n=0.75$, $p_{on}=0.1$)
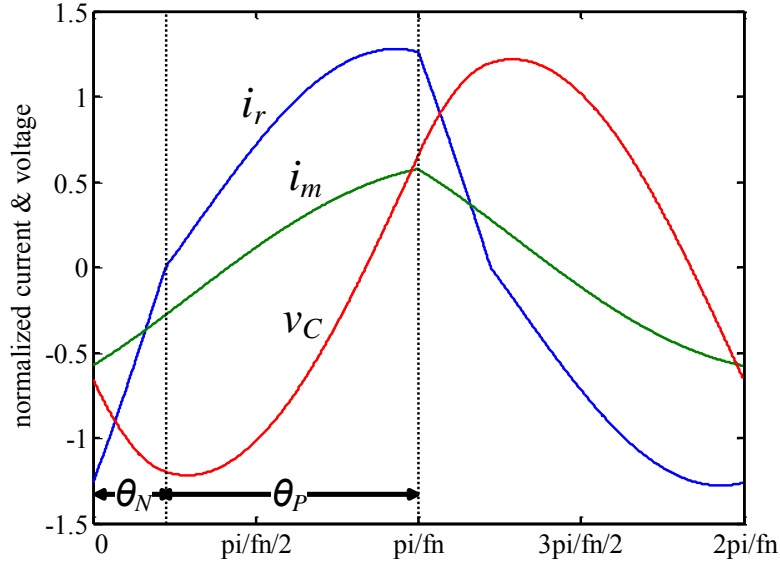
Figure 5.26 The CLL operating waveforms in NP mode ($m=4$, $f_n=1.4$, $p_{on}=0.8$)
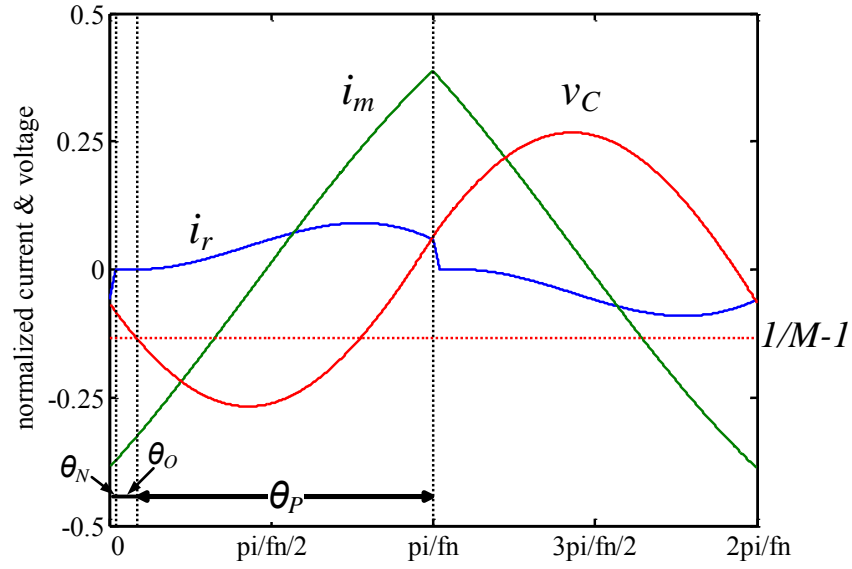
Figure 5.27 The CLL operating waveforms in NOP mode ($m=3$, $f_n=1.4$, $p_{on}=0.05$)

The voltage gain of CLL can be calculated from the operation mode equations, which is shown in Figure 5.28. To make a comparison, in Figure 5.28 the gain of LLC with the same p_{on} and m parameters are also plotted in dash lines. For CLL, the gain curves also converge at the

resonant frequency, but the resonant point gain is $m/(m-1)$ rather than unity. If we normalize

the CLL gain to unity, which matches the gain level of LLC, the peak gain of the former will be

smaller than the latter at the same m and load condition. It means that CLL's capability in

handling wide range input voltage is not as good as LLC. The CLL is beneficial for voltage step-

up conversion application, since the output current is smaller than the input, and the inductor

conduction loss is smaller by putting the resonant inductor to the secondary side of the

transformer than in the primary side.
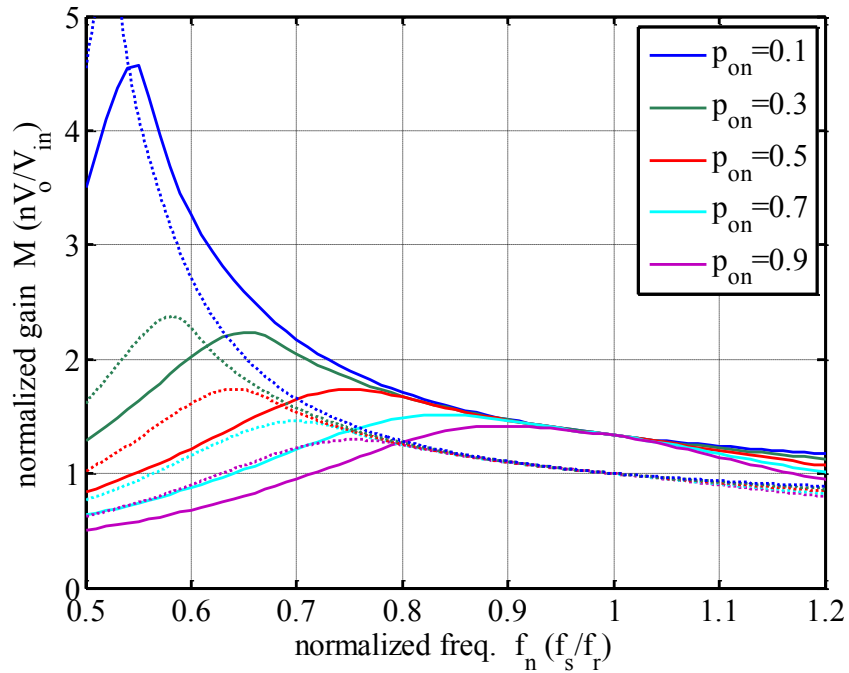
Figure 5.28 The voltage gain comparison between CLL (solid lines) and LLC (dash lines) under different loads (both *m=4*)

CHAPTER SIX: CONCLUSIONS AND FUTURE WORK

6.1 Conclusions

The continuous developments in energy and electronic technology are driving the power conversion techniques towards higher power efficiency and power density. In the field of renewable energy, solar photovoltaic is growing exponentially and the grid-tied PV micro-inverter structure is gaining attentions for its advantage in flexibility, safety and high efficiency. Due to the nature of solar source, the power converter stage should be able to deal with the high fluctuation voltage of PV panels output and in the meantime achieve low power losses and small profile size. In computing and telecommunication devices, the front-end converter is an integral part of power supplies, which also require the DC-DC converter stage to have high efficiency over a large input voltage and load range and operate in high frequency in order to shrink the converter size. Resonant DC-DC converters are suitable candidates for these applications. The LLC resonant converter with the advantage of achieving soft switching for a wide input voltage and load condition is becoming popular in many applications.

In Chapter Two, several LLC analysis methods are examined and discussed. The fundamental harmonic analysis (FHA) approach is a widely used frequency domain analysis method, which is simple and intuitive to use but has poor accuracy. The state-plane methods and time domain analysis methods can provide a precise description of the resonant behavior of the converter, but the study on the LLC is incomplete as not all the operation modes are explored. An operation mode analysis is proposed to fill the gaps of LLC study. It's a time domain approach based on constructing and solving the resonant variable equations for different resonant stages and

modes. Six major operation modes are presented and their resonant current/voltage waveforms and DC gain characteristics are described in detailed. Among these modes, it is found that PO mode is the most preferable operation mode for its features of achieving ZVS, no reverse recovery loss and narrow gain variation caused by load fluctuation. The boundaries of each mode and the load, gain and frequency distributions of each mode are given to better understand the transition and characteristics between different modes. Through the generalized analysis, the operation of the LLC can be precisely described and predicted.

To employ the operation mode model in practical use, approximation is needed to bypass the complex nonlinear equation solving process. The numerical approximation of the LLC analysis is presented in Chapter Three. Unlike prior approximation approaches introduced in the second section of this chapter, we focus on peak gains and PO mode boundary as the targets. The peak of a converter's DC gain curve defines its maximum voltage conversion ratio and also serves as the boundary between ZVS and ZCS region, and therefore it is a vital parameter in LLC design. The occurrence mechanism of peak points are studied that they happen in PON and PN mode constrained by the zero resonant current crossing condition. In PN mode, explicit solutions for peak gain points are derived. In PON mode, a numerical approximation is developed to provide a straightforward calculation method and provides relatively accurate results. In the PO mode study, it is found that its load-frequency boundary line resembles a linear line, and therefore a linear curve-fitting method is developed. Knowing the mode boundary can help restrict the LLC operation within this preferable mode.

In Chapter Four, the design optimization of the LLC resonant converter is studied. As the literature review shows the lack of clear optimal design methods for the LLC, especially in

178

determining the L-C component values, to address this problem we develop three optimal design methods based on the previous presented operation mode analysis and the approximation method can be applied to facilitate the design process. The relation between resonant/magnetizing currents and the converter parameters are discussed, which find the product of inductor ratios m and the characteristic impedance Z_r as an optimization target: the larger this product is, the smaller the conduction losses become. The optimization goal is therefore established as making tank currents as small as possible while satisfying the gain range requirement of the design specifications. The three methods are according to three different design scenarios: one is for narrow input voltage variation, and the design focuses on the resonant point performance of the converter, as it accounts for the normal operation condition and can provides the highest efficiency of the LLC; another method is called peak gain placement, in which by placing the peak point of the full load condition gain curve at the required max gain and minimum frequency the LLC tank can achieve the maximum optimization target; the third method is for the design that has strict restriction on no reverse recovery, which means that the LLC operation should be limited only in PO and OPO mode, and the method following the principle of peak gain placement use the PO/PON boundary information to find the optimal tank parameters. The LLC design can be generalized using normalized model to free from the association of certain design specifications. The general design procedure narrows the required specs to two parameters, the gain margin and the frequency margin, and simplifies the optimization targets to two parameters, the inductors ratio m and the normalized full load power p_{on}, and employs the same idea of the peak gain placement. The correlation between the normalized specs and the optimization targets can therefore be obtained.

In Chapter Five, the analysis of resonant converters is summarized into a generalized procedure. Inspired by the operation mode analysis of LLC converters, a resonant converter

179

topology can be divided into three resonant stages, and then be represented by simplified and normalized equivalent L-C circuits. An iterative process is developed to acquire the resonant variable functions. The boundary conditions of a resonant mode are summarized, which can be applied to solve the unknowns of the resonant variable functions. From this analysis process, various operation waveforms along with the DC characteristics of a resonant converter are obtainable. The process is easy to implement by numerical computing tools, and is useful in resonant converter design and evaluation. The presented analysis examples prove the effectiveness of this standardized procedure.

6.2 Future Works

Further simplification of the proposed LLC operation mode analysis is needed, as the current method involving multiple nonlinear equations solving is complex to use. Besides the DC characteristics, more other useful information can be extracted from the operation mode, such as the voltage/current stresses on the converter components, and their relations with each resonant tank parameters can be further explored and possible approximation methods exists for quickly obtaining these relations. Another area that is not covered in the LLC analysis is the impact of the parasitic elements, as ideal components are used throughout the analysis. It is possible to include some parasitic components in the operation mode analysis to achieve even higher accuracy.

The proposed optimization methods are for the selection of L-C resonant tank parameters, while there are other circuit parameters that can be included in the optimization consideration, such as the dead time, the output capacitance, the selection of inductor and transformer core structure. Also, the actual components used in the converter circuit may, in turn, affect the

effectiveness of the optimal parameters, and post-adjustment can be carried out to improve the converter performance.

The control scheme for the resonant converter is another important research topic. Besides the fixed-duty-cycle frequency control method, other possible control methods like phase shift control will change the resonant behavior of the converter. To design a closed-loop control, the small signal analysis is a must. The resonant converter lacks an easy to use small signal model, and it should be the focused for the future studies.

REFERENCES

[1]   "Renewables 2011 Global Status Report ". [Online]. Available: http://www.ren21.net/

[2]   "Technology Roadmap - Solar Photovoltaic Energy". [Online]. Available: www.iea.org

[3]   S. B. Kjaer, J. K. Pedersen, and F. Blaabjerg, "A review of single-phase grid-connected inverters for photovoltaic modules," *Industry Applications, IEEE Transactions on,* vol. 41, pp. 1292-1306, 2005.

[4]   Y. Xue, L. Chang, S. B. Kjaer, J. Bordonau, and T. Shimizu, "Topologies of single-phase inverters for small distributed power generators: an overview," *Power Electronics, IEEE Transactions on,* vol. 19, pp. 1305-1314, 2004.

[5]   E. Roman, R. Alonso, P. Ibanez, S. Elorduizapatarietxe, and D. Goitia, "Intelligent PV Module for Grid-Connected PV Systems," *Industrial Electronics, IEEE Transactions on,* vol. 53, pp. 1066-1073, 2006.

[6]   C. Citro, A. Luna, J. Rocabert, R. S. Munoz-Aguilar, I. Candela, and P. Rodriguez, "Overview of power processing structures for embedding Energy Storage in PV power converters," in *IECON 2011 - 37th Annual Conference on IEEE Industrial Electronics Society*, 2011, pp. 2492-2498.

[7]   Q. Li and P. Wolfs, "A Review of the Single Phase Photovoltaic Module Integrated Converter Topologies With Three Different DC Link Configurations," *Power Electronics, IEEE Transactions on,* vol. 23, pp. 1320-1333, 2008.

[8]   H. Patel and V. Agarwal, "MPPT Scheme for a PV-Fed Single-Phase Single-Stage Grid-Connected Inverter Operating in CCM With Only One Current Sensor," *Energy Conversion, IEEE Transactions on,* vol. 24, pp. 256-263, 2009.

[9]   H. Hu, W. Al-Hoor, N. H. Kutkut, I. Batarseh, and Z. J. Shen, "Efficiency Improvement of Grid-Tied Inverters at Low Input Power Using Pulse-Skipping Control Strategy," *Power Electronics, IEEE Transactions on,* vol. 25, pp. 3129-3138, 2010.

[10]   W. A. Tabisz, M. M. Jovanovic, and F. C. Lee, "Present and future of distributed power systems," in *Applied Power Electronics Conference and Exposition, 1992. APEC '92. Conference Proceedings 1992., Seventh Annual*, 1992, pp. 11-18.

[11]   F. C. Lee, P. Barbosa, P. Xu, J. Zhang, B. Yang, and F. Canales, "Topologies and design considerations for distributed power system applications," *Proceedings of the IEEE,* vol. 89, pp. 939-950, 2001.

[12]   S. Luo, "A review of distributed power systems part I: DC distributed power system," *Aerospace and Electronic Systems Magazine, IEEE,* vol. 20, pp. 5-16, 2005.

[13]   C. D. Xu and K. W. E. Cheng, "A survey of distributed power system — AC versus DC distributed power system," in *Power Electronics Systems and Applications (PESA), 2011 4th International Conference on*, 2011, pp. 1-12.

[14]   F. C. Lee, W. Shuo, K. Pengju, W. Chuanyun, and F. Dianbo, "Power architecture design with improved system efficiency, EMI and power density," in *Power Electronics Specialists Conference, 2008. PESC 2008. IEEE*, 2008, pp. 4131-4137.

[15]   M. M. Jovanovic, "Power Supply Technology - Past, Present, and Future," presented at the China Conf. for Power Electronics (PCIM China) 2007.

[16]   J. W. Kolar, U. Drofenik, J. Biela, M. L. Heldwein, H. Ertl, T. Friedli, and S. D. Round, "PWM Converter Power Density Barriers," in *Power Conversion Conference - Nagoya, 2007. PCC '07*, 2007, pp. P-9-P-29.

[17]   G. Majumdar, "Recent technologies and trends of power devices," in *Physics of Semiconductor Devices, 2007. IWPSD 2007. International Workshop on*, 2007, pp. 787-792.

[18]   "Power Technology Roadmap Report 2009," Power Sources Manufacturers Association (PSMA), http://www.psma.com/, 2009.

[19]   R. W. Erickson and D. Maksimović, *Fundamentals of Power Electronics*, 2nd. ed.: Kluwer Academic Publishers, 2001.

[20]   M. K. Kazimierczuk and D. Czarkowski, *Resonant Power Converters*, 2nd. ed.: John Wiley & Sons, Inc., 2011.

[21]   M. D. Bellar, T. S. Wu, A. Tchamdjou, J. Mahdavi, and M. Ehsani, "A review of soft-switched DC-AC converters," *Industry Applications, IEEE Transactions on,* vol. 34, pp. 847-860, 1998.

[22]   S. R. Sanders, J. M. Noworolski, X. Z. Liu, and G. C. Verghese, "Generalized averaging method for power conversion circuits," *Power Electronics, IEEE Transactions on,* vol. 6, pp. 251-259, 1991.

[23]   J. A. Sabate, V. Vlatkovic, R. B. Ridley, F. C. Lee, and B. H. Cho, "Design considerations for high-voltage high-power full-bridge zero-voltage-switched PWM converter," in *Applied Power Electronics Conference and Exposition, 1990. APEC '90, Conference Proceedings 1990., Fifth Annual*, 1990, pp. 275-284.

[24]   J. Sun, D. M. Mitchell, M. F. Greuel, P. T. Krein, and R. M. Bass, "Averaged modeling of PWM converters operating in discontinuous conduction mode," *Power Electronics, IEEE Transactions on,* vol. 16, pp. 482-492, 2001.

[25]   W. Chen, F. C. Lee, M. M. Jovanovic, and J. A. Sabate, "A comparative study of a class of full bridge zero-voltage-switched PWM converters," in *Applied Power Electronics Conference and*

Exposition, 1995. APEC '95. Conference Proceedings 1995., Tenth Annual, 1995, pp. 893-899 vol.2.

[26]   R. P. Severns, "Topologies for three-element resonant converters," *Power Electronics, IEEE Transactions on,* vol. 7, pp. 89-98, 1992.

[27]   C. M. Lai and K. K. Shyu, "A single-stage AC/DC converter based on zero voltage switching LLC resonant topology," *Electric Power Applications, IET,* vol. 1, pp. 743-752, 2007.

[28]   C. Chin and G. Bruning, "Voltage-fed half-bridge resonant converter for multiple lamp independent operation," in *Industry Applications Conference, 2001. Thirty-Sixth IAS Annual Meeting. Conference Record of the 2001 IEEE*, 2001, pp. 218-222 vol.1.

[29]   Y. Fang, D. Xu, Y. Zhang, F. Gao, L. Zhu, and Y. Chen, "Standby Mode Control Circuit Design of LLC Resonant Converter," in *Power Electronics Specialists Conference, 2007. PESC 2007. IEEE*, 2007, pp. 726-730.

[30]   M. Z. Youssef and P. K. Jain, "A front end self-sustained LLC resonant converter," in *Power Electronics Specialists Conference, 2004. PESC 04. 2004 IEEE 35th Annual*, 2004, pp. 2651-2656 Vol.4.

[31]   X. Wu, G. Hua, J. Zhang, and Z. Qian, "A New Current-Driven Synchronous Rectifier for Series-Parallel Resonant (LLC) DC-DC Converter," *Industrial Electronics, IEEE Transactions on,* vol. 58, pp. 289-297, 2011.

[32]   R. Beiranvand, B. Rashidian, M. R. Zolghadri, and S. M. H. Alavi, "Designing an Adjustable Wide Range Regulated Current Source," *Power Electronics, IEEE Transactions on,* vol. 25, pp. 197-208, 2010.

[33]   K. Jin, X. Ruan, M. Yang, and M. Xu, "A Hybrid Fuel Cell Power System," *Industrial Electronics, IEEE Transactions on,* vol. 56, pp. 1212-1222, 2009.

[34]   Z. Liang, R. Guo, J. Li, and A. Q. Huang, "A High-Efficiency PV Module-Integrated DC/DC Converter for PV Energy Harvest in FREEDM Systems," *Power Electronics, IEEE Transactions on,* vol. 26, pp. 897-909, 2011.

[35]   Y. Chen, X. Wu, Z. Qian, and W. Zhang, "Design and optimization of a wide output voltage range LED driver based on LLC resonant topology," in *Power Electronics and ECCE Asia (ICPE & ECCE), 2011 IEEE 8th International Conference on*, 2011, pp. 2831-2837.

[36]   A. K. S. Bhat, "Analysis and design of a series-parallel resonant converter," *Power Electronics, IEEE Transactions on,* vol. 8, pp. 1-11, 1993.

[37]   M. K. Kazimierczuk, N. Thirunarayan, and S. Wang, "Analysis of series-parallel resonant converter," *Aerospace and Electronic Systems, IEEE Transactions on,* vol. 29, pp. 88-99, 1993.

[38]   M. Zaki, A. Bonsall, and I. Batarseh, "Performance characteristics for the series-parallel resonant converter," in *Southcon/94. Conference Record*, 1994, pp. 573-577.

[39]   H. Choi, "Analysis and Design of LLC Resonant Converter with Integrated Transformer," in *Applied Power Electronics Conference, APEC 2007 - Twenty Second Annual IEEE*, 2007, pp. 1630-1635.

[40]   Y. Liang, W. Liu, B. Lu, and J. D. van Wyk, "Design of integrated passive component for a 1 MHz 1 kW half-bridge LLC resonant converter," in *Industry Applications Conference, 2005. Fourtieth IAS Annual Meeting. Conference Record of the 2005*, 2005, pp. 2223-2228 Vol. 3.

[41]   B. Yang, R. Chen, and F. C. Lee, "Integrated magnetic for LLC resonant converter," in *Applied Power Electronics Conference and Exposition, 2002. APEC 2002. Seventeenth Annual IEEE*, 2002, pp. 346-351 vol.1.

[42]   A. K. S. Bhat, "Analysis and design of LCL-type series resonant converter," *Industrial Electronics, IEEE Transactions on,* vol. 41, pp. 118-124, 1994.

[43]   X. Fang, H. Hu, J. Shen, and I. Batarseh, "Operation Mode Analysis and Peak Gain Approximation of the LLC Resonant Converter," *Power Electronics, IEEE Transactions on,* vol. 27, pp. 1985-1995, 2012.

[44]   J. F. Lazar and R. Martinelli, "Steady-state analysis of the LLC series resonant converter," in *Applied Power Electronics Conference and Exposition, 2001. APEC 2001. Sixteenth Annual IEEE*, 2001, pp. 728-735 vol.2.

[45]   R. L. Steigerwald, "A comparison of half-bridge resonant converter topologies," *Power Electronics, IEEE Transactions on,* vol. 3, pp. 174-182, 1988.

[46]   B.-H. Lee, M.-Y. Kim, C.-E. Kim, K.-B. Park, and G.-W. Moon, "Analysis of LLC Resonant Converter considering effects of parasitic components," in *Telecommunications Energy Conference, 2009. INTELEC 2009. 31st International*, 2009, pp. 1-6.

[47]   J.-H. Kim, C.-E. Kim, J.-K. Kim, and G.-W. Moon, "Analysis for LLC resonant converter considering parasitic components at very light load condition," in *Power Electronics and ECCE Asia (ICPE & ECCE), 2011 IEEE 8th International Conference on*, 2011, pp. 1863-1868.

[48]   "Half-bridge LLC Resonant Converter Design Using FSFR-series Fairchild Power Switch". [Online Application Note]. Available: www.fairchildsemi.com

[49]   A. K. S. Bhat, "A generalized steady-state analysis of resonant converters using two-port model and Fourier-series approach," *Power Electronics, IEEE Transactions on,* vol. 13, pp. 142-151, 1998.

[50]   A. J. Forsyth, G. A. Ward, and S. V. Mollov, "Extended fundamental frequency analysis of the LCC resonant converter," *Power Electronics, IEEE Transactions on,* vol. 18, pp. 1286-1292, 2003.

[51]   M. P. Foster, C. R. Gould, A. J. Gilbert, D. A. Stone, and C. M. Bingham, "Analysis of CLL Voltage-Output Resonant Converters Using Describing Functions," *Power Electronics, IEEE Transactions on,* vol. 23, pp. 1772-1781, 2008.

[52]   H. A. Kojori, J. D. Lavers, and S. B. Dewan, "State plane analysis of a resonant DC-DC converter incorporating integrated magnetics," *Magnetics, IEEE Transactions on,* vol. 24, pp. 2898-2900, 1988.

[53]   I. Batarseh and C. Q. Lee, "Steady-state analysis of the parallel resonant converter with LLCC-type commutation network," *Power Electronics, IEEE Transactions on,* vol. 6, pp. 525-538, 1991.

[54]   K. Siri, I. Batarseh, and C. Q. Lee, "Frequency response for the conventional parallel resonant converter based on the state-plane diagram," *Circuits and Systems I: Fundamental Theory and Applications, IEEE Transactions on,* vol. 40, pp. 33-42, 1993.

[55]   I. Batarseh, R. Liu, A. Ortiz-Conde, A. Yacoub, and K. Siri, "Steady state analysis and performance characteristics of the LLC-type parallel resonant converter," in *Power Electronics Specialists Conference, PESC '94 Record., 25th Annual IEEE*, 1994, pp. 597-606 vol.1.

[56]   C. Q. Lee and K. Siri, "Design of series-resonant convertor with normalised state-plane diagram," *Electronics Letters,* vol. 22, pp. 718-719, 1986.

[57]   R. Oruganti and F. C. Lee, "Resonant Power Processors, Part I---State Plane Analysis," *Industry Applications, IEEE Transactions on,* vol. IA-21, pp. 1453-1460, 1985.

[58]   F.-S. Tsai, Y. Chin, and F. C. Lee, "State-Plane Analysis of Clamped-Mode Parallel-Resonant Converter," in *Telecommunications Energy Conference, 1987. INTELEC '87. The Ninth International*, 1987, pp. 220-227.

[59]   M. Vuksic, S. M. Beros, and L. Vuksic, "The Multiresonant Converter Steady-State Analysis Based on Dominant Resonant Process," *Power Electronics, IEEE Transactions on,* vol. 26, pp. 1452-1468, 2011.

[60]   I. Batarseh, "State-plane approach for the analysis of half-bridge parallel resonant converters," *Circuits, Devices and Systems, IEE Proceedings -,* vol. 142, pp. 200-204, 1995.

[61]   N. H. Kutkut, C. Q. Lee, and I. Batarseh, "A generalized program for extracting the control characteristics of resonant converters via the state-plane diagram," *Power Electronics, IEEE Transactions on,* vol. 13, pp. 58-66, 1998.

[62]   H. de Groot, E. Janssen, R. Pagano, and K. Schetters, "Design of a 1-MHz LLC Resonant Converter Based on a DSP-Driven SOI Half-Bridge Power MOS Module," *Power Electronics, IEEE Transactions on,* vol. 22, pp. 2307-2320, 2007.

[63]   T. Liu, Z. Zhou, A. Xiong, J. Zeng, and J. Ying, "A Novel Precise Design Method for LLC Series Resonant Converter," in *Telecommunications Energy Conference, 2006. INTELEC '06. 28th Annual International*, 2006, pp. 1-6.

[64]   C. Gould, D. A. Stone, M. P. Foster, and C. Bingham, "State-variable modelling of CLL resonant converters," in *Power Electronics, Machines and Drives, 2004. (PEMD 2004). Second International Conference on (Conf. Publ. No. 498)*, 2004, pp. 214-219 Vol.1.

[65]   H. J. Jiang and G. Maggetto, "Identification of steady-state operational modes of the series resonant DC-DC converter based on loosely coupled transformers in below-resonance operation," *Power Electronics, IEEE Transactions on,* vol. 14, pp. 359-371, 1999.

[66]   "An Introduction to LLC Resonant Half-bridge Converter", AN2644. [Online]. Available: www.st.com

[67]   C. Adragna, S. De Simone, and C. Spini, "A design methodology for LLC resonant converters based on inspection of resonant tank currents," in *Applied Power Electronics Conference and Exposition, 2008. APEC 2008. Twenty-Third Annual IEEE*, 2008, pp. 1361-1367.

[68]   G. Ivensky, S. Bronshtein, and A. Abramovitz, "Approximate Analysis of Resonant LLC DC-DC Converter," *Power Electronics, IEEE Transactions on,* vol. 26, pp. 3274-3284, 2011.

[69]   B. Lu, W. Liu, Y. Liang, F. C. Lee, and J. D. van Wyk, "Optimal design methodology for LLC resonant converter," in *Applied Power Electronics Conference and Exposition, 2006. APEC '06. Twenty-First Annual IEEE*, 2006, p. 6 pp.

[70]   Y. Liu, "High Efficiency Optimization of LLC Resonant Converter for Wide Load Range," M.S Thesis, Virginia Polytechnic Institute and State University, 2007.

[71]   C. Chakraborty, M. Ishida, and T. Hori, "Performance, design and pulse width control of a CLL resonant DC/DC converter operating at constant frequency in the lagging power factor mode," in *Power Electronics and Drive Systems, 1999. PEDS '99. Proceedings of the IEEE 1999 International Conference on*, 1999, pp. 767-772 vol.2.

[72]   J. Sosa, M. Castilla, N. Berbel, J. M. Guerrero, and L. G. de Vicuna, "Analysis, design and practical evaluation of an input-output linearization controller for the CLL-T dc-dc resonant converter," in *IEEE Industrial Electronics, IECON 2006 - 32nd Annual Conference on*, 2006, pp. 2593-2598.

[73]   D. Huang, D. Fu, F. C. Lee, and P. Kong, "High-Frequency High-Efficiency CLL Resonant Converters With Synchronous Rectifiers," *Industrial Electronics, IEEE Transactions on,* vol. 58, pp. 3461-3470, 2011.